Masterarbeit

Investigation of flow phenomena in a compressor cascade using Particle Tracking Velocimetry (PTV)

Herr BSc Julián Sánchez Riera

August 2018

Nr. 1475

Institut für Luftfahrtantriebe
Universität Stuttgart
Direktor: Prof. Dr.-Ing. S. Staudacher

INSTITUT FÜR LUFTFAHRTANTRIEBE
UNIVERSITÄT STUTTGART

Prof. Dr.-Ing. S. Staudacher

Institut Für Luftfahrtantriebe

Pfaffenwaldring 6
D-70569 Stuttgart

Telefon (0711) 685 63520
Telefax (0711) 685 63505

Masterarbeit

für

Herrn Julián Sánchez Riera

Untersuchung von Strömungsphänomenen in einer Verdichter-Kaskade mit Hilfe der Particle Tracking Velocimetry

Hintergrund

Das Institut für Luftfahrtantriebe betreibt einen großen Flachbettwasserkanal. In der Messstrecke des Kanals befindet sich eine Verdichter-Kaskade zur Untersuchung der Strömungsphänomene bei unterschiedlichen Anströmwinkeln. Die Spaltströmung und deren Wechselwirkung mit der Passagenströmung führen zu sehr komplexen Strömungsphänomenen mit einer erheblichen Bedeutung für die Turbomaschine. Die Spitzenspaltströmung hat einen wesentlichen Einfluss auf den Wirkungsgrad und auf das Stabilitätsverhalten des Verdichters.

Zielformulierung

Am Flachbettwasserkanal des Instituts soll die Strömung im Schaufelspitzen-Spalt-Bereich einer Verdichter-Kaskade untersucht werden. Von besonderem Interesse sind hierbei die auftretenden Phänomene an der Stabilitätsgrenze. Die Particle Tracking Velocimetry (PTV) erlaubt die Untersuchung der Strömung, ohne dass störende Sonden eingesetzt werden müssten.

Arbeitspunkte

- Einarbeitung in die Thematik/ Literaturrecherche,
- Planung des Einsatzes der PTV im stabilen und instabilen Betriebsbereich,
- Festlegung einer geeigneten Mess- und Auswerteprozedur zur Untersuchung der Strömung,
- Detaillierte Untersuchung der stabilen und instabilen Strömungsphänomene,
- Auswertung, Interpretation und Dokumentation der Ergebnisse.

Betreuer: Prof. Dr.-Ing. S. Staudacher, Dr.-Ing. Markus Leitner

Erklärung des Kandidaten

Ich versichere, dass diese Masterarbeit selbständig von mir verfasst wurde – abgesehen von der Mitwirkung der genannten Betreuer – und dass nur die angegebenen Quellen und Hilfsmittel verwendet wurden.

27.08.2018
Datum


Unterschrift

Termine

Ausgabe : 1.3.2018 bestätigt :

Zeitraum für Besprechung :

Unterbrechung : genehmigt durch Prüfungsausschuss am :

Verlängerung : genehmigt durch Prüfungsausschuss am :

Seminarvortrag:

Abgabe : bestätigt :

Erklärung

Hiermit versichere ich, dass ich diese Masterarbeit selbstständig mit Unterstützung des Betreuers / der Betreuer angefertigt und keine anderen als die angegebenen Quellen und Hilfsmittel verwendet habe.

Die Arbeit oder wesentliche Bestandteile davon sind weder an dieser noch an einer anderen Bildungseinrichtung bereits zur Erlangung eines Abschlusses eingereicht worden.

Ich erkläre weiterhin, bei der Erstellung der Arbeit die einschlägigen Bestimmungen zum Urheberschutz fremder Beiträge entsprechend den Regeln guter wissenschaftlicher Praxis[1] eingehalten zu haben. Soweit meine Arbeit fremde Beiträge (z.B. Bilder, Zeichnungen, Textpassagen etc.) enthält, habe ich diese Beiträge als solche gekennzeichnet (Zitat, Quellenangabe) und eventuell erforderlich gewordene Zustimmungen der Urheber zur Nutzung dieser Beiträge in meiner Arbeit eingeholt. Mir ist bekannt, dass ich im Falle einer schuldhaften Verletzung dieser Pflichten die daraus entstehenden Konsequenzen zu tragen habe.

Stuttgart, 27.08.2018

Ort, Datum, Unterschrift

1 Nachzulesen in den DFG-Empfehlungen zur „Sicherung guter wissenschaftlicher Praxis" bzw. in der Satzung der Universität Stuttgart zur „Sicherung der Integrität wissenschaftlicher Praxis und zum Umgang mit Fehlverhalten in der Wissenschaft"

Contents

List of Figures

List of Tables

Nomenclature

Abbreviations

A	—	Fitting Constant	[Pa · s]
A_s	—	Characteristic Area	[m^2]
a	—	Flow Acceleration	[m/s^2]
B	—	Fitting Constant	[K]
C	—	Fitting Constant	[K]
C_p	—	Pressure Coefficient	[–]
c_{ax}	—	Flow Axial Velocity	[m/s]
c	—	Blade Chord Length	[mm]
h	—	Specific Enthalpy	[J/kg]
H	—	Blade Height Length	[mm]
i	—	Incidence Angle	[°]
L	—	Characteristic Length	[m]
$\dot{m}$	—	Mass Flow	[kg/s]
N	—	Rotor Blade Speed	[rpm]
n	—	Refraction Index of a medium	[–]
p	—	Pressure	[Pa]
R	—	Specific Ideal Gas Constant for Air	[J/kg · K]
Re	—	Reynolds Number	[–]
s	—	Particle Position	[m]
T	—	Temperature	[K] or [°C]
t	—	Time	[s]
u	—	Flow Velocity	[m/s]
U	—	Rotor Blade Speed	[m/s]
x	—	Particle Position	[m]

Greek Letters

β_1	—	Inlet Air angle	[°]
β_1'	—	Design Inlet Air angle	[°]
η_c	—	Compressor Efficiency	[–]
θ	—	Angle of Incidence or Refraction	[°]
μ	—	Dynamic Viscosity	[kg/m s]
ν	—	Kinematic Viscosity	[m^2/s]
π	—	Pressure Ratio	[–]

ρ	—	Density	[kg/m^3]
σ_0	—	Standard Deviation	
φ	—	Flow Coefficient	[–]
ψ	—	Load Coefficient	[–]

Acronyms

BLF	—	Boundary Layer Flow
DV	—	Double Vortex Structure
HSV	—	Horseshoe Vortex
LDA	—	Laser Doppler Anemometry
PIV	—	Particle Image Velocimetry
PTV	—	Particle Tracking Velocimetry
RKE	—	Relative Kinetic Energy
RMS	—	Root Mean Squared
TLF	—	Tip Leakage Flow
TLFV	—	Tip Leakage Vortex
LE	—	Leading Edge
TE	—	Trailing Edge

Chapter 1

Introduction

The Aerospace and Aeronautical Industry has experienced over the last decades a huge growth motivated by the increase in the number of passengers transported every year by all the commercial airlines. This increase in passengers generates an increment in the number of aircrafts flying in the skies at any moment in any place of the world. But, this fact has brought some other drawbacks: airspace saturation, pollution (CO2 and NOx), noise levels... Nowadays, these issues are of utmost importance in regions such as Europe or North America, where the skies are completely saturated with aircrafts flying 24h per day. The increase in the number of aircrafts increments the amount of CO2 and NOx emissions, which is also raised by the saturation of the skies and the delays in the flights that it causes. So, more airplanes flying more time produce huge amounts of pollutants. Some ideas are come up with to solve these situations, like the "Smarter Skies" Airbus idea for 2050 [1]. Hence, shorter term solutions are needed.

Moreover, the changes in society, which requires shorter and faster flights, cheaper fares and on-board comfort, introduce some other variables in the equation such as reaching a compromise between more powerful and highly efficient engines with bigger aircrafts. In the area we are focused on, the production of more powerful and efficient aircrafts at the same time enters in a complicated trade-off that requires a better understanding of the engine operation every day, in order to maximize both parameters and satisfy all the requirements. For that reason, the planification in the reduction of the fuel consumption (better fuel efficiency) in a 1.5% and a reduction of pollutants emission of aircraft engines in a 50% for 2050 needs a deeper understanding of the performance of an engine [2].

At the end of 20th Century, the efficiency of gas turbines was around 40% [3]. That means that only 40% of the energy of the flow is useful for propulsion, while the other 60% is useless, normally classified as losses. All these losses are due to different factors: thermal losses, flow losses, pressure losses, cycle losses, transmission losses... Then, designing engines as efficient as possible means to know all the reasons and phenomena involved in every type of loss, so they could be analysed and in any way reduced their effects in the overall engine performance.

Inside a compressor, there are many losses, such as the aerodynamic or profile losses, the secondary losses or the tip gap losses. This last group is related with the existence of a tip clearance between the rotor and the casing. In turbomachineries, this gap is left for allowing the free rotation of the rotor. The existence of a space between tip and casing causes the presence of a flow from one side of the blade to another (Tip Leakage Flow), generating a vortex and originating a sort of pressure and flow losses.

At first sight, it could be thought that this tip gap should remain constant, or invariant through time, but it is not the case. The turbomachine can work under very different pressure, temperature, humidity and speed conditions. All these factors influence in the dilatation, deformation and vibration of the rotor, so different tip clearance can be found in the same turbomachine. Additionally, compressors can work under different operating points. Therefore, these different conditions may affect the behaviour of the Tip Leakage Flow, and hence, the losses and the perturbation of the flow in the turbomachine.

In that sense, this project is focused on the investigation of the flow phenomena around the tip blade in a compressor cascade. This study has been performed in the water channel facilities of the "Institut für Luftfahrtantriebe" (ILA) at the Universität Stuttgart. Before the realization of this research, some papers have been already published related to this topic [4, 5], which carried out the investigation with colour ink visualization. Papayannis [6] used a colour visualization of the flow trajectories too. Kuke [7] studied the suitability of the water channel facilities to adapt them for carrying out PTV experiments. Al-Taie [8] undertook the first measurements of the Tip Leakage Flow with the PTV experimental procedure. In further investigations and projects, Schwäble [9] initiated the deeper investigations of the flow characteristics under unstable conditions.

With the realization of this research, this project will try to take another step in the analysis of the TLF phenomena by analysing and comparing the flow behaviour and characteristics under stable and unstable conditions. The instability of the flow phenomena is defined by the Operating Point of the Compressor, and its situation with respects to the Stability Limit. When crossing this Limit, the behaviour of the compressor will turn unstable and the main characteristics of the flow will change. The flow does not behave in the same way as in stable conditions, since it presents some strange phenomena, which are not expected in the normal or general flow performance.

Due to this fact, the first thing to do in this study is centering and laying down the key characteristics of the flow performance in stable operating conditions, so a base can be established and can help to compare other different performance points of the compressor. Then, unstable conditions will be analysed trying to observe which structures previously defined are present this time and which ones not. Moreover, the appearance of different flow structures would lead to different flow phenomena that influence the compressor performance by making worse its operation.

To understand the behaviour of the flow in any kind of operating situation is a powerful tool in the design and research of more efficient and powerful new engines. The better comprehension of all the flow phenomena allows us to focus on the main points where the biggest losses are located.

To investigate the TLF effects, it will be used an optical measuring method: the Particle Tracking Velocimetry, or PTV. The PTV is a measuring technique that uses cameras to track tracer particles in a 3D-space by taking pictures of them. This method not only allows obtaining qualitative data, such as the trajectory or the velocity direction, but also quantitative values of the velocity, acceleration or relative kinetic energy.

By adjusting the position of a rotating plate, the incidence angle of the compressor cascade can be modified, thus the flow can be analysed under different operating point conditions. Moreover, the casing is simulated by the presence of a cover plate on top of the blades, whose distance to them can be adjusted with four holdings. Hence, both the incidence and the tip clearance can be tested in a wide range. Additionally, the flow velocity of the experiment can be modified, depending on the amount of water mass flow that is allowed to enter in the water channel. In this situation, all main parameters that could have important influences in the flow behaviour can be tested. In the present project two different incidence angles, under three different Reynolds number conditions with the same tip clearance, have been studied.

Chapter 2

Theoretical Background

Before the development of the actual project, it is necessary to present the general topics, which cover the movement description of the flow and the importance of the Reynolds number in the PTV experiment, the compressor operation in both stable and unstable operation and the Tip Leackage importance in the compressor instabilities.

2.1 Lagrangian and Eulerian description of the flow

It exists two different ways to describe the movement of the fluid flow. Basically, the Eulerian description observes the properties of the flow in a fix point or location of the entire fluid domain. On the other side, the Lagrangian notation centres the analysis in specific volumes of the flow domain, usually named as control volume. This analysis is focused on the properties and tracking of single particles.

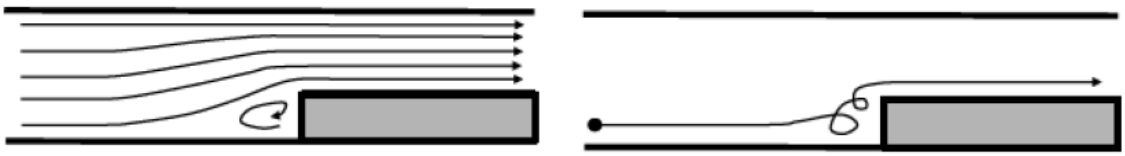

(a) Eulerian Description (b) Lagrangian Description

Figure 2.1: Fluid Flow Description

The general Fluid Mechanics is defined by the Eulerian methodology, which considers the flow as a whole.

The Particle Tracking Velocimetry (PTV) is a methodology that works by means of the image recording of the flow with different cameras, located in different orientations and locations, during a period of time. This type of experimental technique is useful to follow and capture the trajectory of single particles introduced in the flow, allowing the users to observe the different flow patterns. That is the reason why, the PTV is considered a Lagrangian method, since it analyses the trajectory of every particle.

2.2 Viscosity and Reynolds number

A fluid flow element in motion suffers forces from the surroundings, including the viscous stresses, which cause deformations in the fluid. These viscous stresses can be approximated by a viscous stress tensor, denoted by τ. This stress tensor can be scaled with the gradient of the velocity field.

A Newtonian fluid can be defined as a fluid whose viscous stresses are directly proportional to the velocity gradient. This proportionality constant is the Viscosity, that can be expressed in terms of the dynamic, μ in $kg/m \cdot s$, or kinematic viscosity, ν in m^2/s. The kinematic viscosity can be related with the dynamic viscosity by means of the density: $\nu = \mu/\rho$.

The flow motion can be characterized in two different ways. The first one of them is defined by a linear motion of the fluid, generally at low velocities. The second type of movement is a random motion of the fluid, normally present at high velocities. Both different patterns are named Laminar and Turbulent, respectively. The transition between both flow regimes can be determined by the use of the *Re* number, which relates the inertial forces of the flow with respect to the viscous forces (or the friction).

The *Re* number is a parameter that allows determining similarity between different flow conditions. Hence, when keeping the *Re* in a similar range in different experiments, it can be assumed that the flow phenomena in both situations are similar or present the same general characteristics.

$$Re = \frac{\rho u L}{\mu} = \frac{u L}{\nu} \tag{2.1}$$

2.3 Experimental Similarity

One of the most important features when performing an experiment in a laboratory is the similarity between the model and the prototype.

In first place, the model must satisfy the Geometric Similarity. Essentially, the size of the model in all directions must be proportional to the real object, by the same proportionality constant. This fact will ensure that the flow follows the same flow pattern.

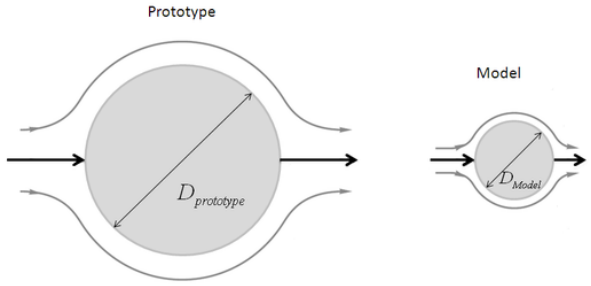

Figure 2.2: Geometric Similarity [10]

Besides, the fluid must present the same pressure distribution all along the surface of both the model and the real body, so both situations represent the same phenomenon. In this case, the Reynolds number similarity ensures this important point. By assuring a Re similarity in both situations, the flow represents the same flow profile in both cases. As previously described, the Reynolds number relates the inertial and the friction forces in the flow, so the Re similarity in an experiment leads to the similarity in pressure gradients around both bodies.

When both similarities are fulfilled, the streamlines and the pressure distribution over the original and the model are similar and they are assumed to represent the same physical phenomena, even when both situations have different geometrical size, velocity field and study fluid.

And third, there is the Mach number, Ma, similarity. Ma is defined as the ratio between the velocity of the flow with respect the speed of sound, a_0.

$$Ma = \frac{u}{a_0} \tag{2.2}$$

The Ma similarity relates the similarity between the model and the real prototype in terms of flow compressibility. It is known that for $Ma \leq 0.3$, the flow can be assumed as incompressible. For higher values, flow is assumed as compressible. But this is only for gases. In the case of a liquid, all liquids are assumed to be incompressible.

2.3.1 Similarity in a Water Channel

To achieve the requirement of Re similarity, the compressor cascade to be analyzed should have the similar size and flow velocity as in a real compressor cascade, if the experiment would be carried out with air. But that fact would lead to air flow velocities of hundreds of m/s under really special pressure and temperature conditions. So, an alternative methodolgy is to carry out the experiment substituting the air by water as a fluid flow.

By performing the analysis with water instead of air in a smaller compressor cascade, the velocities required for the experiment are lower, and hence attainable in a small research facility such a water channel. Therefore, the *Re* similarity could be fulfilled even in such different conditions.

But there is an important issue regarding the use of water: it has higher viscosity than the air. So, no complete Reynolds similarity can be achieved in a water channel. But even in this situation, as the study is focused on the Tip Leakage Flow (a type of Secondary Flow), it can be assumed that the basic structures involved in the secondary flow does not change at higher Reynolds numbers than in the water channel [11].

Furthermore, the water, contrary to the air which is a gas, is a liquid, and by definition, all liquids are incompressible, so even when in a air compressor we can find compressibility effects depending on *Ma*, in the water channel those effects cannot be reproduced. But this consequence has a minimal effect in our study since the compressibility effects are not a keypoint nor object of research in this study.

Hence, the flow used in our study is water and its properties of density, ρ, and dynamic viscosity, μ, have been establisched looking into the literature. It can be observed here that the density of liquid water varies less than a 0.5% between 0-30ºC at ambient pressure conditions [12], so since the experiments have been carried out at that range of temperatures, the density has been assumed constant and equal to 1000 kg/m^3 (value of liquid water density at 4ºC and 1 atm).

Contrary to the density, the dynamic viscosity depends on the temperature and the pressure. For that purpose, and considering that the ambient pressure at every experiment is equal to 1 atm, a correlation from literature has been considered for the dynamic viscosity. This correlation has been taken from [13] and has the following form:

$$\mu[Pa \cdot s] = A \cdot 10^{B/(T-C)} \tag{2.3}$$

where $A = 2.414 \cdot 10^{-5} Pa \cdot s$, $B = 247.8K$ and $C = 140K$ are constants and T is the temperature of the water in K.

2.4 Compressor

2.4.1 General Characteristics

A compressor is a mechanical machine that increases the pressure of a fluid, essentially, by reducing its volume. The type of compressor that is going to be analyzed by means of our experiment is an axial compressor, in which the air flow passes through the machine in axial direction [14].

Basically, an axial compressor is a dynamic rotating machine that compresses the fluid by adding kinetic energy (velocity) to the fluid through the rotor, or rotating unit, and then increasing the potential energy (static pressure) by slowing down the velocity of the fluid in a diffuser, or stator unit [14].

Both the rotor and stator units for axial compressors are designed like a normal fan with airfoils, which are the ones that contribute to the fluid compression. Every set of rotor and stator is defined as one stage, and as a general rule, axial compressors are normally multi-stage, in order to achieve higher overall pressure ratios through the whole machine, since the pressure rise achievable with only one stage is not high enough to reach the actual performance requirements.

2.4.2 Stage Characteristics. Load and Flow Coefficients

To describe the compressor operation, different dimensional and dimensionless parameters are commonly used for that task. These groups are defined in order to describe and settle the main operation characteristics of the turbomachinery. These main parameters are the Load, ψ, and Flow Coefficients, φ.

The Load Coefficient ψ is defined as follows:

$$\psi = \frac{\Delta h}{U^2/2} \tag{2.4}$$

ψ represents the amount of energy available in the fluid. In the particular case of a compressor, it is the energy introduced in the flow for generating a pressure rise.

The Flow Coefficient φ is defined as follows:

$$\varphi = \frac{c_{ax}}{U} \tag{2.5}$$

φ represents the amount of mass flow that passes through the turbomachine.

Besides both of them, another parameters well used for defining the operation of a compressor are the Pressure Ratio and the Mass Flow Parameter. These variables are defined as follows:

$$\pi = \frac{p_{out}}{p_{in}} \tag{2.6}$$

$$\dot{m}_{parameter} = \frac{\dot{m}\sqrt{RT_t}}{p_t A_s} \tag{2.7}$$

Both the Pressure Ratio and the Mass Flow Parameter are related with the Load and Flow Coefficient, respectively, due to the fact that both pairs represent the same physical phenomena. So, at the end it is almost the same to express the Operation of a Compressor in terms of ψ-φ or π-$\dot{m}_{parameter}$. Essentially, the ψ-φ is a generalization of the more extended π-$\dot{m}_{parameter}$ maps.

Finally, the Operation of a Compressor can be represented by means of the Stage Characteristics, a sort of graphical demonstration between the relation of the work and flow parameters. In the other side, the representation of π-$\dot{m}_{parameter}$ gives us what are known as Compressor Maps.

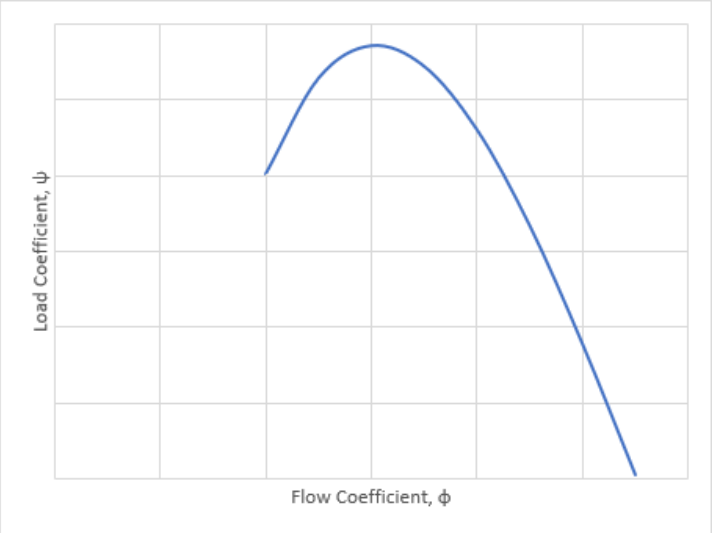

Figure 2.3: Non-Dimensional Compressor Stage Characteristics

The graphical representation of the Stage Characteristics leads to a first conclusion in the operational behaviour: the Load and Flow coefficients are inversely related. For decreasing φ, the ψ increases until reaching a maximum where the stage reaches the maximum pressure rise. From that point, the continuous decrease in φ leads into a abrupt decrease in ψ. When entering this region of operation, the compressor shows an unstable state, heading into the compressor instabilities: stall and surge.

The stable operation, shown in Figure 2.3, is also known as First Characteristic. The unstable regions are called Secondary and Tertiary Characteristics [15] and are representations of the compressor behaviour under unstable conditions.

This graphic representation of both parameters has a huge importance in the analysis of single-stage compressor at a given rotational speed. In practise, not all the Stage Characteristics lines with different constant rotational speeds coincide into a single curve, but their trends are comparable and they are used not only in off-design calculation, but also in design performance predictions [3].

2.4.3 Incidence angle in Stage Characteristics

As described in previous sections, a compressor stage is formed by two parts: a rotor and a stator. Both parts are composed by blades, which have a certain orientation with respect the incoming flow.

The orientation in which are located the blades with respect to the incoming flow is defined by the Incidence Angle, i. This incidence angle is defined as the difference between the Inlet Air Angle, β_1', and the Design Inlet Angle of the Blade, $\beta 1$.

$$i = \beta_1' - \beta_1 \tag{2.8}$$

The β_1 angle is a parameter defined by the cascade design, which is meant to be the angle of the flow in Design Point. β_1 is the angle formed by the Camber Line of the blade in the Leading Edge and the axial direction of the cascade (Figure 4.8).

Depending on the value of the incidence, three different situations can be found in the operation of a compressor cascade. For an incidence of 0^o, the stage is working in Design conditions. If the incidence is positive, the incoming flow enters into the cascade by hitting first the pressure side of the blade. But, if the incidence is negative, the flow would hit first the suction side.

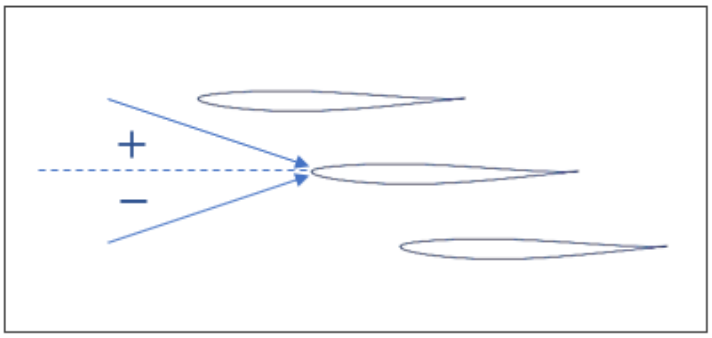

Figure 2.4: Incidence Angle

2.5 Compressor Instabilities

As it has been demonstrated in Section 2.4.2, the operational behaviour of a compressor can be represented by means of the Stage Characteristics (Figure 2.3) as a simplified picture of the compressor performance. Moreover, the performance is also shown with the help of the known as Compressor Maps (Figure 2.5). This kind of graphical representation collects the main operational parameters of the turbomachinery considering the "Stage Stacking", concept regarding the assemble of multiple compressor stages in one single turbomachinery.

In Figure 2.5 a Compressor Map is shown. Here the relation of the Pressure Rise in the compressor is related depending on the Mass Flow Parameter, plotted also over a contour map of the Isentropic Efficiency (dashed elliptical contour lines) and the Rotational Speed Parameter (black curved lines), with the representation of their corresponding trends. Besides, the red line represents the Stability Line, border between the stable and unstable operation of a compressor. The distance between the operational point and this Line is called Stability Margin.

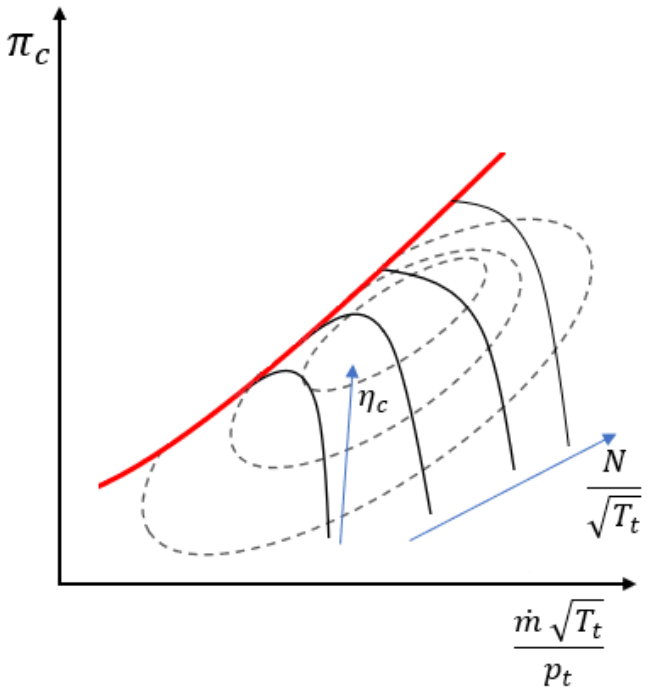

Figure 2.5: Axial Compressor Map

When the operating point of the compressor is located in the unstable region, the behavior of the compressor could be characterized in two different ways: Rotating Stall and Surge. Although the performance of the turbomachinery can be classified in those two general forms, both instability types are very complex and unstable phenomena.

2.5.1 Rotating Stall

Stall is a phenomenon related to the boundary layer separation over the surface of an airfoil: isolated (in the case of an airplace wing or stabilizer) or enclosed (in a turbomachinery). In a turbomachinery, the stall of an airfoil leads to the blockage of the passages in between airfoils due to its growth [15]. Even though the stall of the airfoils does not destabilize the compressor performance, it just reduces the effectiveness of the compression along the turbomachine.

These ”stall cells” have a particular behavior: they propagate around the annulus in circumferential direction, opposite to the blade rotational speed direction, passing from one passage to another. This flow structure is globally stable, but unsteady in time and it is named as ”Rotating Stall” [16]. The velocity of propagation varies depending on the kind of Rotating Stall: Full or Part Span, but it is around 50% of the blade rotational speed [15].

The rotation of the stall cells is caused by the blockage of the stall cells itself. The blockage causes the redirection of the inlet flow towards the adjacent passages. On one side, the flow is happened to have positive incidence. On the other side, the airfoils have negative incidence. This causes the airfoils in the positive incidence side to ”stall”, and the ones in the negative side, to reattach the flow, inducing the rotation of the stall cells.

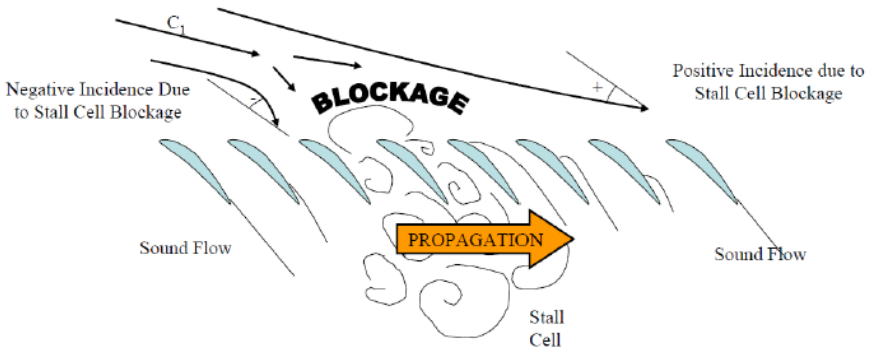

Figure 2.6: Rotating Stall propagation [15]

Once a stall cell is developed, it can extend to the entire blade span. If it covers from tip to hub, it is named as ”Full Span Stall”. But when it covers only part of the blade, it receives the name of ”Part Span Stall”.

The stall condition happens when the operational point of the compressor exceeds the stability line, but it can develope in two different ways. For small reductions of mass flow and hence pressure rise, the operating point movement is small, and it is called ”Progressive Stall”, typical in ”Part Span Stall”. But when the instability causes a huge drop in the pressure ratio and mass flow parameter, the instability is called ”Abrupt Stall”, common in ”Full Span Stall” [15].

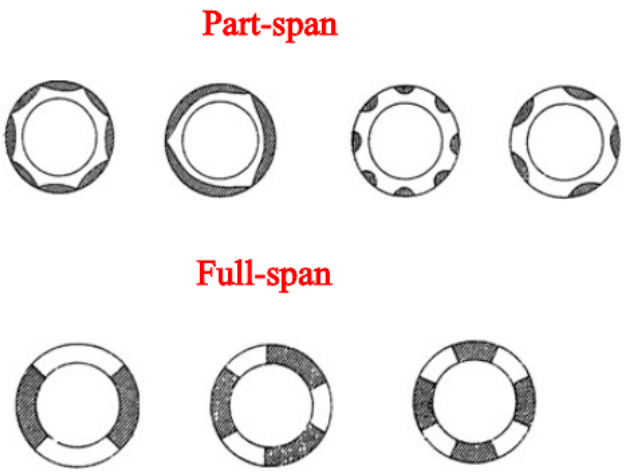

Figure 2.7: Types of Rotating Stall [17]

2.5.2 Surge

When talking about the Surge, it is not assumed as an instability of an isolated compressor, but an instability of the whole system: compressor, valves, pipes, chambers. In this situation, when trespassing the Stability Line, the compressor works with a high pressure ratio and a reduced mass flow.

Under those conditions, the compressor is unable to maintain the working point, so the previously air compressed crosses again the compressor in opposite direction, which can generate in some cases reverse flow. Hot gases coming from the Combustion Chamber can be sucked into the compressor, and they could even exit through the air intake. At this point, the compressor will recover its initial state, once the pressure gradient through the compressor is reduced and it is able to sustain a stable air flow. But, if the conditions that generated the stall remain, the compressor will enter again in surge conditions.

When a compressor is in surge, the compressor moves around a whole new loop, different from the line of the Stage Compressor Characteristics. This loop can have small or large amplitude [15].

A typical Compressor Surge Cycle can be seen in Figure 2.8. The Stage Characteristics (Primary, Secondary and Tertiary) is represented by a blue continuous line and the Surge Line by a dashed red line.

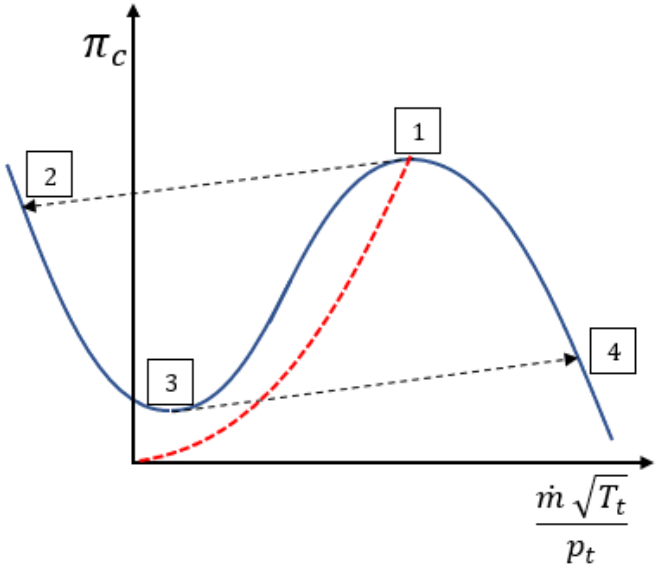

Figure 2.8: Compressor Surge Cycle

When achieving the Surge Line in Point 1, the compressor trespasses the Stability Point and enters in Surge. As it has been previously explained, the compressor is unable to maintain the working point due to the pressure and mass flow conditions, so the previously compressed air comes across the compressor backwards. Reducing the mass flow and the pressure, even being possible to achieve reverse flow (Point 2).

Once the pressure is reduced, the compressor starts to recover its operation and increses the mass flow (Point 3). Since in this point the back pressure at the outlet of the compressor is low, a huge increase in the mass flow can be found, leading to a rapid recovery until it is reached again the Stage Characteristics (Point 4). From this state, the compressor behavior follows the Stage Characteristics, until Point 1 is reached again, and the looped is repeated again.

These huge sudden movements of the flow, charging and discharging the compressor, genererate also abrupt changes in the pressure along the whole system. Then, high levels of vibrations are induced in the components, resulting in high engine wear and even damage, which could even be destructive, in the case of components breaking, due to ingestion and fatal damage in downstream components, such as the Combustion Chamber or the Turbine.

2.6 Secondary Flow

The main goal of this Investigation Study is to better understand the flow phenomena existing around a blade in a compressor cascade. And therefore, one of the targets to look at is the Secondary Flow.

In this group we can include diverse type of flows and pattern, since the definition of Secondary flow is not a closed statement and their natures vary a little bit. But even when the Secondary Flow is not the main part of the main flow in a blade cascade, their effects on it are appreciable and play a huge role in the efficiency of aeroengines or gas turbine power equipments [18]. And since the flow structure is very complicated in a turbomachinery, time-dependent, three-dimensional flow, centrifugal and Coriolis forces, blade interaction, tip clearance, viscosity and turbulence, etc, its understanding has been the center of studies in the recent time, with the objective of improving the efficiency and performance of turbomachinery [18].

Generally, the ”Primary Flow” can be considered to be the flow that follows the preset direction, stablished by the blade design. Therefore, the ”Secondary Flow” could be defined as the result of the interaction between the boundary layer flow and the pressure gradients in a blade [19].

Due to this fact, the Secondary Flow is determined as the main reason of losses in a turbomachinery. In these flows, the kinetic energy is bounded to vortices and cannot be introduced in the main flow and, furthermore, the velocity gradients related to these vortices produce the dissipation of energy. Since this kind of flow has a lower momentum (lower energy), it is also prone to separation [19].

Inside of this group, we can find different types of structures, among which we can find the ”Horseshoe Vortex”, the ”Passage Vortex” and the ”Tip Leakage Vortex”.

2.6.1 Horseshoe Vortex

The Horseshoe Vortex has been studied a lot during the last decades, as a phenomenon that appears around vertical cylinders wih an end-wall, but also in turbomachinery blades [19], as a special case, where instead of a cylinder, there are blades. This Horseshoe Vortex appears in the flow approaching the end-wall boundary layer thickness in the verical cylinder [18].

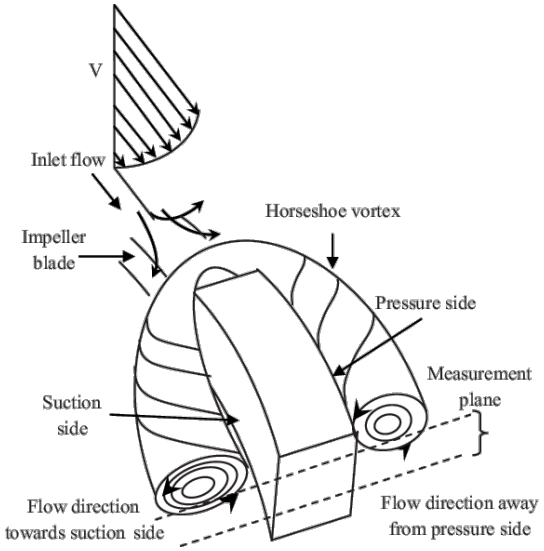

Figure 2.9: Formation of a Horseshoe Vortex pair [20]

In the case of turbomachinery blades, the Horseshoe Vortex develops at the stagnation point in the leading edge, near the end-wall. The boundary layer flow is decelerated at the stagnation point in the leading edge, generating a gradient of static pressure. As a result, a vortex is generated [19]. This vortex generates two different legs, each one in one side of the blade: pressure-side leg and suction-side leg [18].

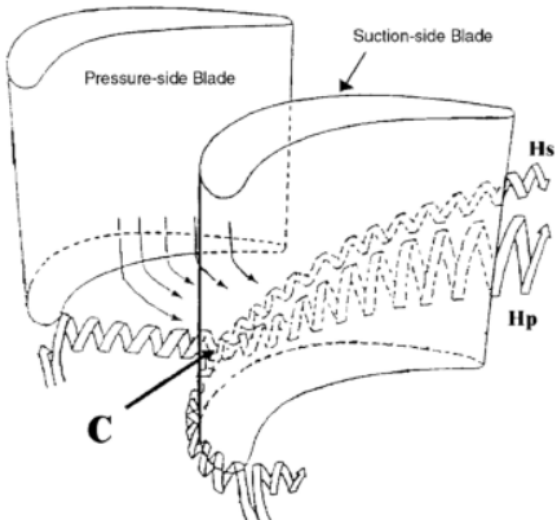

Figure 2.10: Horseshoe Vortex in a blade [21]

In the case of a blade cascade, the pressure leg of the Horseshoe Vortex tends to move towards the suction side of the adjacent blade, due to the pressure gradient existing between pressure and suction side. That causes that the pressure-leg vortex approaches the suction-leg vortex, joining themselves and moving together downstream.

This type of vortices appears also in the Leading Edge Tip Clearance of a blade cascade. In this case, the Horseshoe Vortex is formed by the incoming boundary layer flow from the casing.

As it will be furtherly discuss in the definition of the Tip Leackage Flow and Vortex in Section 2.6.3, the Horseshoe Vortex interacts with the Tip Leakage Flow and, hence, with its Vortex. As the tip leakage vortex is stronger than the Horseshoe Vortex, this last one tends to rotate and move down the tip leakage one along the blade passage. Both vortices rotate in different directions.

2.6.2 Passage Vortex

The Passage Vortex is the result of the interaction of the incoming boundary layer, the boundary layer at the casing and the hub with the existing pressure gradients in radial direction and between pressure and suction side. Due to the low-energy flow existing near the pressure and suction surfaces, the pressure gradient forces the flow to move from the pressure side to the suction side, in both casing and hub end-walls. Both vortices generated near the casing and the hub rotate in opposite directions [18].

2.6.3 Tip Leakage Flow and Vortex Breakdown

The Tip Leakage Flow is produced due to the existence of a tip clearance in the rotor blade row that allow the free rotation of it. As a result of the pressure difference between the pressure and the suction side, a leakage flow is driven across the tip clearance [4]. Despite the tip clearance is small compared to the blade or the surrounding casing, as well as its leakage flow, its effects are of utmost importance on the aerodynamic efficiency of the blade [18]. The losses related to the tip clearance are not only caused by the leaking flow, but also its interaction with the main flow, as well as with the boundary layers [4].

Another effects resulting of the presence of the tip leakage flow that can be found in a compressor cascade are, for instance, the partial blockage of the passages and the interaction with the Passage Vortex and the Horseshoe Vortex. The representation of this last one can be seen in Figure 2.11. The resulting aerodynamic losses present in a compressor cascade are due to the strong level of this interaction. Tackling all the repercussions that the tip clearance has, the leakage flow has adverse impacts in the efficiency and stability of axial compressors [4].

Different levels of clearance and working points of the compressor have different consequences on the leakage flow behavior, and hence, on the general compressor stability. So, a better understanding of these phenomena and their influences on the flow would lead to a reduction in the overall losses in a compressor and, as a result, an optimization of the efficiency and stability perfomance of axial compressors.

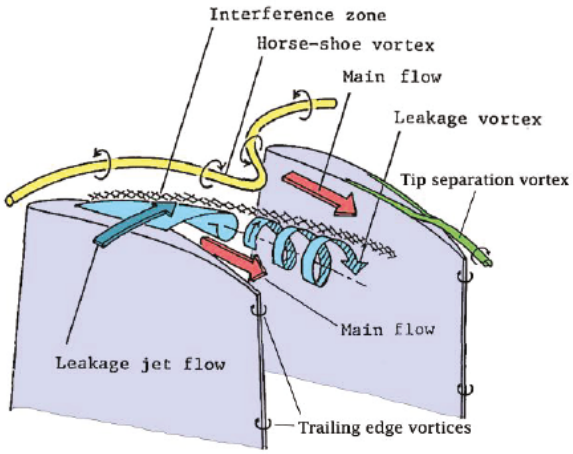

Figure 2.11: Flow Phenomena at the tip region of the blades [22]

The complex phenomena existing around the tip blade near the casing is shown in Figure 2.11. As a result of the pressure gradient between the pressure and suction side of the blade, a leakage flow is driven through the clearance. This leakage flows rolls up into a vortex (Tip Leakage Vortex), interacting with an incoming Horseshoe Vortex. This region is the cause of the main portion of losses [22].

The total magnitude of the tip leakage flow is related to the blade loading. It is acceptable to think that when the blade cascade is working at a higher loading (higher overall pressure rise), the pressure gradient across the clearance would be bigger, and hence, the amount of tip leakage flow.

The unstable behavior of axial compressors has demonstrated the importance of knowing and understanding the processes governing the rotating stall initiation. Two main types of stall inception could be found in literature [23]: ”modal” and ”spike”. However, many axial compressors show a spike stall initiation [23]. And in many cases, the tip leakage flow is the origin of this spike stall onset. This occurs at high blading loading or low flow coefficient.

The explanation that links the tip leakage flow with the blade stall lies in the blockage of the passage caused by the tip leakage flow. As the flow coefficient decreases, the tip leakage flow grows, enlarging its vortex until the tip leakage vortex covers the whole passage, even achieving the hub [24]. Two different criteria were proposed by Vo [24] for the tip leakage blockage:

- Alignment of the incoming flow and tip leakage flow with the leading edge plane.
- Tip leakage backflow from contiguous blade passages at the trailing edge.

The first statement can be seen in the Figure 2.12 by Hoying et al. [25]. Here it can be observed that when reducing the flow coefficient, the tip leakage vortex grows, occuping the entire passage, until the tip leakage vortex is aligned with the plane formed by the leading edge of the blades. In this situation, the passage is blocked, initiating stall.

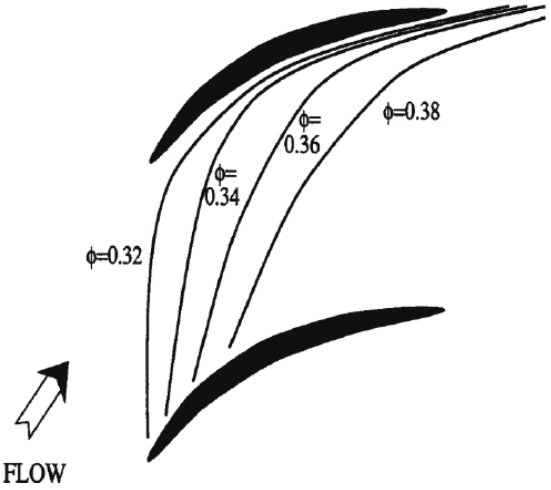

Figure 2.12: Trajectories of the tip clearance vortex for different flow coefficients [25]

At this point, the growth of the tip leakage vortex could have been considered stable, since the structures and the development are the same for different values of the flow coefficient. When stall occurs, the behavior and development of the tip leakage vortex is no more stable. At stall, the flow breakdown develops.

The Vortex Breakdown is a disturbance in the flow, characterized by the formation of an internal stagnation point, followed by reversed flow. There exist two main forms of vortex breakdown that predominate, one is called ”axisymmetric”, or ”bubble-type”, and the other, ”spiral”. The first type is characterized to be shaped like an ”axisymmetric bubble-shaped” structure, like a revolution body. And the ”spiral” one has an helicoidal shape, twisting the flow [26]. Both vortex breakdown types can be seen in the following figures.

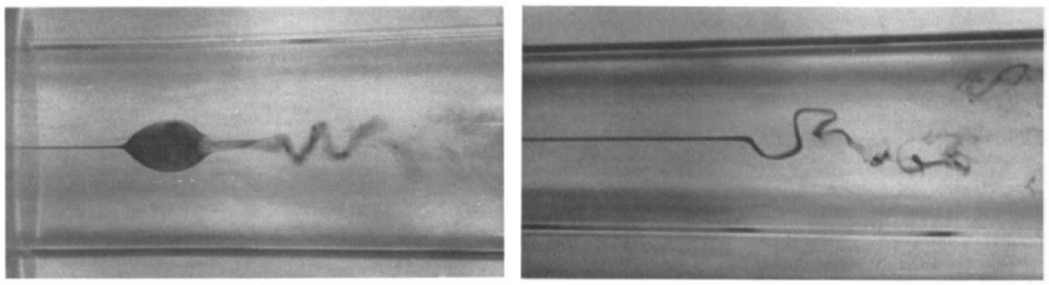

(a) Bubble-type (b) Spiral

Figure 2.13: Vortex Breakdown types [26]

The breakdown of the leakage vortex plays a major role in the initiation of the stall. Furukawa et al. [27] investigated the influence of the vortex breakdown with decreasing mass flow rate. As mass flow rate is reduced, it appears a bubble-type breakdown in the core of the tip leakage vortex, which size grows when reducing the mass flow rate. This bubble forms a recirculation zone in the center of the vortex that acts like a blockage, which together with the fact that in this region the flow is decelerated, the vortex is prone to expand.

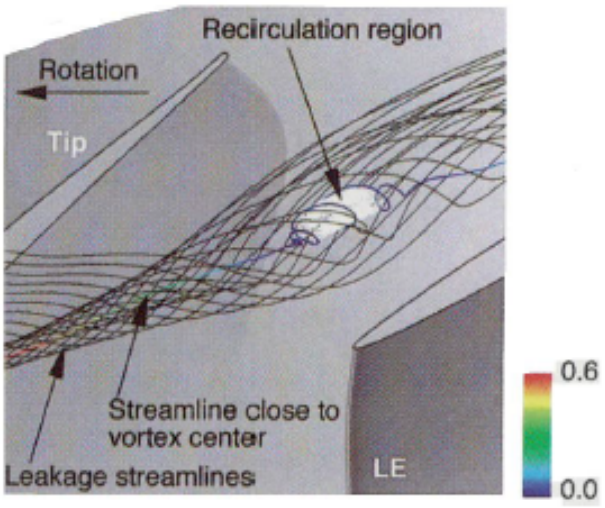

Figure 2.14: Streamlines at tip leakage vortex breakdown [27]

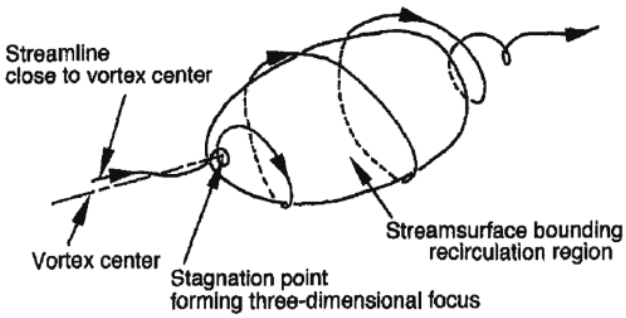

Figure 2.15: Flow topology of vortex breakdown [27]

The main point of this bubble-type vortex breakdown is the existence of an stagnation poing, as well as, large-scale fluctuations [5]. The breakdown of the vortex generates perceptible changes in the vortex structure, being its expansion the main reason for the blockage of the passages, and therefore, the origin of stall.

Chapter 3

Particle Tracking Velocimetry

3.1 Introduction

In every flow experiment, the measurement techniques to be used must have been related with the variable or variables to be measured and, even more important, they must be able to obtain the proper data from the physical phenomena to analyse with the fewest interference as possible.

Usually, the main variable tested in a flow experiment is the velocity: magnitude, direction or both. Knowing the velocity field around a body provides additional information, apart from velocity trends, such as accelerations, pressure field, etc. The velocity is also a key parameter when knowing the regime of a flow, by means of the Reynolds number.

When measuring the velocity in a flow it exists different techniques. One of the most simple ones is the Hot-Wire (or Hot-Plate) Anemometry. Another type of velocity measuring techniques are the optical techniques. In this group they can be find the Particle Image Velocimetry (PIV), the Laser Doppler Anemometry (LDA) and the Particle Tracking Velocimetry (PTV).

The PTV is an optical technique that allows obtaining the trajectories of particles in the flow by taking consecutive pictures over a time period with several cameras at the same time. The PTV allows the tracking of particles in 3D using several cameras and triangulating the position of every particle in the 3D space. The velocity is obtained knowing the space covered by the particle over the time step between consecutive images.

The main aim of the present project is the study of the flow phenomena in a blade cascade with tip clearance. This objective requires the knowledge or determination of the trajectories that the flow follows, so the behaviour of the flow can be studied under the conditions tested. Hence, the method used for studying the flow is the Particle Tracking Anemometry (PTV).

3.1.1 Particle Tracking Velocimetry. Definition and Characteristics

The PTV is a velocimetry methodology for measuring the velocity of particles introduced in a fluid flow. In this technique, the particles are followed and tracked individually, so the physical approach of the PTV is Lagrangian. This approach differs from the one used, for instance, in the PIV, which is an Eulerian method that measures the flow velocity at a complete domain.

The scheme of the PTV can be given in 2D or 3D, depending on the experimental method. The one that is going to be carried out in this project is the 3D-PTV. It is based on the utilization of several cameras, usually between 3-4, to capture the particles trajectories in a three-dimensions control volume, using photogrammetric principles [28].

By means of the images captured with several cameras, it is possible to obtain the spatial coordinates of every particle in every time step by optical triangulation. After knowing the position of all particles in different time steps, the software proceeds to match every particle from every image with its own representation in the following time steps, obtaining trajectories in consecutive time steps with positions in different time steps. This is based on the "nearest neighbour principle" [29]. When ambiguities in the position determination are found, additional criteria is needed, such as "minimum acceleration" along a particle trajectory or "minimum change of acceleration" along such trajectories.

Once the position of every particle all over the time period of measurement is obtained, the velocity and the acceleration of the particles can be determined using the relation between the position and the velocity and acceleration.

Considering that every time step and space displacement is sufficiently small, those relations can be expressed as follows by means of the Central Method [30]:

$$u_i = \frac{1}{2}\frac{x_i(t+\Delta t) - x_i(t-\Delta t)}{\Delta t} \tag{3.1}$$

$$a_i = \frac{1}{2\Delta t^2}\left(x_i(t+\Delta t) - 2x_i(t) + x_i(t-\Delta t)\right) \tag{3.2}$$

The index $i = 1,2,3$ makes reference to the spatial component in the three directions: x, y, z.

3.2 Flow of data

The data processing of the measurements must pass some procedures from the Image Capturing until the final Trajectory Display, before the data could be interpreted. For that reason, the data is treated with different routines. Apart from acquiring the images from the flow and the particles whose trajectories are going to be analysed, some calibration images must be got for calibrating the tracking and position triangulation program.

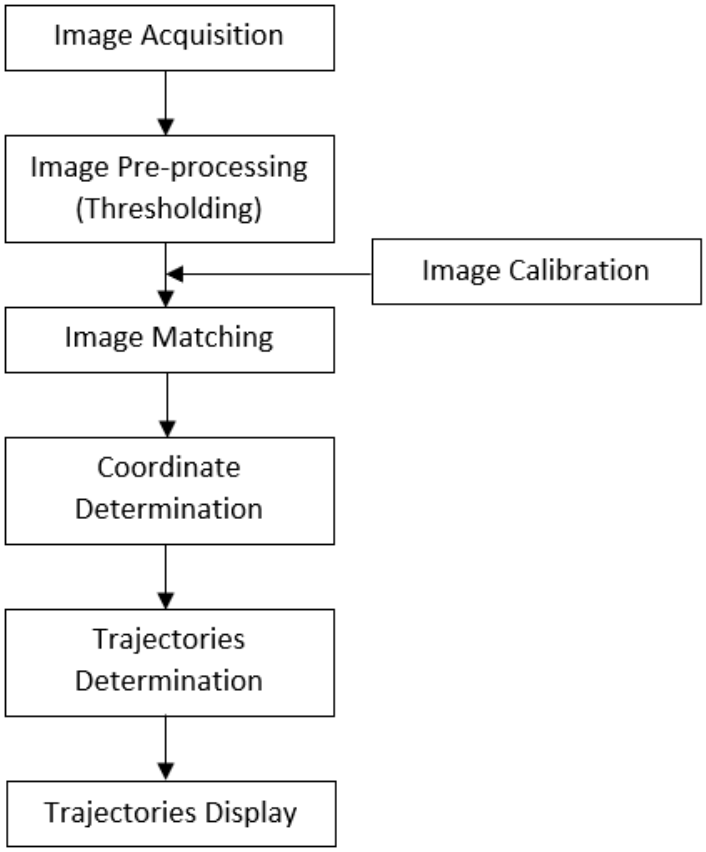

Figure 3.1: Work Flow during the data processing from Image Acquisition to Trajectory Display [8]

The first task to perform to the images is the High Pass Filtering (Thresholding). By filtering the images taken directly from the water channel by means of the cameras set, all the background and reflections are eliminated. When applying the thresholding to the image, it is intended to highlight the particles with respect to the background, so they are easily identified by the following program routines.

Afterwards, the coordinates of every particle in every time step (picture number) are triangulated by finding the same particle in the images of the different cameras for every time step. The procedure for finding the coordinates is performed by means of mathematical methods of photogrammetic principles.

When the coordinates of every particle are known, the next stage of the data processing is computing the different kynematic variables, such as the velocity and acceleration of every trajectory. The velocity allows calculating the Relative Kinetic Energy, which is defined as the square of the ratio between the velocity in one point of the fluid domain and the inlet flow velocity.

3.3 Working Procedure. Software

The working flow diagram displayed in Figure 3.1 is a schematic representation of all the steps carried out during the analysis of the data taken at the water channel. In this section, every stage in Figure 3.1 will be linked with its corresponding processing program in the correct order explaining in detail the purpose and characteristics of every program and step.

- The procedure of every measurement has been initiated by calculating the Reynolds number of tests with a simple Matlab routine.

- Next, it has been proceeded to acquire the images of the flow from the water channel, by means of the ”MovieRam-Recorder Software” installed in the computer of the water channel.

- After obtaining the images, they have to be filtered in order to eliminate the reflections and the surroundings, so the particles are highlighted and the next software (3D-PTV) recognizes them easier. This is made with a Matlab routine called ”*Mittelungsprogram*” (Averaging Program).

- The ”3D-PTV” program takes the images and performs the triangulation of the particles in the images and determines the trajectories, after previous calibration of the domain by calibrating the cameras position and orientation.

- The ”PostProcess.exe” takes the data from ”3D-PTV” and adds several parameters to the data already processed, such as the viscosity, the maximum velocity of the particles and the acquisition frequency.

- With the ”Datenkrake” Matlab routine, all the ”.txt” files produced by ”PostProcess.exe” are merged in a single ”.txt” file with the proper format for the next program, ”Paraview”.

- For the visualization of all the trajectories calculated in previous steps of the processing work flow, it has been used the program ”Paraview”.

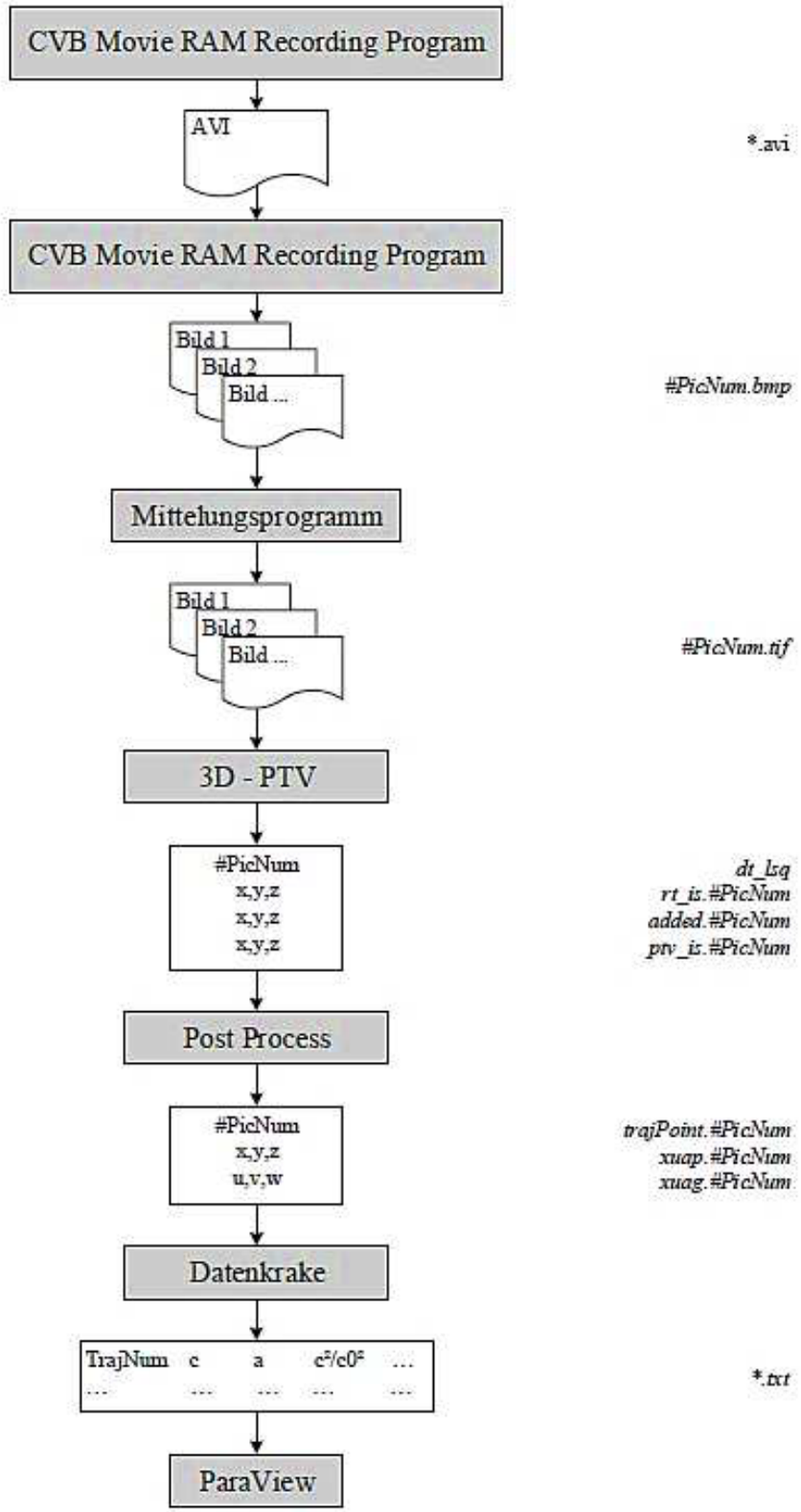

Figure 3.2: Programs utilized in the Work Flow during the data processing [7]

3.3.1 Reynolds number calculation. Matlab routine

The first step in the project when taking measurements from the water channel is getting the Reynolds number of the experiments. Knowing the *Re* allows us to know the flow conditions in which the measurements are being carried out. Calculating the *Re* also helps to the possibility of performing a Reynolds study inside the project, so different *Re* can be tested.

The Reynolds Number is defined as follows:

$$Re = \frac{\rho u L}{\mu} = \frac{uL}{\nu} \tag{3.3}$$

In Section 2.3.1 it has been concluded that the density of the water can be kept as a constant and with a value equal to 1000 kg/m^3 (value of liquid water density at 4ºC and 1 atm). The value of the dynamic viscosity, μ, is given by the Equation 2.3, whose value depends only on the Temperature of the water in *K*. The characteristic length, *L*, of the problem is given by the length of the blade chord, equal to 100mm. And u is given by the value of the flow velocity.

At this point only two parameter must be obtained in order to calculate the *Re*: the water temperature and the flow velocity.

- The Water Temperature is measured in ºC with the utilization of a termometer, whose sensing end is introduced in the water channel in the plenum chamber zone.
- The Flow Velocity is measured in m/s and it is got in an indirect way. From its definition, the velocity is the ration between the space and the time needed to cover that space.

$$u = \frac{s}{t} \tag{3.4}$$

  The measurement of the velocity has been done timing in seconds the time that a ink flow needs to cover a given distance at the entrance of the measurement region, right in front of the blade cascade.

  The distance to be covered has been established by placing a Ruler of 25cm long in the water channel, so when the ink flow crosses the inlet of the measuring zone, crosses first across the ruler, so using a timer, the time and hence the velocity can be guessed.

  For trying to avoid the human error in the time measurements (by the eye perception) at least 5 different measurements of the time are done and then the value taken for the velocity is the average of all of them.

The value of the Reynolds Number is an important parameter when analysing the flow. It represents and shows the characteristics of the pressure flow field in a fluid mechanics problem. So, obtaining correctly the *Re* allows performing identical or very similar experiments of the reality.

3.3.2 MovieRAM-Recorder Software

The image acquisition of the measurements is performed with the MovieRAM-Recorder Software. This software allows the user to record with different setting parameters. Among the most used parameters it can be found the Recorging Frequency, the Number of Pictures and the Exposure Time.

- The Recording frequency, in Hz, is the frequency with which the images are taken. The cameras and the software allow the image recording up to 120Hz. But, when the frequency is higher than 64Hz, the size of the image is reduced from 1024 to 512 pixels in image height. In this study, frequencies of 50 and 60Hz are commonly used. Only for 3 measurements have been used 120 Hz for proving the capabilities of the camera/software system.

- The Number of Pictures defines the number of images that the camera and the software record. Depending on the Recording Frequency, both parameters define the Period of Time that every measurement covers.

  Normally, 200-250 pictures per measurement have been used. In the tests with 120Hz have been used 400-500 pictures due to the reduction of the Period of Time of the measurements.

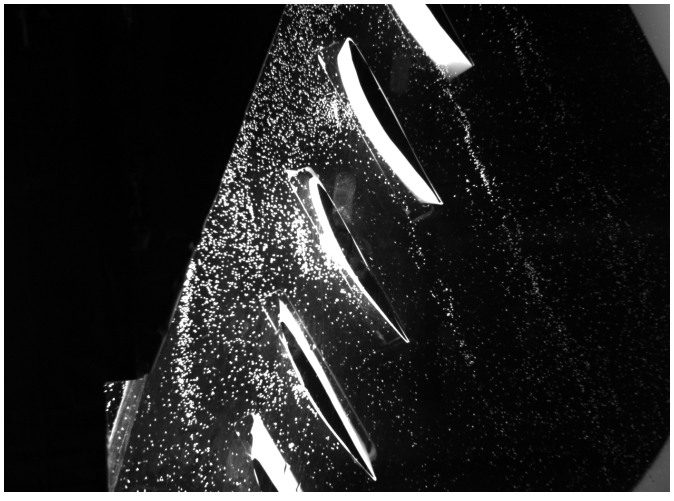

Figure 3.3: Picture of the Image Recording

- The Exposure Time is a parameter that defines the time of exposure of every camera in μs. High values, i.e. 15.000 μs, increase the time of exposure of the camera lenses, so more light is capture by the recording device and the images are brighter. Lower values, i.e. 2.500 μs, decrease the exposure time, less light is got by the camera and the images are darker. A too high value of the Exposure Time can saturate the camera sensors, so the images are shown completely white, but more important, that could lead to damage in the camera cells.

  For normal measurements, the Exposure Time is around 3.000-5.000 μs depending on the camera. But for the acquisiton of the calibration images, monochromatic (green) light is used, so for a better visualization of the calibration plate (Figure 3.4), the Exposure Time must be rised until 15.000 μs, only for this situation.

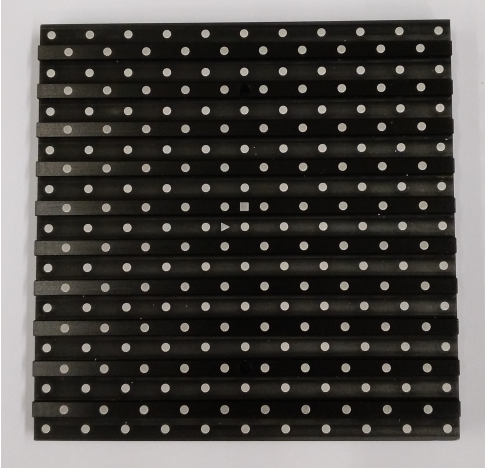

Figure 3.4: Calibration Plate

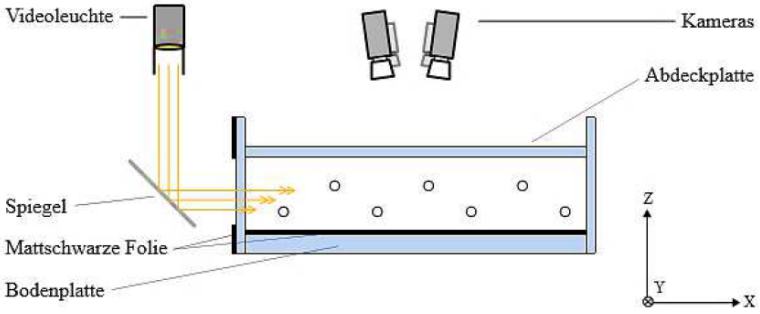

Figure 3.5: Position and Orientation of Cameras [7]

Every camera has its own Hard Disk in which they store the images that they record. Actually, the cameras record an AVI-file video and afterwards, the software also ”breaks” the video into the different BMP-file images, which are the ones that are being used in further stages [8].

3.3.3 Mittelungsprogram. Matlab routine

As already explained at the beginning of this section, the next step in the image processing is to perform a High-Pass Filtering of the images in order to eliminate, mainly, light reflections and to highlight the particles with respect to the background. The main purpose of this part is improving the particle detection effectiveness [8].

Even using some sort of shielding against stray light, unwanted scattered light from the surroundings and reflections in the glass cover surface or due to scratches are present in the images, hence a filtering is needed to eliminate these issues and improve the particle detection in further stages.

All bright spots that do not match with the brightness of the particles, high brightness areas or steady spots and zones are eliminated and blackened from the images by averaging them. The brightness level of every pixel is averaged over all the frames. If the difference of the brightness level of one pixel in one frame and the averaged brightness level of this pixel is zero, the pixel is darkened, and hence, eliminated. Because of this procedure, only moving particles are kept in the images.

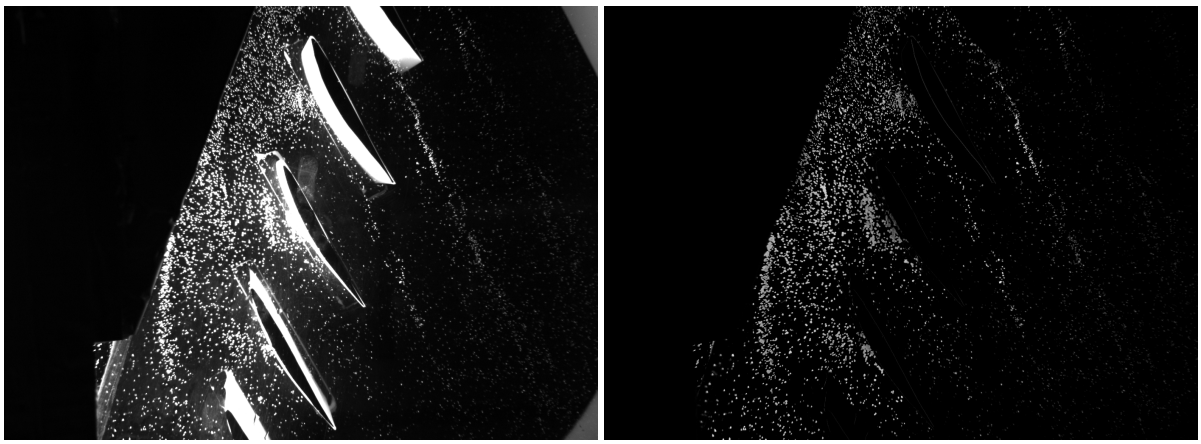

(a) Image Recording (b) After Averaging (Thresholding)

Figure 3.6: Picture from Image Recording. Before and After the Averaging

Not only the images from the particle trajectories must be filtered, but also the images of the calibration plate for the calibration of the tracking program. The images of the calibration plate do not have to be processed with the ”Mittelungsprogram”, because they are static images of the calibration plate and they are only one picture per camera. So, the processing and high-pass filtering must be done manually by means of image editor programs, such as Paint or Irfanview.

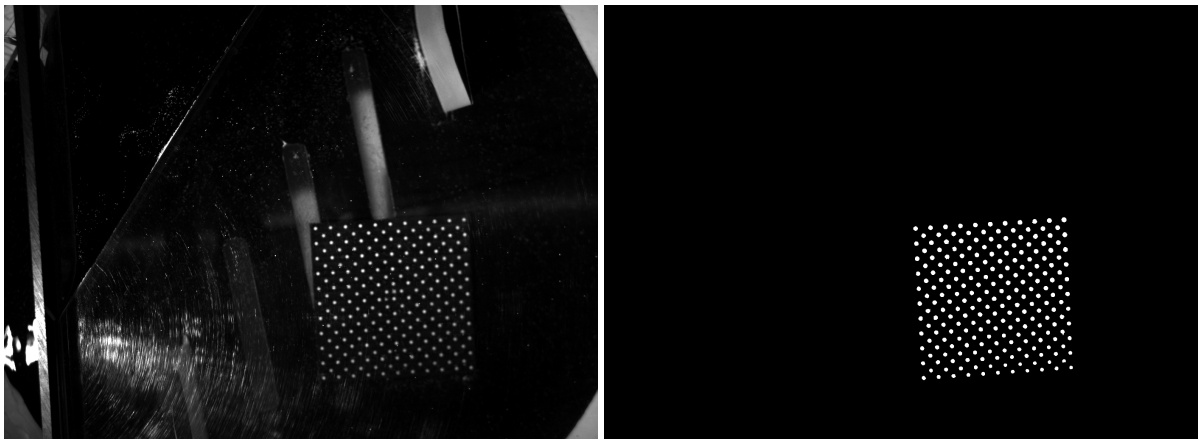

(a) Image Recording (b) After Averaging (Thresholding)

Figure 3.7: Calibration plate. Before and After the Averaging

This stage is also useful for modifying the file format of the images, both the calibration and the particle images. The original format of the images is BMP. So, they must be converted into TIFF. The conversion of the particle images is done in the "Mittelungsprogram" and the conversion of the calibration ones is done with Irfanview, storing the images in TIFF format.

The recent update of the MovieRAM-Recorder Software made necessary an update in the "*Mittelungsprogram*" routine by changing the numbering of the images, adjusting it [9].

3.3.4 3D-PTV

The main part of this study is the matching of the particles trajectories along the different images or frames in which one measurement is made up. This stage is realized with the program "3D-PTV", developed by Hans-Gerd Maas and Beat Lüthi [7, 31], as a Dissertation project. Essentially, the images are first filtered by a grey filter. Subsequently, the particles positions are obtained by triangulation using the same frame from all cameras at the same given time. With the command "Tracking/Show Trajectories" all the particles trajectories can be displayed in 2D for every camera. For evaluating the quality of the tracking, the program shows for every measurement the RMS (Root Mean Squared) and the Standard Deviation, σ_0. Also the ratio Links/Lost can be used as an indicator of the quality of the procedure.

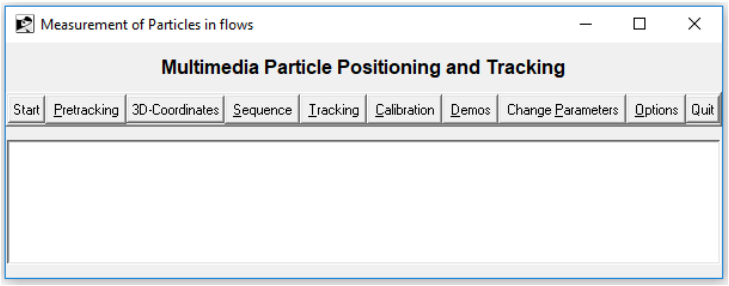

Figure 3.8: 3D-PTV User Interface

3.3.4.1 Operating Procedure

The PTV method used in the program is based on the Algorithm of Basic Photogrammetry of Maas [31], which obtains the three-dimensional coordinates of the flow particles from two-dimensional pictures.

The successful particle detection and its trajectory tracking is determined by different characteristics of the particles used in the experiments. These main characteristics are the neutral-buoyancy of the particles in the fluid, so they follow the flow as a part of it and the reflection properties [31].

The first step is to process the images with a high-pass filter, which allows the program to detect the particles and distinguish them from the background. The software determines the particles coordinates by matching the paticles of every image row, using a the Collinearity Principles and the Epipolar Geometry.

To obtain the particles coordinates in the 3D-space after matching its representations in the different images of every camera, the system must be calibrated. The Calibration process has been perfomed with the placement of a Calibration Plate (Figure 3.4) in the measurement zone. This plate has a specific points distribution, which is introduced in the program. Additionally, the software requires the relative position of the cameras with respect to the calibration plate. A Manual Orientation gives a rough position of the plate and the cameras and the software calculates internally its position. Furthermore, a calibration process can be done after every tracking process, called ”Shaking”. The ”Shaking” calibration uses the calculated position of the particles in the flow to re-calculate and re-orientate the previous position and orientation of the cameras with respect to the calibration plate. This procedure works as a ”Feedback” process.

After successful calibration, the following stage of the procedure is finally calculating the coordinates of the particles and its trajectories. The search of the particles trajectories can be limited to a given space region. The matching of one particle along the different frames can also be configured to determine the zones whether the program must look for the continuity of the trajectories along time.

3.3.4.2 Particle Correspondence

To compute the particle correspondences among the images taken from different cameras, the Collinearity Principles and the Epipolar Geometry are used. The Epipolar Geometry identifies the particles in the different images of all the cameras and the equations of the Collinearity Principle determine the 3D-spatial coordinates of them with the 2D-pictures.

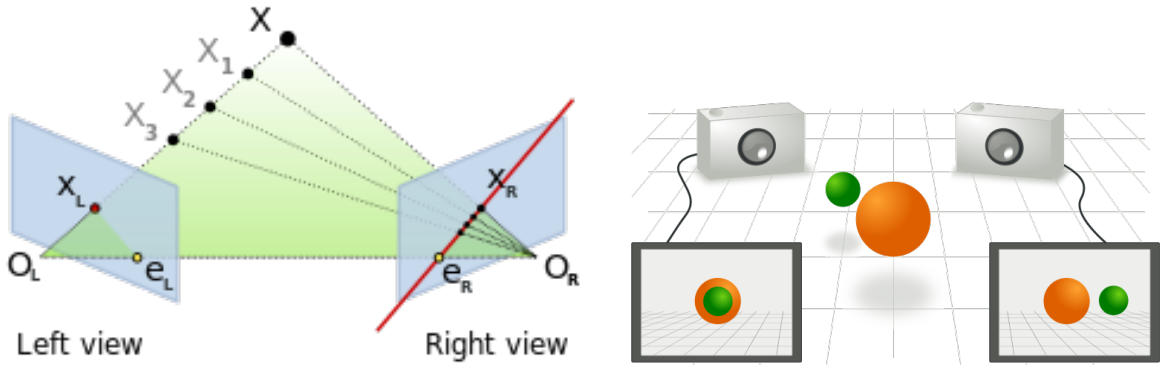

(a) Epipolar Geometry Representation

(b) Epipolar Geometry in Image Acquisiton with Cameras

Figure 3.9: Images for Epipolar Geometry [32]

The mathematical formulation derived for the Epipolar Geometry is based on the assumption that the cameras can be approximated to pinhole camera model. This model consists of the camera aperture being described as a point and no lenses are used to focus the light. Geometric distorsion or blurring of unfocused objects are not considered. The presence of several different mediums is not considered by the pinhole model too.

For instance, in the measurements, the light beams must cross 3 different mediums: air, glass and water. The direction of light propagation changes when crossing different mediums, according to Snell's Law. This change in the refraction characteristics depends on the material properties.

The Snell's Law of Refraction relates the change in the direction of propagation of a wave depending on the media:

$$n_1 \cdot sin\theta_1 = n_2 \cdot sin\theta_2 \tag{3.5}$$

In this particular case the light waves cross 3 mediums in the measurements, so the Snell's Law is extended (Figure 3.10):

$$n_1 \cdot sin\theta_1 = n_2 \cdot sin\theta_2 = n_3 \cdot sin\theta_3 \tag{3.6}$$

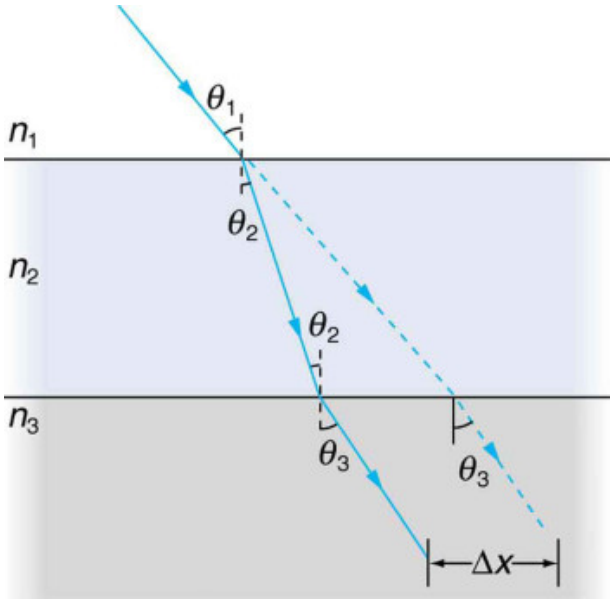

Figure 3.10: Snell's Law of Refraction through 3 different materials [33]

The repercussion of the Snell's Law in the Epipolar Geometry and the Collinear Principles can be seen in the following Figure 3.11 taken from Maas [31]:

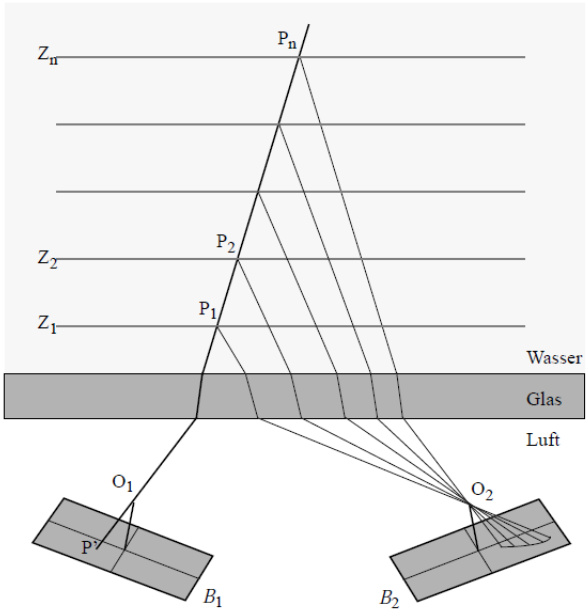

Figure 3.11: Epipolar Geometry for several mediums [31]

The different indexes of refraction of the different material change the direction of propagation of the light wave, as in Figure 3.11, so this eventuality must be taken into account in the matching of the particles.

The determination of the coordinates of a point with a single camera is sometimes hard. Only one camera leads to many ambiguities for one object location. Hence, more than one must be used. Using two cameras with different points of view reduces the number of ambiguities, since the second camera gives another imaging beam. [31]. But even when using two different cameras, the presence of multiple particles at the same time in the same space leads to the possibility of diverse matching possibilities [31]. The solution is the addition of a third, or even a forth camera, which all together work simultaneously, reducing ambiguities and increasing the precision of the tracking [7].

As a result, the utilization of several cameras shows a tolerance width in the matching of particles with the different cameras. This guessing area is called "Epipolar Band", and it is an important parameter in the calibration and tracking of the software. Depending on the number of cameras, the points detected and matched among different pictures of an image row are called Duplets (two cameras), Triplets (three) or Quadruplets (four). The utilization of 4 cameras reduces the number of ambiguities to near-zero [8].

3.3.4.3 Particle Coordinates Calculation

The correspondence of the particles among different images is done by means of the principles of the Epipolar Geometry. But the calculation of the coordinates of the actual detected and matched particles is done with the equations of the Principles of Collinearity. Thus, the knowledge of the Outer and Inner Orientation of the system is of utmost importance.

The Outer Orientation defines the camera position and orientation in the Global System of Reference. For that reason, every camera has 6 defining parameters: 3 defining their position (in X-, Y-, Z-axis) and their orientation (θ, ω, κ) [8].

The coordinates of the point P of the object are given by:

$$P = (X, Y, Z)$$

And the coordinates of the projection center are given by:

$$X_o = (X_o, Y_o, Z_o)$$

These positions must be tranlated into the coordinates of the image, which implies transforming 3D-coordinates (space) into 2D-coordinates (image). This change of System of Reference is done by a Translation and a Rotation. Both changes are controlled by the position (coordinates of projection center) and the orientation (θ, ω, κ angles) of the camera [34]. The matrix of rotation is a 3x3 matrix:

$$R = \begin{Bmatrix} R11 & R12 & R13 \\ R11 & R12 & R13 \\ R11 & R12 & R13 \end{Bmatrix}$$

The Inner Orientation describes the position of the projection center with respect to the image plane. The coordinates of the point P of the object, the coordinates of the projection center and the coordinates of any point in the sensor plane (image) are given below [34]:

$$(x_P, y_P, z_P)$$

$$O = (x_o, y_o, z_o)$$

$$P' = (x, y, z)$$

As a consequence of the projection method, there is the same ratio between $x - x_o$ and $x_o - x_P$, $y - y_o$ and $y_o - y_P$ and $z_o = c$ and $z_P - x_o$. This ratio is denoted as λ [34]. Solving this expressions for λ and applying the translation and the rotation of the camera system and substituting, these expressions lead to two equations known as Collinearity Equations [34, 35]:

$$x - x_o = -c\frac{R_{11}(X - X_o) + R_{21}(Y - Y_o) + R_{31}(Z - Z_o)}{R_{13}(X - X_o) + R_{23}(Y - Y_o) + R_{33}(Z - Z_o)} \tag{3.7}$$

$$y - y_o = -c\frac{R_{12}(X - X_o) + R_{22}(Y - Y_o) + R_{32}(Z - Z_o)}{R_{13}(X - X_o) + R_{23}(Y - Y_o) + R_{33}(Z - Z_o)} \tag{3.8}$$

3.3.4.4 Calibration

Eventually, the parameters needed for the Inner and Outer Calibration are not given, so it is usual to use the calibration of images, in order to get a rough preorientation. For that reason, the Calibration process of the system is of main importance to ensure a high accuracy in the PTV calculations.

The calibration process is done to obtain the main parameters needed for the Inner and Outer Orientations. Furthermore, the calibration takes place in two different stages.

The first stage of the calibration is done with a preorientation which involves the placement of a Calibration Plate (Figure 3.4) in the middle of the measurements zone. Here is performed a photo to the plate with every camera, so the system can state a relation with the image coordinates and the 3D-space coordinates. The Calibration Plate has a predefined grid of point, whose spatial coordinates have been given to the software. Additionally to the calibration recordings, the system needs a first estimation of the Inner and Outer Orientation parameter. A simple measurement of the cameras position and orientations has been proved to be sufficient [7]. These values are displayed in Table 3.1 and 3.2

	X[mm]	**Y[mm]**	**Z[mm]**	ω **[º] (X-axis)**	φ **[º] (Y-axis)**	κ **[º] (Z-axis)**
Cam 1	-45	40	650	-3	-2	0
Cam 2	40	35	650	-2	3	0
Cam 3	-45	-30	650	2	-2	0
Cam 4	40	-40	650	3	2	0

Table 3.1: Outer Orientation. Position and Orientation of every camera

	x_P**[mm]**	y_P**[mm]**	z_P**[mm]**
Cam 1-4	0	0	17

Table 3.2: Inner Orientation. Position of every camera

These initial parameters define the default orientation settings of the cameras. Additionally, the calibration process, perfomed by automatical assignation and manual correction, allows determining the predefined coordinates of every point of the calibration plate grid. Both processes together complete the orientation calibration. After that, a first tracking process can be initiated.

After performing a tracking procedure, further calibrations processes can be carried out in order to refine the orientation parameters and improve the accuracy of the particles coordinates, correspondences and tracking. This fine calibration is referred as "Shaking". In the Shaking Calibration, the data of the measurement series is used. In this case, the data of the detected and matched particles is used as reference points for the orientation.

The main input parameters for the fine calibration are the number of images to use and the Epipolar Band parameter. The Epipolar Band is a parameter that measures the tolerance band of the Epipolar Geometry calculations when finding correspondences among images of the different cameras. It is normal to start with large tolerances, around 0.2 mm, and start reducing it when iterative shaking processes are carried out, until reaching a value as small as possible, for example, equal to 0.1 mm.

The quantification of the accuracy of the tracking and the calibration is done by paying attention to three different parameters. The first of them is the RMS (Root Mean Squared), which is defined as "the standard deviation of all particle distances to their associated epipolars" [8]. The second parameter is the Standard Deviation, σ_0, defined as "the standard deviation of the distances of all identified particles from each other within the image plane" [8]. The third parameter is the Links/Lost ratio that represents the ratio between the particles that are tracked in the measurement volume and the number of particles that are not. A high Links/Lost ratio represents a high quality of the calculations [7].

3.3.4.5 Tracking

The last stage of the 3D-PTV measurements is the tracking of the particles in the control volume, according to the approach of the Lagrangian notation. With the recording of succesive images along a time period, the program is able to follow and track the trajectories of every particle and show them in a display view.

For a good particle trajectories tracking, it is important the relation between the mean distance between particles and the mean displacement of the particles [8]. Ideally, this ratio must be high, so the displacements of the particles are small compared with the distance to each other. A high value in the mean displacements is a sign of chaotic movement of the particles, so the tracking is almost impossible [8]. This situation causes the loss of particles during the tracking, and hence, short trajectories. This is usual in recirculation or vortices regions. A possible solution is the increase of particles density in these areas or the increase in the image acquisition frequency [8].

The algorithm implemented in the 3D-PTV software is the one developed by Maas [31]. These routines have a diverse number of parameter to adjust and calibrate the tracking of the particles. Mainly, three groups of parameters are needed: the Velocity Limit of the particles in the 3 axis (dv_x, dv_y, dv_z), the Limit of the Acceleration ($dacc$) and the angle of the search cone ($angle\ [gon]$).

Every particle has 3 degrees of freedom that correspond to the 3 translation directions (if we do not consider any rotation) [8]. Thus, the motion of every particle must be limited, so the algorithm can distinguish which pixels of different images corresponds to each particle, limiting the maximum displacement possible of every of them.

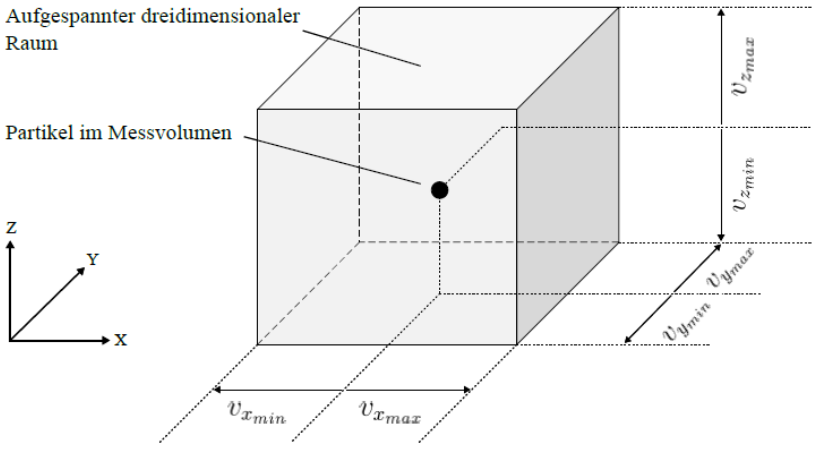

Figure 3.12: Search Control Volume [7]

Depending on the flow regime and the shape of the bodies, the flow can either experience accelerations or decelerations. They suffer changes in both direction and magnitude. This is controlled by the parameter *dacc*, which limitates the Lagrangian Acceleration [8]. Additionally, the *angle* [*gon*] parameter defines the size of the Search Cone in which the program looks for the particle. It can take values between 0º and 360º, depending on flow conditions. Too low values may produce losses in particles information [7].

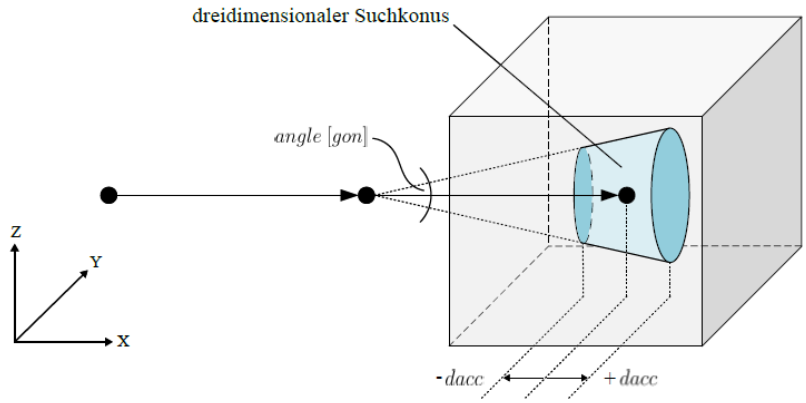

Figure 3.13: Search Cone [7]

All these paramters previously described take the following values in the 3D-PTV program (Figure 3.14):

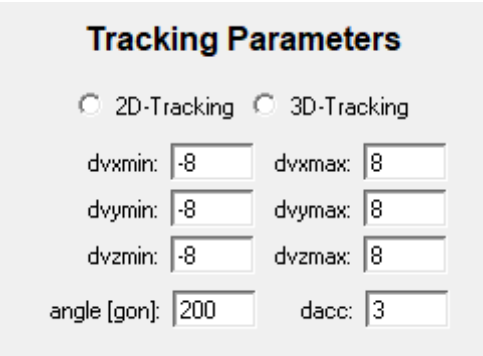

Figure 3.14: 3D-PTV Option Panel. Tracking Parameters

Additionally, other parameters are used in the 3D-PTV program. For example, the Refractive indices, which are needed during the high-pass filtering done by 3D-PTV. This parameter take values between 1-10. The next important group of parameters is all the variables that define the minimum and maximum size of the particles to be detected.

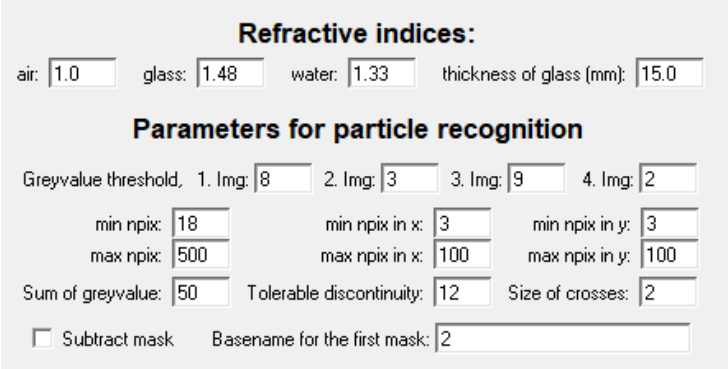

Figure 3.15: 3D-PTV Option Panel. Parameters for Particle Recognition

Finally, it can be also modified the size of the space in which the program looks for the particles to track and to generate the trajectories. This is defined by the parameters in the ”Iluminated Layer Data” set. Here are defined the height of the data analysed (Zmin and Zmax) and the left and right limits of the images, defined by Xmin and Xmax.

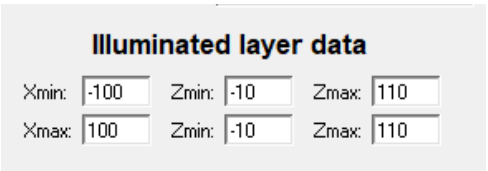

Figure 3.16: 3D-PTV Option Panel. Iluminated Layer

3.3.5 Post Process.exe

After the tracking analysis with 3D-PTV, the data obtained is now processed by the program ”Post Process.exe”. This code includes in the data results from 3D-PTV another different physical properties, such as velocity and accelerations. This new program requires some inputs like the kinematic viscosity of the water and the Recording frequency, in order to perform all its calculations.

3.3.6 Datenkrake. Matlab routine

At this point of the post-process of the results, the data is still stored separated in several individual files which correspond to every single image. With the Matlab routine ”*Datenkrake*”, all these single files, called ”trajPoint” are merged in one unique ”.txt” file. In these files all the information about the particles and the trajectories is saved: spatial coordinates, velocity, acceleration, etc. The program only needs the adjustment of the initial and final name of the images and the flow velocity at the inlet of the measuring zone, before the blade cascade.

The program has been modified to include the representation of the particle distribution above the blade. Additionally, this routine includes the calculation of the Relative Kinetic Energy, obtained with the utilization of the inlet flow velocity [8].

The output of this routine is a ".txt" file in which all results are merged in table structure. This file is configured and organized in order to be loaded in the next processing software, ParaView.

3.3.7 ParaView

The last stage of the data processing is the utilization of the software Paraview. With this program, more than processing the data, it will display all the trajectories in a 3D-environment (Figure 3.17). ParaView is an open source application for interactive visualization for scientific applications [36]. It is used for data analysis and visualization, both qualitative and quantitative.

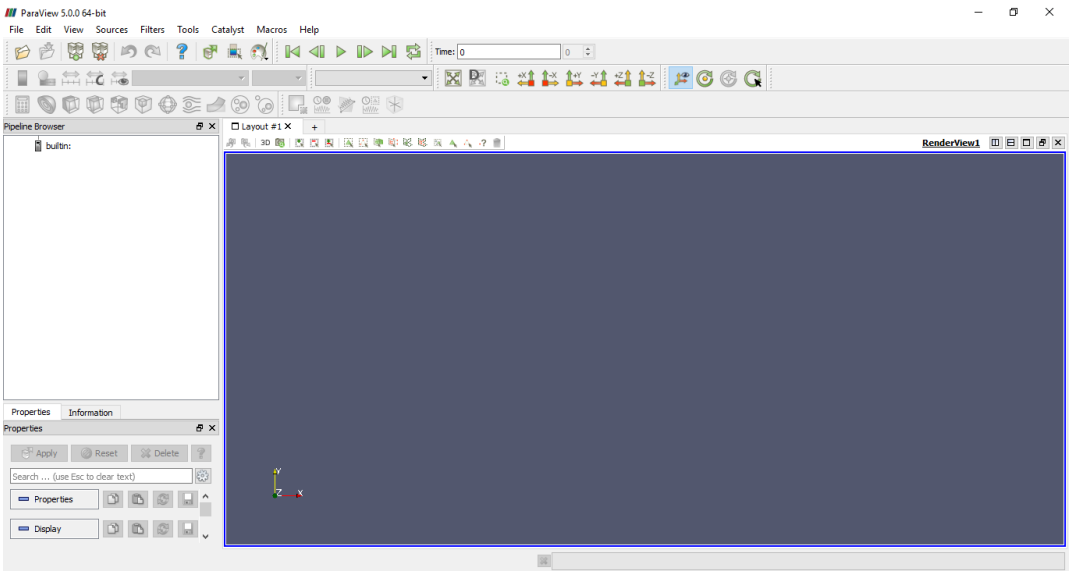

Figure 3.17: ParaView User Interface

All the data processed in the previous programs and rearranged with the Matlab routine "*Datenkrake*" can be loaded directly into ParaView. But before displaying all the trajectories, the ".txt" file must be correctly integrated in the program.

The ".txt" file has a structure of a table, so the first thing to do in ParaView is to load and build that table inside the program. The command "TableToPoints" fulfill this task and assigns the spatials coordinates of the file in the program. Afterwards, the vectorial representation of the trajectories must be obtained and displayed in the command window. For this purpose, the filter "Calculator" is used, which calculates the trajectories of the particles as velocity vectors. The filter "Glyph" finally represents the trajectories in ParaView in the 3D-space.

Once all the data is introduced in ParaView, it is possible now to start the analysis of all the trajectories, the behaviour of the flow and the different flow patterns that exist in the core of the flow in a compressor cascade.

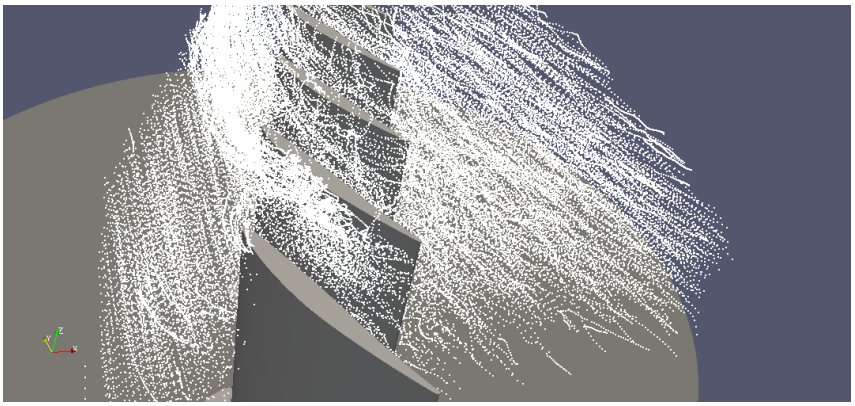

(a) Loading of Data points

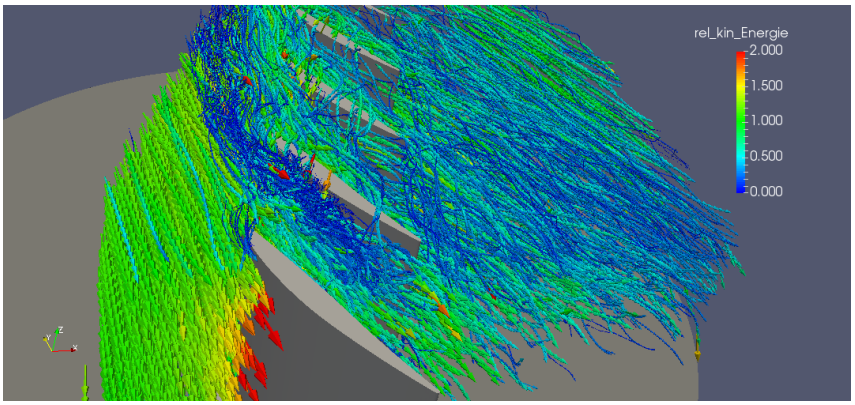

(b) Creation of Flow Trajectories

Figure 3.18: Representation of the particles trajectories in ParaView

Figure 3.18(a) represents the spatial coordinates of all the particles detected during the whole acquisition time of the cameras. After applying the ”Calculator” tool, all the trajectories, consisting of velocity vectors, are obtained. After applying the ”Glyph” tool, the trajectories are displayed, as shown in Figure 3.18(b). This representation of the trajectories is the final result of the data post-process taken from the water channel, which is going to be analysed in order to observe the flow phenomena existing in a compressor blade cascade.

Chapter 4

Experimental Layout. Water Channel

4.1 Water channel Distribution

The realization of the PTV measurements of blade cascade has been carried out in a flat water channel, where a linear cascade is installed. Following, the main characteristics of the water channel are described, as well as the key aspects of the different elements also present in the measurement facilities.

The Study of the flow has been carried out in the facilities of the Institut für Luftfarhtantriebe (ILA) of the Universität Stuttgart (Insitute of Aircraft Propulsion). There are two different water channels in the ILA. The measurements have been done with the Flat Water Channel. The fluid, in this case water, moves in a controlled cycle, in which the blade cascade is located in the measuring zone, which allows the study and analysis of the different flow phenomena.

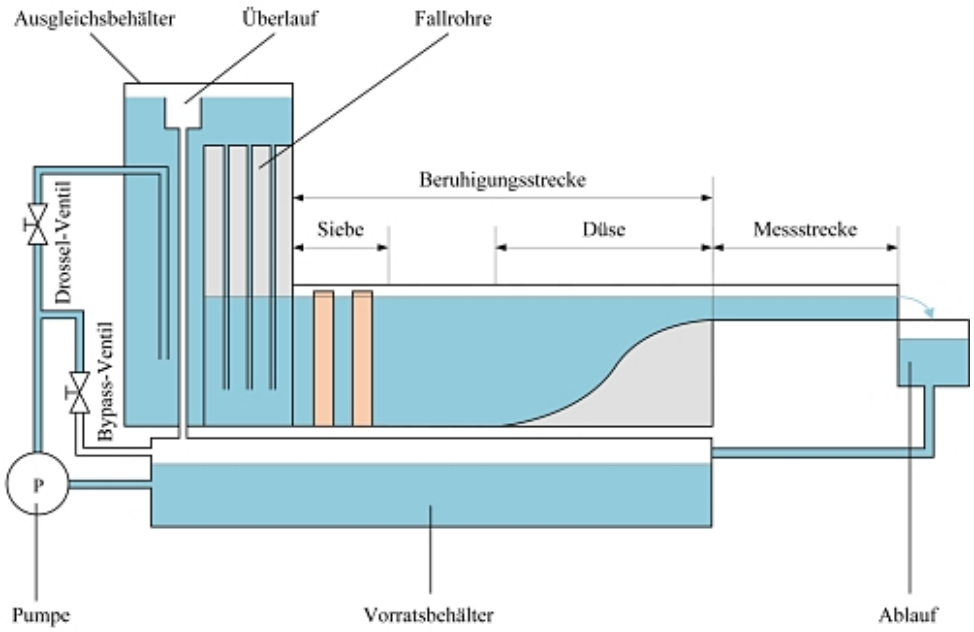

Figure 4.1: Schematic Representation of the Flat Water channel [37]

The general structure of the Flat Water Channel is shown in Figure 4.1. In the Measuring Zone (*Messstrecke*) we can find the object of study in the water channel, the blade cascade in this case. This zone can be observe with Figures 4.2 and 4.3. Above the linear blade cascade, the four cameras used for the image acquisition are located, as shown in Figures 4.9 and 4.10.

The water flow that crosses the Measurements Zone is collected at its end by an Outlet Drainage (*Ablauf*) and redirected to the Main Storage Tanks (*Vorratsbehälter*). Here the water is collected from the Measuring Zone and with the help of a pump (*Pumpe*) the fluid is introduced in the Surge Tank (*Ausgleichsbehälter*). The amount of water provided to the Surge Tank is controlled by two valves: the Throttle (*Drossel-Ventil*) and the Bypass valves (*Bypass-Ventil*). The first one controls the flow of water that enters in the Surge Tank and the second one provides water to the Main Tank after the pump in case the water level in it drops below a minimum level, so the pump is not damaged.

In the Surge Tank there are a sort of Vertical Pipes (*Fallrohre*) that connect it with the Becalming Region (*Beruhigungsstrecke*) of the water channel. The Vertical Pipes control the amount of water flow that enters in this section of the channel and the velocity that reaches the flow in the measruring zone. To reduce the water flow, screws are placed on top of the Vertical Pipes so the flow is limited. In case of overflow, the Surge Tank has an Overflow Pipe (*Überlauf*). If the water level in the Surge Tank is too high, water would flow through this pipe to the Main Tanks.

At the entrance of the Becalming Region, there are some Screens (*Siebe*), so the falling of the water of the Vertical Pipes does not propagates and reaches the Measuring Zone and perturbates the measurements. Right in front of the Measurement Zone a Nozzle (*Düse*) can be found. Here the flow is accelerated and redirected to the measuring zone. When the water flow crosses the Measurement Zone, it reaches the Outlet Drainage, hence the flow cycle is closed.

4.2 Measurement Zone Distribution

The Measurement Zone referred in Figure 4.1 is shown in representation of Figure 4.2. The whole Measurement Zone can be divided in three zones.

- The First one is the inlet section of the flow in the blade cascade. This part is the ending of the Nozzle of the Becalming Region and accelerates and redirects the flow towards the blade cascade.

- The Second region is the linear blade cascade. It is placed on a circular plate which allows its rotation, letting the modification of the incidence angle of the tests. The adjustable walls present in this area are of utmost importance.

When changing the incidence angle, the flow is deflected by the blades, so this adjustable side walls must follow the deflection angle of the flow, thus no unwanted disturbances from downstream are introduced in the linear cascade. On top of the cascade is found the cover plate. It acts as if it was the casing of the compressor rotor. There are adjustable holdings supporting the plate, so the plate can be located at different heights, and hence, different tip clearances can be tested.

- And the Third zone is the end of the measurement zone, where the Weir is located. This Weir is used to control and modify the water level in the measurement zone. It allows adjusting the water level according to the height of the cover plate.

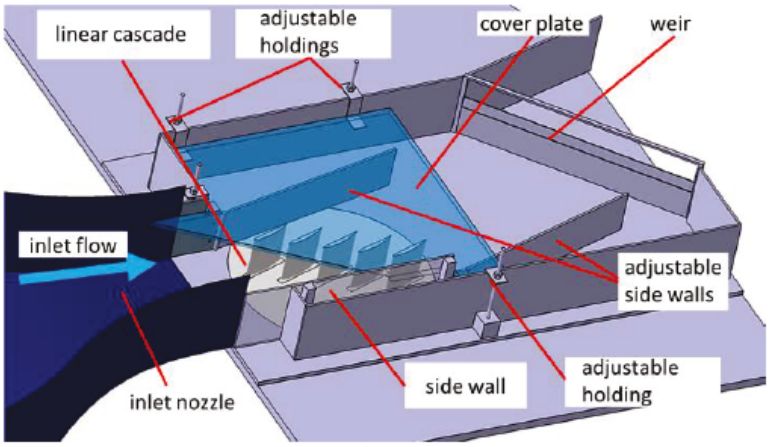

Figure 4.2: Measuring Zone in the Water Channel [4]

Figure 4.3 shows the measurement zone from downstreams. Both the side walls and the adjustable holdings are shown. The inlet nozzle can be observed before the blades. Here the rotating plate in which the blades are mounted can be clearly seen with a black tape. This plate allows the rotation of the blades, hence the modification of the incidence angle. The black tape covering the rotating plate, the tip blade and the top part of the side walls is used to avoid reflections of the light from those surfaces. So, the cameras do not capture them and they increase the contrast between the particles and the background.

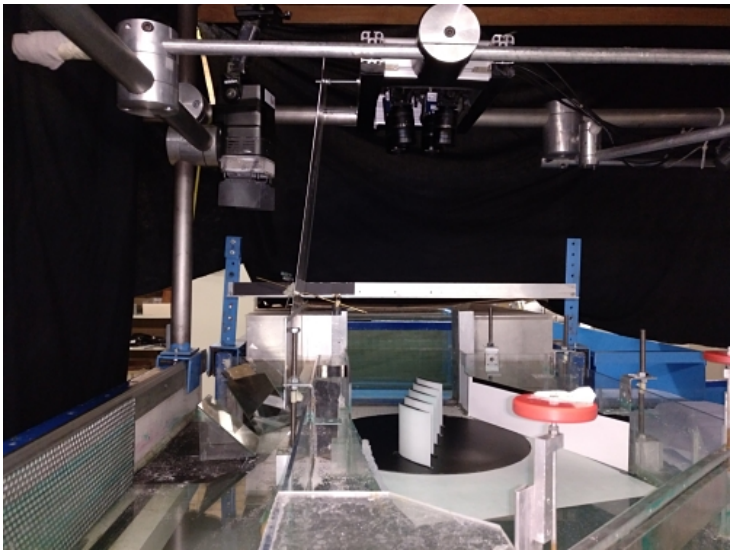

Figure 4.3: Measuring Zone seen from downstreams

At the bottom of the image can be seen the weir. After that weir there is a fall, and then the Outlet Drainage. In this picture, one of the adjustable side walls can be observed at the right part of the image, with similar orientation as the blades. While a finite and linear blade cascade is being tested, in reality, a circular rotor cascade seems to be ”infinity” from the point of view of every blade, since it ”seems” for every blade that there is no side-endings of the cascade. Then, to avoid unwanted perturbations of the measurement facilities, adjusting these walls is important to redirect the flow and minimize the cause of these perturbations.

4.2.1 Blade Design

The blade design utilized for the experiment in the water channel linear cascade is a NACA-65 profile [4]. Its contour is shown in Figure 4.4. This type of profiles is a standard compressor profile, whose chamber line is defined with a single circular arc. The maximum thickness of the chosen profile is 10% of the chord, the leading edge radius is 0.687% of the chord and the trailing edge radius is 0.8% of the chord.

Both the blade chord and height are 100 mm length and the Design Inlet angle of the blade is 55^{o}, parameters included in Table 4.1 with other cascade key parameters.

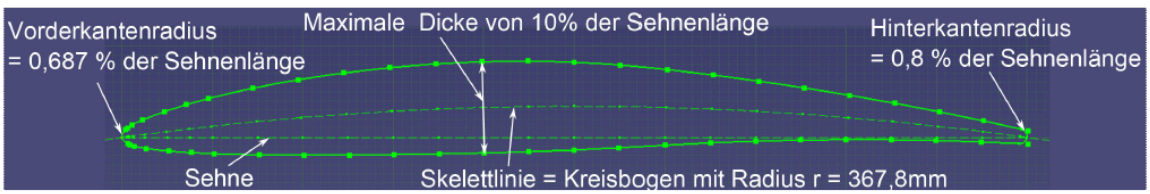

Figure 4.4: NACA-65 profile. Contour [38]

One single blade is shown in Figure 4.5. Not only the blade tip, but also the blade base are covered with black tape. The blades are made with plastic material of colour white, so when light is projected over their surfaces, it is reflected. Both the tip and the base are perpedicular surfaces to the cameras and their light reflections are captured by the cameras, so they must be covered. The side walls are not mandatory to be covered, they scatter the light in other directions, so the cameras do not catch the reflections, or at least not an important amount. As it is described in further chapters, this may have some importance under certain conditions, when these reflections cause disturbances in the visualization of the trajectories.

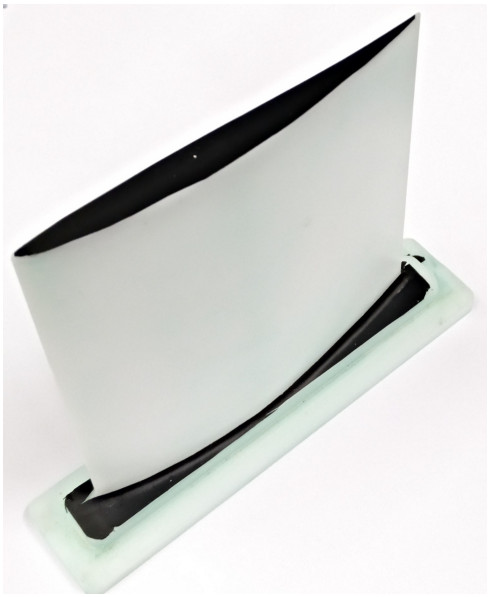

Figure 4.5: NACA-65 profile. Water channel Blade

The design of the cascade is shown in Figure 4.6, taken from Weimer [38]. The key parameters of the cascade design are shown in the image and its values are collected in Table 4.1. The cascade has 5 blades distributed linearly in it.

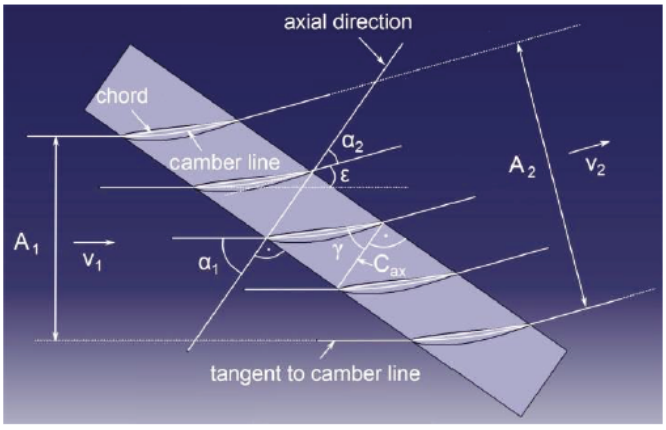

Figure 4.6: Linear Compressor Cascade Design [38]

Design Parameters		
Diffusion Factor	DF	0.45
de Haller Number	dH	0.742
Blade Chord	C	100 mm
Blade Height	h	100 mm
Inlet Angle	α_1	55º
Outlet Angle	α_2	39.37º
Turning Angle	ϵ	15.6º
Stagger Angle	γ	47.19º
Axial Chord	C_{ax}	68 mm
Pitch	S	74.9 mm

Table 4.1: Design Data of the Linear Cascade [4]

4.2.2 Change in Incidence Angle

One of the most important aspects of this study is being able to analyse the cascade behaviour under different operating conditions. This can be achieved by changing the incidence angle of the blade cascade. This has been done by mounting the blades in a rotating plate in the middle of the measurement zone. As explained before, the plate and the blades tip are covered with a black tape to avoid and eliminated light reflections on the cameras.

Figure 4.3 shows the location and distribution of the plate and the blades in the water channel. In Figure 4.7, an isolated representation of the blades and the plate is shown.

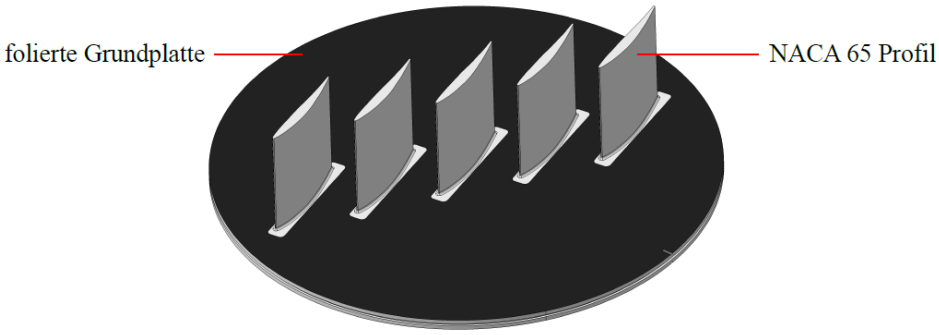

Figure 4.7: Rotating Plate with Blades [7]

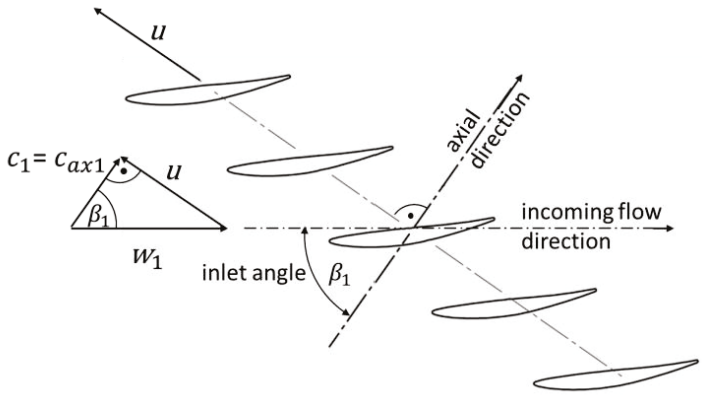

Figure 4.8: Velocity Triangle of the Compressor Cascade [4]

To take into account the rotating frame of reference of the blade cascade, it is assumed a relative velocity of the flow, w, which can be considered as the inlet velocity of the measuring section [4]. This fact requires a rotor blade speed, U. From the velocity triangle of the stage in Figure 4.8 can be deduced the following:

$$tan\beta_1 = \frac{U}{c_{ax}} = \frac{1}{\varphi} \tag{4.1}$$

Considering Off-Design conditions by means of the incidence angle and the Design Inlet Air angle, the Flow Coefficient of the stage can be expressed as follows:

$$\varphi = \frac{1}{tan\,(55^o + i)} \tag{4.2}$$

This leads to the flow coefficient being only a function of the incidence, which is modified in this experiment in the water channel by the turning the rotating plate in the experimental setup [4], instead of considering a rotational speed. This fact allows performing the experiment with a linear cascade.

4.3 Measuring System. Cameras Distribution

The disposition and mounting of the cameras above the measurement zone in the water channel are shown in Figure 4.9 and based on the design of Kuke [7]. The cameras are mounted on a Platform (*Kameraplattform*) above the Measuring Zone (*Messstrecke*).

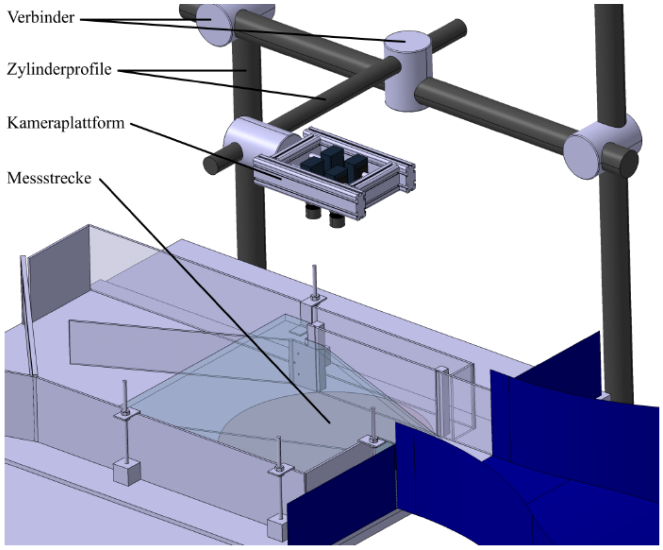

Figure 4.9: Measurement Section with Cameras Platform [7]

All cameras are oriented in different angles to the compressor blade cascade (Figure 4.10), as already noted in the rotation parameter of Table 3.1.

Figure 4.10: Camera Platform

Kuke also introduced the Coordinate System used by the cameras and all the equipments. It is defined by the position of the Calibration Plate in the water channel when performing the calibration. The side edge of the calibration plate must be oriented in flow direction, so flow direction is established in Y-axis direction (Figure 4.11).

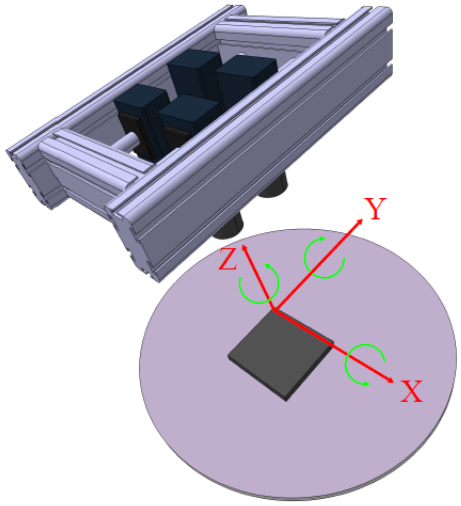

Figure 4.11: Coordinate System [7]

The Center of the Coordinate is defined as the upper left point of the Calibration Plate. This point has been made to coincide with the center of rotation of the Plate where the blades are mounted. Hence, the Blade Plate center of rotation is established as the Center of the Coordinate System of the Measuring Layout.

4.4 Measurement Conditions

In the study of the TLF, there are three main parameters that determine its behaviour: incidence angle, Reynolds Number and Tip Clearance. In this particular project, only two of these variables are studied: the incidence and the *Re*. The Tip Clearance is not object of study in this project.

4.4.1 Modification of Incidence Angle

As it has been explained in previous sections, one of the most important aspects of the study is being able to modify the operating conditions of the blade cascade. This is achieved by changing the incidence angle of the cascade. For that reason, the cascade is mounted in a rotating plate, as explained in Section 4.2.2.

4.4.2 Modification of Reynolds Number

To vary the Reynolds Number, the only way to do it for a given fluid and characteristic length is modifying the flow velocity. Under constant cross-section conditions in the water channel with an incompressible fluid, the way to increase the flow velocity is increasing the mass flow that passes through the water channel. This is achieved by opening more number of Vertical Pipes in the Surge Tank.

Figure 4.12 shows 4 open Pipes. These conditions are given for a low Reynolds Number test. For high Reynolds Number measurements, the number of open Pipes must be increased up to 8 pipes.

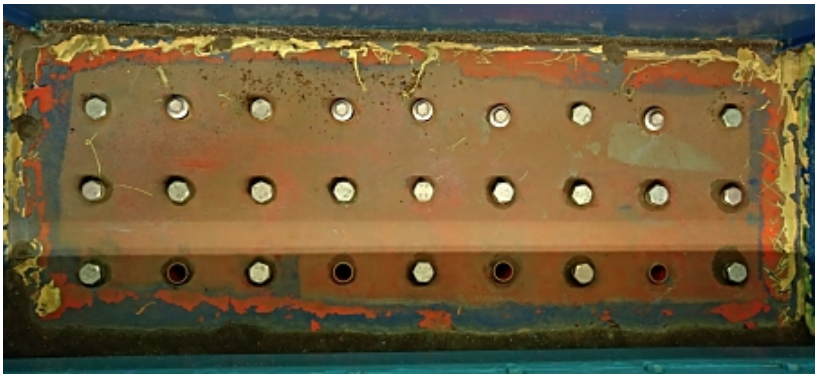

Figure 4.12: Openings of Vertical Pipes in Surge Tank

In order to reduce possible unwanted disturbances in the flow velocity distribution, the disposition of pipes opening must be symmetric with respect the vertical axis of the image. In this way, we try to ensure that roughly the same mass flow is entering in every point in pitchwise direction. The pipes should be opened, as much as possible, in the same row, as Figure 4.12 shows.

4.5 Tracer Particles and Particles Characteristics

In this type of experiments, like PTV, the particle (or tracer particles) characteristics are very important. The key point for the suitability of one type of tracer over another is related with the behaviour of the particle in the fluid and the optical detection characteristics.

First of all, the particles must follow the fluid flow without any kind of slippage or unrealistic movement. For this reason, the particles should be as small and light as possible. Typically, the size of the particles is the range of μm and tenths of mm. In case, the particle density matches the fluid density, it can be spoken of neutral-density properties. That means that the particles does not sink, but the follow the flow without slippage or any influence on the flow behaviour [7].

Additionally, the optical characteristics of the particles must be sufficient for allowing the tracking, when iluminating the measurement volume. The particles should be able to reflect enough light, so they can be distinguished with respect the background, and hence, they can be tracked. Because of this reason, a particle must have a large surface, or large diameter. But, bigger particles tend to slip in the flow. So the particle size is a compromise between visibility and flow performance.

In this study, *Poraver* particles have been used, with a diameter between 250-500 μm and a particle density of $\rho_p = 650\text{-}1000\ \text{kg/m}^3$.

Chapter 5

Flow Analysis

The present report shows and collects the results and conclusions taken from the study done of the flow around a compressor cascade in the flat water channel at the ILA-Universität Stuttgart installations. The study has involved the analysis of different angles of incidence of the flow, changing the Reynolds number, and getting the effects that both parameters have in the behaviour of the flow in a compressor cascade. In the flat water channel, the measurements have been done in a linear compressor cascade formed by 5 blades. The central one is defined as our "study blade", because it is far from the walls, so their effects can be avoided or neglected, and the blade "feels" like it is in an infinite plane. Thus, the results taken from this blade can be extrapolated to a whole compressor rotor, by assuming its behaviour periodical.

The aim of this study is to analyse the flow phenomena around a compressor blade cascade with tip clearance. The flow phenomena changes under different operating conditions that involve different flow coefficients, so this has been considered by measuring the cascade with different angle of incidences, achieving it by means of mounting the linear cascade on a rotating plate [5].

5.1 Measurements Experimental Conditions

For the investigation of the flow phenomena induced by the leakage flow of the blade tip clearance, two different incidence angles have been tested, 10^o and 19^o, under three different Reynolds number conditions each one (low, medium and high). The tip clearance utilized for the measurements has been 4mm, which corresponds to the 4% of the chord length.

The main point is the study and description of the flow phenomena existing in the blade passage, related to the existence of the tip leakage flow. Table 5.1 shows the experimental conditions of the different measurements carried out in the water channel.

Incidence	Reynolds Number	Tip Clearance (%Chord)	Camera Frequency
10º	15.803	4%	50Hz
10º	21.937	4%	50-60Hz
10º	27.422	4%	60Hz
19º	16.590	4%	50Hz
19º	19.065	4%	50-60Hz
19º	30.023	4%	60Hz

Table 5.1: Experimental Conditions of the Measurements in the Water Channel

For every flow conditions, at least 10 different measurements have been performed, which makes a total amount of around 60 data tests. The capture of the images has been performed under different Camera Frequencies (50 and 60Hz), but in all cases the duration of data collection is around 3s.

For the analysis of the data collected from the image recording in the water channel, it has been used a dimensionless parameter, the Relative Kinetic Energy (RKE). Which relates the ratio between the flow velocity in any point of the flow domain, c, with the inlet flow velocity, c_0.

$$RKE = \frac{\frac{1}{2}m \cdot c^2}{\frac{1}{2}m \cdot c_0^2} = \frac{c^2}{c_0^2} \tag{5.1}$$

being m the mass of the tracking particles in the flow.

The usage of the RKE expression is really important in the analysis of the flow. It relates the kinetic energy of the flow in any point of the streamline with respect the kinetic energy of the inlet flow. Thus, it can be analysed the variations in energy of the flow in any part of the flow domain with respect the incoming flow. So, when a region with low RKE is found, it can be deduced that in that zone some kind of energy dissipation is occuring, normal characteristic in recirculation regions.

If considering the Bernoulli's Principle for one streamline, the RKE can be releated to the Pressure Coefficient. From the Bernoulli's Principle, without considering the gravity effects, we get the following expression:

$$p - p_0 = \frac{1}{2}\rho c_0^2 - \frac{1}{2}\rho c^2 = \frac{1}{2}\rho c_0^2 \left(1 - \frac{c^2}{c_0^2}\right) \tag{5.2}$$

$$C_p = \frac{p - p_0}{\frac{1}{2}\rho c_0^2} = 1 - \frac{c^2}{c_0^2} = 1 - RKE \tag{5.3}$$

The Pressure Coefficient is a dimensionless parameter that relates the static pressure change in one point of a streamline with respect the freestream, and the dynamic pressure of the flow in the freestream. In other words, the C_p shows the pressure variations in a flow with respect the incoming free flow. Values higher than 0 represent a rise in the static pressure of the flow. Meanwhile, values lower than 0 mean a decrease in the static pressure.

The second most used parameter in the analysis of the flow is the Absolute Acceleration, in m/s^2. The acceleration relates the rate of change of the velocity over time, both in magnitude and direction. In this case it is used the absolute acceleration, which is obtained as the norm of the three components in the three axis of the vector acceleration. In the analysis, it is given by a single value without sign, so during the observation of the flow, other parameters such as the RKE must be used for guessing if the flow decelarates/accelerates or rotates in one region.

5.2 Incidence Angle: $i = 10^o$. Stable Behaviour

At first, it is being explained the case in which the compressor cascade presents a stable flow structure, which corresponds to i=10º. The utilization of the term "stable" refers to the stability of the flow situation, which does not vary significantly over time, and it keeps stable in space, too.

It must be considered that in design conditions, a compressor should work with an incidence angle of, ideally, around 0º, defined as the incidence in which the incoming flow direction is tangent to the blade camber line. So, an angle of i=10º is a high incidence to be assumed. This situation can be expected as realistic if the compressor works at a low flow coefficient operating point, for instance, it could be reasonable at the engine starting or take-off [16]. At that stage (take-off), an aircraft has a lower velocity that cruise, so the mass flow in the engine is lower than in design. Moreover, the thrust requirements are higher in this point, so the engine is delivering maximum thrust with low air mass flow. These conditions translated into the compressor operation mean a high loading coefficient and a low flow coefficient.

This combination is found normally with a high incidence, in which the need of higher flow deflections, give low flow coefficients [3]. Thus, a compressor cascade working with i=10º can be considered as working in a high loading setup inside the stability region.

5.2.1 General Flow Characteristics

Following, we can observe the flow inside a passage of our compressor cascade in the following images. Those pictures correspond to two different views of the channel. The first ones seen from top of the blade cascade and the others, from downstream.

Figures 5.1 and 5.3 show the RKE in the passage from the top and show the flow at around 50% of blade height (which corresponds to 50mm from the hub) to ignore, by the moment, the effects of the TLF. The view of the flow at 50% of the blade height has been made by performing a ”Slide” in ParaView and eliminating the trajectories that were above a certain value of blade height.

It can be observed that the flow follows the path guided by the blades in a smooth way, without suffering any radical change of direction inside the passage. The flow enters the passage with a value of RKE that varies slightly around 1 (which means flow velocity equal to inlet flow velocity). Near the suction side of the blade, an acceleration of the flow can be observed, where values closer to an orange colour in the RKE scale show a slight increase of the velocity in that region. But apart from that local spot, the rest of the flow initiates a slow deceleration through the passage. In Figure 5.1, the flow seems to slow down its velocity from the inlet flow velocity (i.e. RKE=1) until values near to RKE=0.75. This fact means a diffusion of the kinetic energy of the flow, in benefit of the pressure.

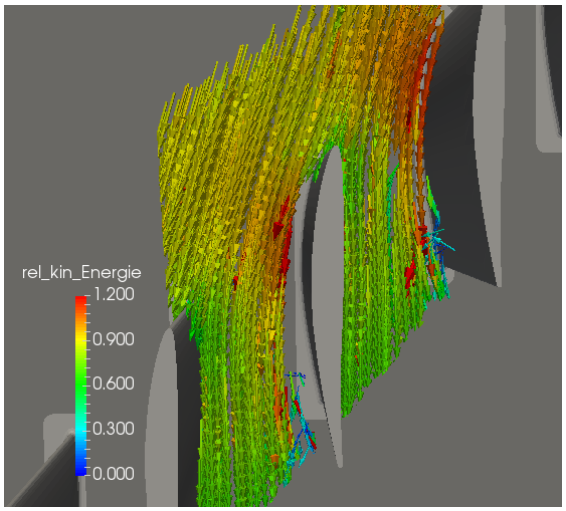

Figure 5.1: Relative Kinetic Energy of the flow around the centre blade. View from top. Cut at 50% blade height (i=10º, Re=21.937, h=4%)

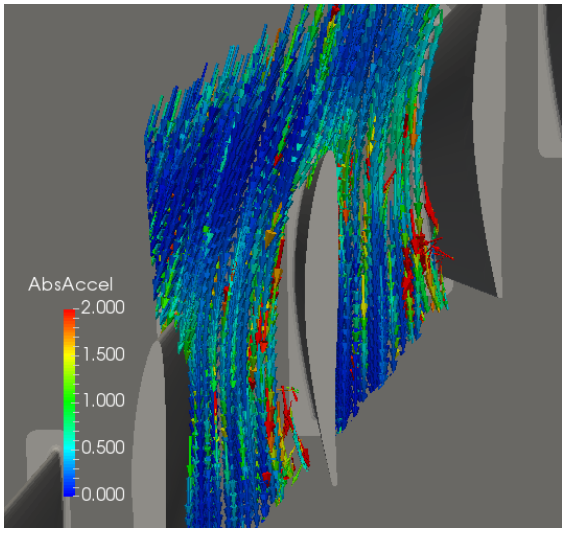

Figure 5.2: Absolute Acceleration in m/s^2 of the flow around the centre blade. View from top. Cut at 50% blade height (i=10º, Re=21.937, h=4%)

Figure 5.3 shows the same phenomena for a higher *Re*. In this case, the values of the RKE appear to be a little bit smaller than in Figure 5.1, but the uniform deceleration and the increased velocity spot in the suction side of the passage can be observed too.

Another important characteristic observed in the images of the RKE is the presence of flow detachment in the surface of the blade. In Figure 5.3, it exists a region near the TE of the blade that shows low values of RKE (and, hence, velocity), lower than 0.4. Observing Figures 5.3 and 5.4 together near the TE, the Absolute Acceleration representation of the flow shows higher values in that part. These high values of acceleration are due to the recirculation of the detachment and the rotation of the flow in it.

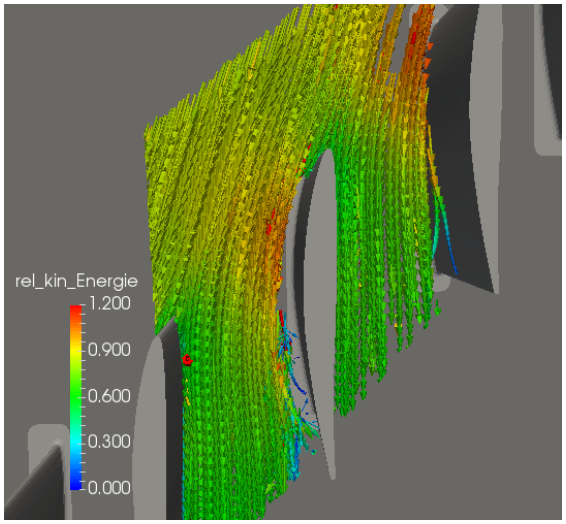

Figure 5.3: Relative Kinetic Energy of the flow around the centre blade. View from top. Cut at 50% blade height (i=10º, Re=27.422, h=4%)

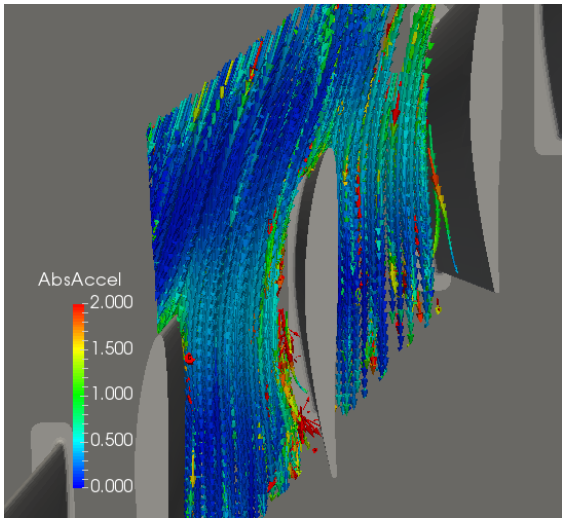

Figure 5.4: Absolute Acceleration in m/s^2 of the flow around the centre blade. View from top. Cut at 50% blade height (i=10º, Re=27.422, h=4%)

The trajectories coloured with the Absolute Acceleration of the flow in the blade passage are shown for the same conditions, as the RKE ones, in Figures 5.2 and 5.4, which correspond to Figures 5.1 and 5.3, respectively. Dark blue colours represent low or near-zero values for the acceleration. With light-blue colour is defined a region at the beginning of the passage with accelerations around 0.5 m/s^2. When comparing the figures of absolute acceleration with the RKE ones, this zone corresponds to the area of increased velocity near the blade suction side and with the mid-part of the passage, where the deceleration of the flow velocity occurs. Besides, in this part, the flow enters to the passage, so the trajectories seem to make a curve when adapting to the blade shape. The flow enters the channel and must adapt to the designed path, hence the higher values of acceleration correspond to the modification in the direction, too. Another areas of interest are the red colour trajectories. These points have high acceleration, near 2 m/s^2. Those values are due to flow detachment.

From these graphical representations of the flow in the blade cascade, it can be seen one last feature. When paying attention to Figures 5.1, 5.2, 5.3 and 5.4, it can be noted a sort of a space near the blade suction side surface where no trajectories are found. This ”gap” near the surface appears in all the representations of the measurements. This space might be caused because of a detachement of the flow, so no particles that could be tracked enter in that recirculation zone, or by some kind of measurement errors. After checking and overlapping different measurements of the same conditions and observing the images directly taken from the cameras (like Figure 3.3), this last hypothesis is confirmed. The orientation of the cameras makes them capture too much light reflected from the side surfaces of the blades. This causes that when a particle is crossing near that region, the blade surface reflections ”hide” the particle, so the tracking software ”loses” it. Due to the cameras position, this fact is crutial near the surface of the blade, so few particles trajectories appear there.

The next group of images corresponds to the trajectories of the general flow from downstream. Here, two subsets of figures are displayed for different Re. The only difference between the two sets is a filtering of the trajectories with respect to the Relative Kinetic Energy. The cut has been performed at 0.30, which corresponds to a flow velocity lower than 55% of the inlet flow velocity. Both sets of images represent the same idea: the detachments or recirculation zone of the flow in the passage. The easiest way to observe it is with the visualization of the velocity, or in this case the RKE, in the regions with low velocity or near-zero.

In the first set (Figures 5.5 and 5.6) it can be seen the difference between the low and mid-RKE (and velocity) regions inside the passage. In both figures, it can be seen the top region of the passage where the TLFV develops, with blue colours. Which can be seen too in the blade on the suction side, near the TE, corresponding to the detachment flow already seen in Figures 5.1-5.4. With both pictures can be demonstrated an important feature of the blade cascade in the water channel: the periodicity in the flow behaviour. This can be observed with the repetition of the flow structures from one passage to the other (Figure 5.6).

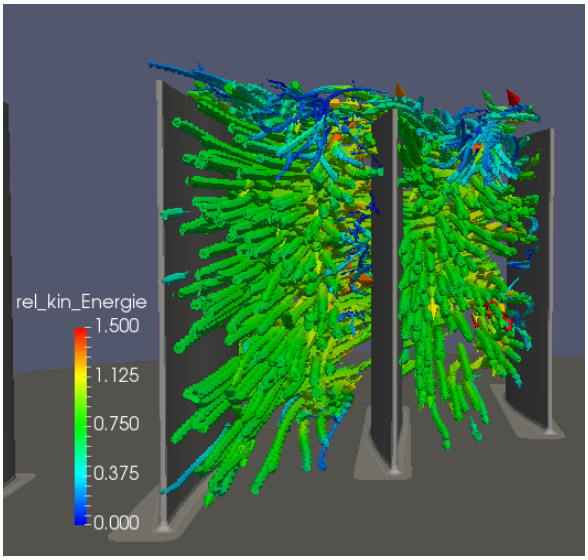

Figure 5.5: Relative Kinetic Energy of the flow around the centre blade. View from downstream (i=10º, Re=21.937, h=4%)

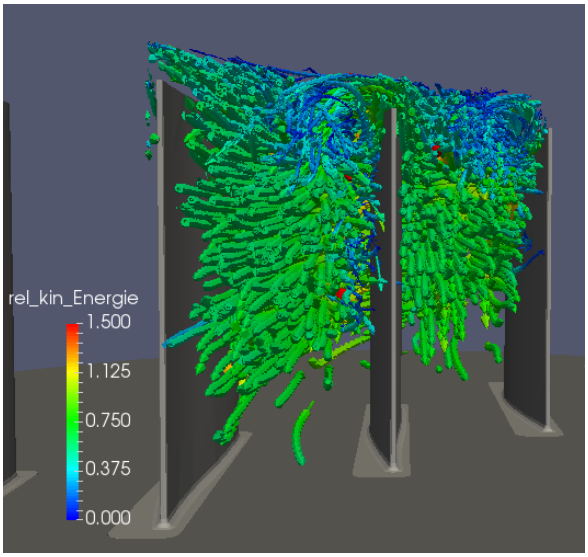

Figure 5.6: Relative Kinetic Energy of the flow around the centre blade. View from downstream (i=10º, Re=27.422, h=4%)

The development of the TLFV and its rotation is perceived in Figure 5.6. The dimensions of the vortex can be guessed by the difference in RKE/velocity between the passage main flow (RKE=0.7) and TLFV (RKE=0.35). This loss in velocity between both flow structures is motivated by the viscous losses as a result of the velocity gradient between the two flow streams, which induce a turbulent dissipation of energy, and hence, velocity. Even when Figures 5.5 and 5.6 have different flow conditions they show the same general flow characteristics. Despite of different *Re*, they have similar RKE, with the high *Re* measurement being slightly smaller.

Following, images of the acceleration are displayed (Figures 5.7 and 5.8). These images represent the same flow conditions as in Figures 5.5 and 5.6, respectively.

Both acceleration images present a low acceleration region at the pressure side of the passage. This region corresponds to the zone where the main flow remains undisturbed by the presence of the TLFV and/or the flow detachment on the blade surface. But if we focus our attention now on the suction side of the passage, we find zones with higher accelerations.

In Figure 5.8 can be seen the difference of acceleration values of the vortex with respect to the surroundings. In this zone, these high acceleration values don't correspond to a high increase of velocity, since it has been proved in previous images (Figure 5.6) that this area has low velocities. So, this higher acceleration is due to high decelerations of the flow, mainly because of the velocity gradients between main flow and TLF, and the energy viscous dissipation. But, since the flow is rotating in the vortex, these values of the accelerations also correspond to a high centripetal acceleration of the vortex, motivated by this rotation.

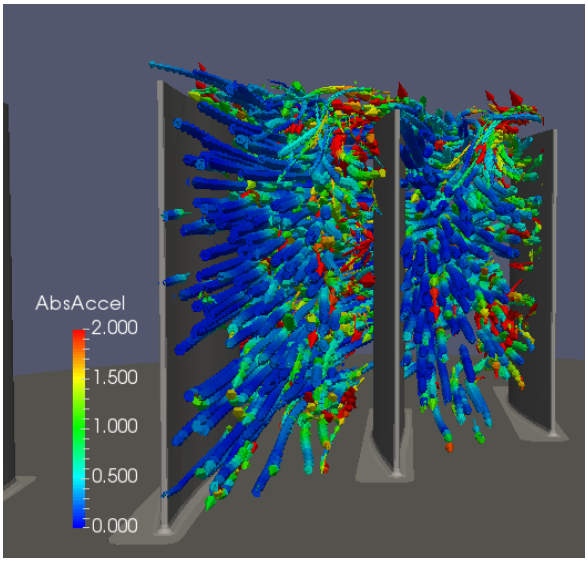

Figure 5.7: Absolute Acceleration in m/s^2 of the flow around the centre blade. View from downstream (i=10º, Re=21.937, h=4%)

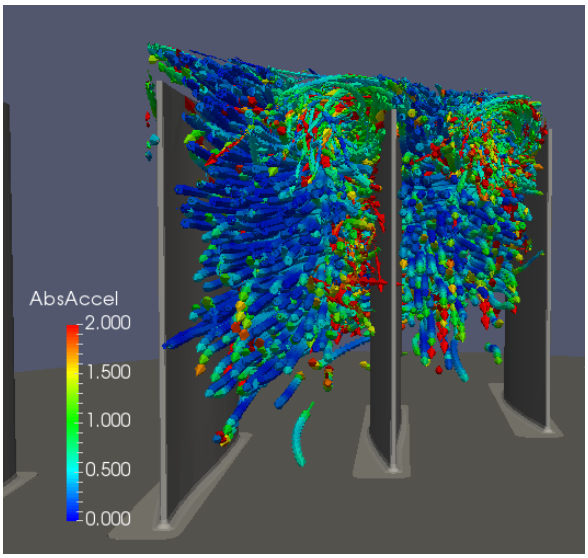

Figure 5.8: Absolute Acceleration in m/s^2 of the flow around the centre blade. View from downstream (i=10º, Re=27.422, h=4%)

One special feature that has been observed in both images is the periodicity of the flow. This has been already pointed out when observing Figure 5.6. It is an importante characteristics to be observed in the analysis of the data. It guarantees that the phenomena observed in one passage/blade can be extrapolated to the rest of passages/blades. Then, the simplification of one blades rotor into a finite linear cascade, when analysing its flow behaviour, is consistent with the real experience, so all the results obtained in the water channel can be assumed that reproduce the same phenomena than a real rotor.

The second set of images (Figure 5.9 and 5.10) just filters part of the trajectories with respect the RKE, leaving the low velocity trajectories. In this pictures, two parts of the flow are distinguished: Boundary Layer Flow and Detached Flow.

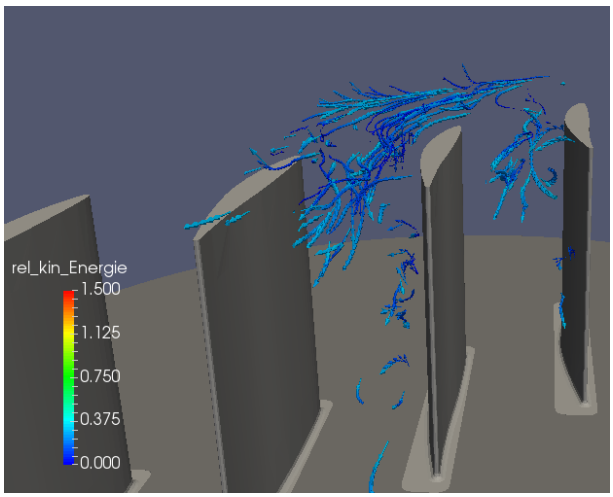

Figure 5.9: Relative Kinetic Energy of the flow around the centre blade. Filtering at RKE lowers than 0.3. View from downstream (i=10º, Re=21.937, h=4%)

As seen in Figure 5.9, the lowest velocities are found in the top of the image, near the tip region of the passage, and close to the TE at the blade suction side. The first ones correspond to the Boundary Layer Flow (BLF). There is also another region of low velocity, which is close to the suction side at the Trailing Edge (TE) of the center blade. These trajectories are the result of the detachment of the flow in the blade surface, due to the increased incidence angle of the cascade. So, even when both types of trajectories have the same range of velocities, they are pretty different. Both they origins and characteristics are completely different.

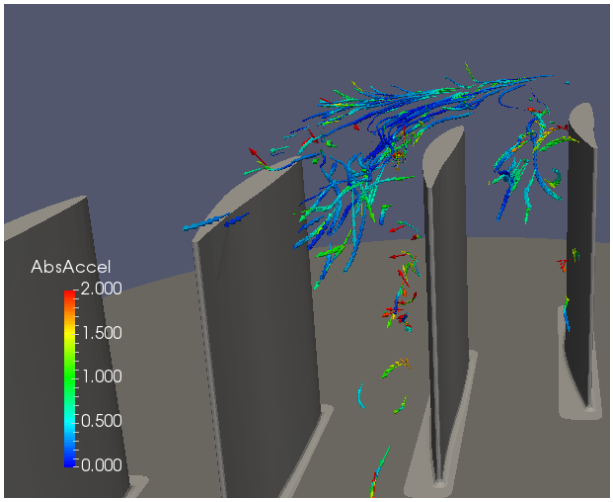

Figure 5.10: Absolute Acceleration in m/s^2 of the flow around the centre blade. Filtering at RKE lowers than 0.3. View from downstream (i=10º, Re=21.937, h=4%)

From Figure 5.10, the same flow trajectories as in Figure 5.9 are shown. It is seen that the BLF, on top of the image, has, generally, low acceleration component. Their values are around 0.2-0.3 m/s^2, but they can reach values from 0.5 to 1 m/s^2 in the middle of the channel. On the other side, the trajectories belonging to the detachment zone present higher values of acceleration. As seen, green, orange and red colours are characteristic of that region, which indicates values between 1-2 m/s^2.

5.2.2 Identification of different Flow Structures

After clarifying the general flow pattern in the compressor cascade, it is time now to start defining each one of the different structures that can be found, especially in the tip region, but in the whole passage. Essentially, the flow is compound by five part flows, that are defined by their origin, location and interaction with the rest of them.

- The first one is formed by all the trajectories that constitute the main flow. These trajectories follow the pre-defined direction specified by the blade contour. They do not suffer any disturbance and follow mainly a straight path, stablished by the blade incidence (showed in the images in Green colour).

- The second group is the tip leakage flow. It is the flow that crosses from the pressure side to the suction side of a blade over its tip through the clearance existing between the blade and the casing. This flow, as defined in previous sections, is one of the main cause of losses in a compressor cascade and one explanation of the rotating stall inception. This flow in contact with the main flow turns into a vortex that rotates clockwise, rotation defined in flow direction (showed in the images in Red colour).

- The third group is defined by the main flow that interacts with the Tip Leakage Flow, changing their trajectory and forming part of the TLFV structure (showed in the images in Yellow colour).

- To the forth group belong all the trajectories that come from the BLF included in the Horseshoe Vortex structure (showed in the images in Yellow colour).

- And the fifth group is defined by all the trajectories in the recirculation region (showed in the images in Blue colour).

The general flow structure is represented in Figure 5.11 using some characteristic trajectories and collecting them by colours. The Green colour trajectories denote the Main Flow of the passage; the Red colour ones are Tip Leakage Flow; and the Yellow ones are disturbed flow, including the BLF and the HSV.

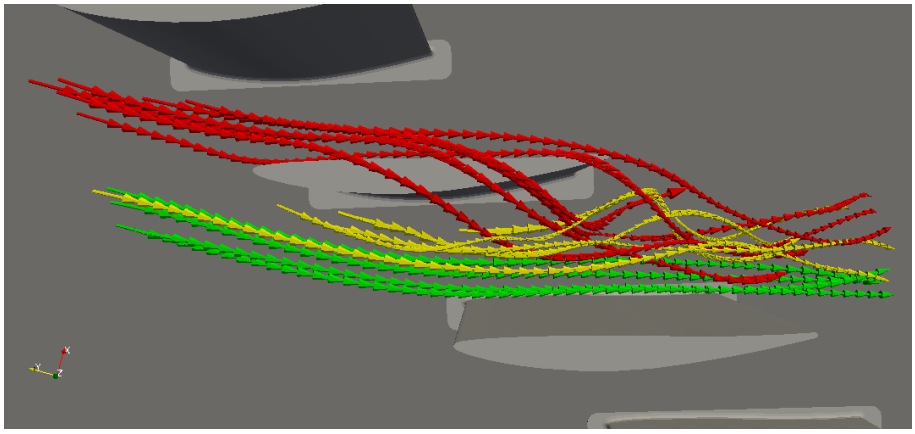

Figure 5.11: Flow characteristic patterns in a compressor cascade. View from top (i=10º, Re=27.422, h=4%)

From Figure 5.11, it can be seen the trajectory lines of the main flow (in green), which enter in the passage following and adjusting to the incidence angle of the cascade and the contour of the blade. And they continue their way, straight, without suffering any perturbation or interaction with any other flow structure.

Furthermore, the trajectory lines of the Tip Leakage Flow (in red) show the crossing of the leakage flow across the tip blade from the pressure side (right side of the blade in the picture) to the suction side (left side). The first thing to notice is the angle of crossing of the TLF. Except from the last two trajectories that are in between the TLF and the Trailing Edge Vortex, all TLF trajectories present at first sight roughly the same crossing angle.

Another element noted from the TLF is the sense of rotation. In Figure 5.11 it can be seen the clockwise turning of it, but its visualization is better in Figure 5.12, image taken from downstream. This movement is motivated to the presence of the casing and the incoming main flow and boundary layer flow.

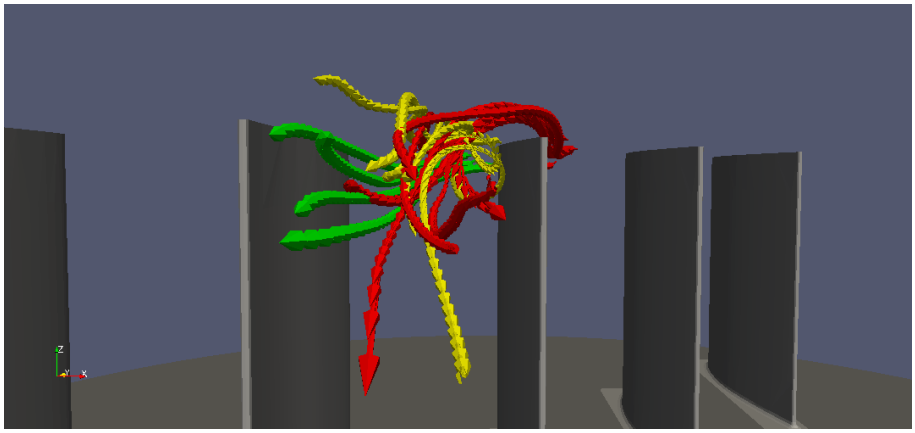

Figure 5.12: Flow characteristic patterns in a compressor cascade. View from downstream (i=10º, Re=27.422, h=4%)

Finally, the interaction of both principal flows (in yellow) can be observed as the third coloured group between the two previously flow structures. It acts like a interaction and combination of both partial flows and separates the zones of predominance of each type of flow structure.

Naturally, when the TLF crosses the tip clearance and enters the nearby passage, it interacts with the main flow coming upstream. The interaction of both flows results in the turning of the main flow in the sense of the TLFV, i.e. clockwise.

As this interacting flow comes, mainly from the vicinity of the Boundary Layer flow, the disturbed main flow experience not only a turning effect, but a change in direction due to this rotation. As it is noted in the downstream image (Figure 5.12) and in the rear-lateral view (Figure 5.13), the Yellow partial mass flow tends to head towards the hub, it gains a negative vertical component in the velocity (in a rotor the sense of the component would be radial towards the rotor centre of rotation).

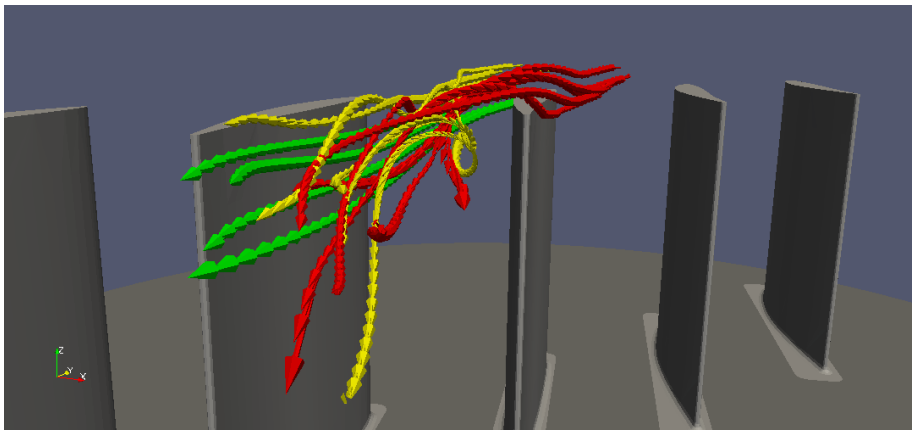

Figure 5.13: Flow characteristic patterns in a compressor cascade. View from lateral right side (i=10º, Re=27.422, h=4%)

Another fact to be noticed from these set of pictures is the existence of a double vortex structure, formed by the TLFV and the pressure-side of an HSV from the BLF. This can be slightly observed in Figure 5.12. The second and the third yellow trajectory counting from left to right seem to have a rotational component in counterclockwise direction, i.e. in opposite sense to the TLFV.

5.2.3 Tip Leakage Flow and Tip Leakage Vortex. Description and Characteristics

The characteristics of the TLF depends mainly on three parameters: the Re number, the incidence angle and the tip clearance, which essentially change the pressure field around the blade and the flow coefficient. And since it has been stated in previous developments that the TLF is driven by the pressure difference between the two sides of the blade; when the pressure field changes, the TLF changes too. This study will be centred in the influence of the incidence in all the flow phenomena in the compressor cascade, but a briefly discussion of the Re number will be done at the end of this section, summing up its contribution. The contribution of the tip clearance to the TLF has not been considered in this study, so its value has been left as a constant value, and then, not analysed its influence.

From the following pictures in Figure 5.14, already displayed in the last section, it can be taken a first view of the size and cover zone of the TLFV. For the conditions we are analysing now, incidence of 10º, the flow phenomena situation is stable and roughly steady, hence the structures seen in the pictures can be seen in the different measurement repetitions.

The TLFV occupies, under these conditions, a reduced portion of the blade span in the tip region, around the 20% of it in spanwise direction, and a bit more than the 50% of the passage width, which results in it occupying around the 10% of the passage, with roughly calculations measuring on the images, only due to the TLFV.

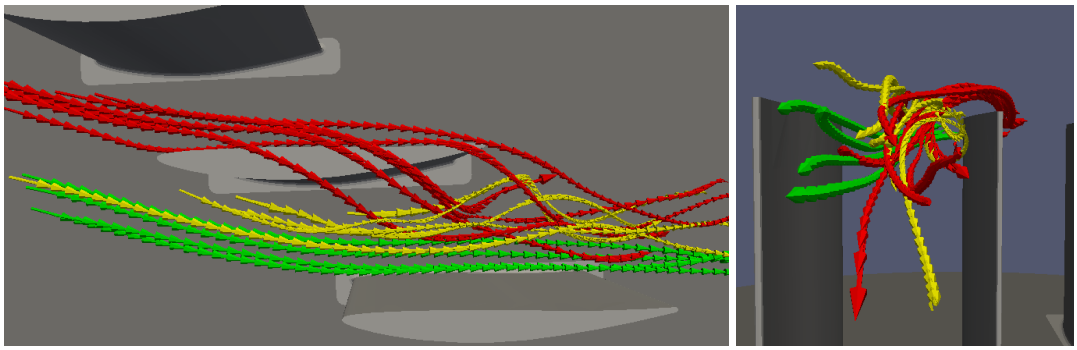

(a) Top view (b) Downstream view

Figure 5.14: Flow characteristic patterns in a compressor cascade (i=10º, Re=27.422, h=4%)

Since the TLF velocity and kinetic energy are low, the general contribution of this partial flow to the general performance is low. Besides, it causes a reduction of the mass flow through the cascade, reducing the effective cross-section area. This happens because of its low velocity component, which makes difficult the course of the flow. Thus, it induces a downwards component in the disturbed main flow, which drives the main flow to adjust to the reduced cross-section area in the passage. This fact is added to the rotation movement that adquires the flow from the vortex rotation.

The first tool used to analyse all the flow structures and phenomena present in a compressor cascade is the RKE, as it is has been used in previous images, like Figure 5.15. Another variable has been thought to give useful information of the flow, it is the Absolute Acceleration (Figure 5.16).

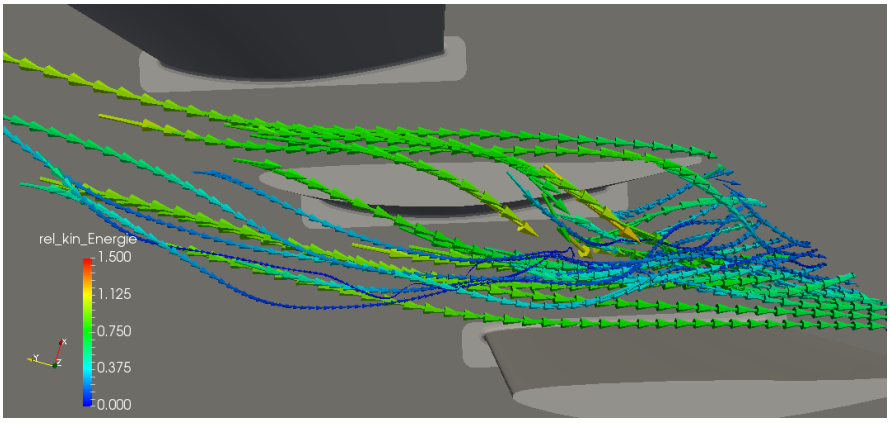

Figure 5.15: Relative Kinetic Energy of the flow around the centre blade. View from top (Compressor Blade view) (i=10º, Re=21.937, h=4%)

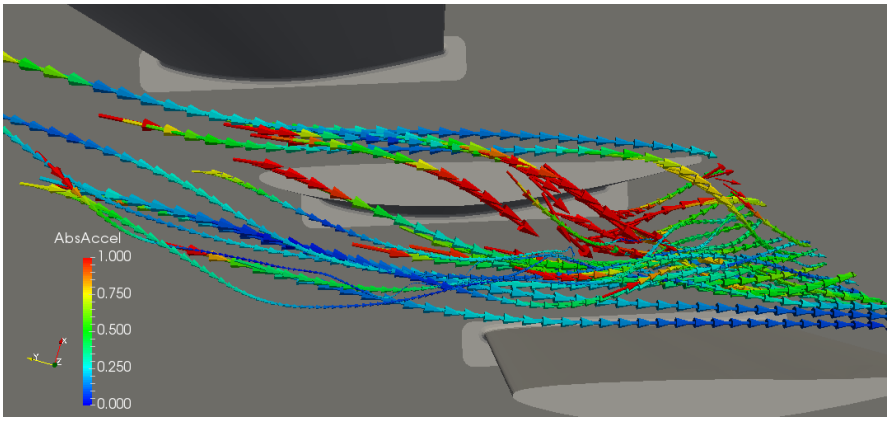

Figure 5.16: Absolute Acceleration in m/s^2 of the flow around the centre blade. View from top (Compressor Blade view) (i=10º, Re=21.937, h=4%)

The Absolute Acceleration gives an easy, fast view of the spots in the flow with high changes in velocity or direction. In comparison with the figure previously displayed (Figure 5.15), the same trajectories have been analysed and displayed this time with the use of the Absolute Acceleration (Figure 5.16). The highest values of acceleration can be found in the blade tip (TLF) and in the TLFV. In first place, the flow from the near passage must climb to the tip region and cross the tip clearance of the blade. This motivates a variation of velocity (Figure 5.15), but most important, a direction change. When the TLF enters the passage, it comes into contact with the main flow of this channel and it turns into a vortex, due to the casing. The high values of acceleration of the TLF are around 1 m/s^2, or even more, and the mid-values of the TLFV at the exit of the passage are kept around 0.25-0.5 m/s^2 (light-blue and green values).

5.2.4 Double Vortex Structure. Tip Leakage Flow and Horseshoe Vortex interactions

Another interesting fact of the flow structure present in the passages of a compressor cascade is, what it has been named as "Double Vortex Structure". This flow structure consists of a group of vortices present in the blade passages, whose own rotation is influenced with the nearby vortex rotation. That means both vortices rotation senses are related and they affect each other.

The "Double Vortex" group is formed by the TLFV and the HSV, which is formed by the incoming BLF of the casing and the flow of its vicinity when approaching the blade, as it has been already explained in Section 2.6.1. It is this HSV structure that interacts with the TLFV and both vortices appear to rotate in opposite senses. In next Figure 5.17, the trajectories that belong to each vortex are highlighted in different colours. The TLFV is brought out in red colour and the HSV, in yellow.

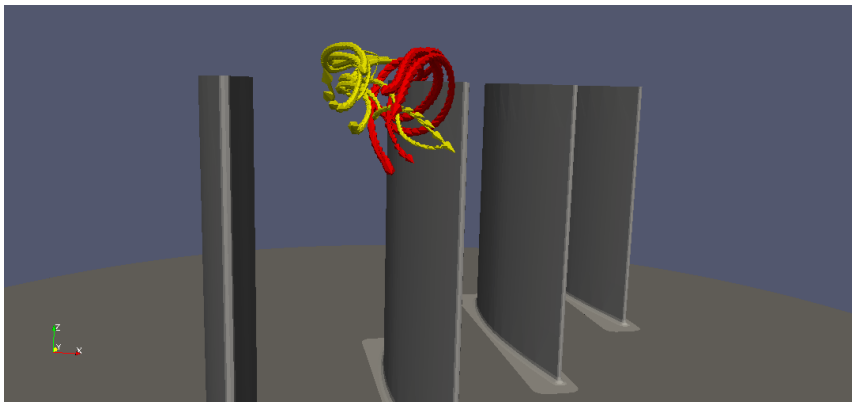

Figure 5.17: Double Vortex Structure: Identification of trajectories. View from downstream (i=10º, Re=27.422, h=4%)

In Figure 5.18 it can be clearly seen the difference between both vortices. The TLFV comes from the tip clearance and when enters in the passages rolls clockwise. And the HSV, which comes from the BLF of the casing, just on top of the image, turns in counterclockwise direction. From the definition of the HSV concept, it has been said that it is weaker than the TLFV [4], so it tends to bend under the TLFV. This fact is observed with the two yellow trajectories at the right of the image and the one at the down part. Those trajectories, especially the two first ones, come from the vicinity of BLF, closest to the Boundary Layer and the casing, so they may belong to the HSV structure. But even when all they seem to come from the vicinity of the casing, they might seem to belong to the main flow. So, they are simply influenced by the HSV and when interacting with the TLF they take part of the Double Vortex in the HSV side.

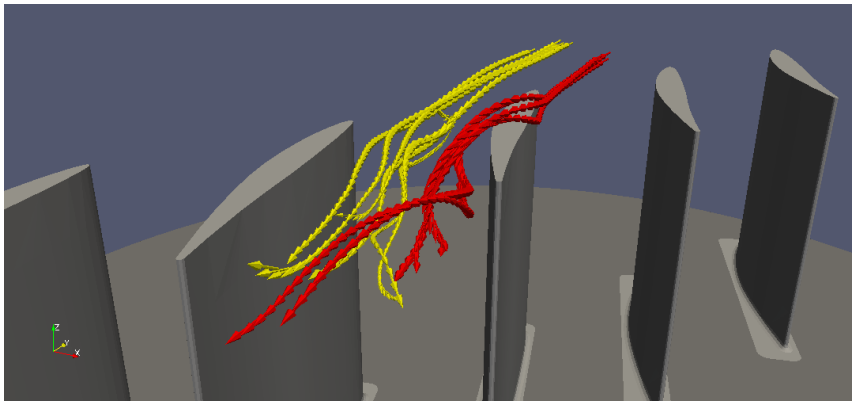

Figure 5.18: Double Vortex Structure: Identification of trajectories. View from downstream (upper right side) (i=10º, Re=27.422, h=4%)

Following, the same trajectories are displayed in Figures 5.19 and 5.20, representing the RKE instead. Both flow parts have similar RKE at the beginning of the trajectories. In both cases, light-green colours point out values of RKE around 0.80-0.90 (Figure 5.20). But when both flow streams (TLFV and HSV) rotate, they lose velocity, which is shown in the blue colours of the trajectories, corresponding to RKE below 0.30 (Figure 5.20).

In this situation, the rotation of the trajectories induces a loss of velocity or RKE (i.e. energy) because of the shear stresses, which appear due to the velocity gradients between the different flow streams. Both vortices have the same velocity range at the end of the trajectories when exiting the passage.

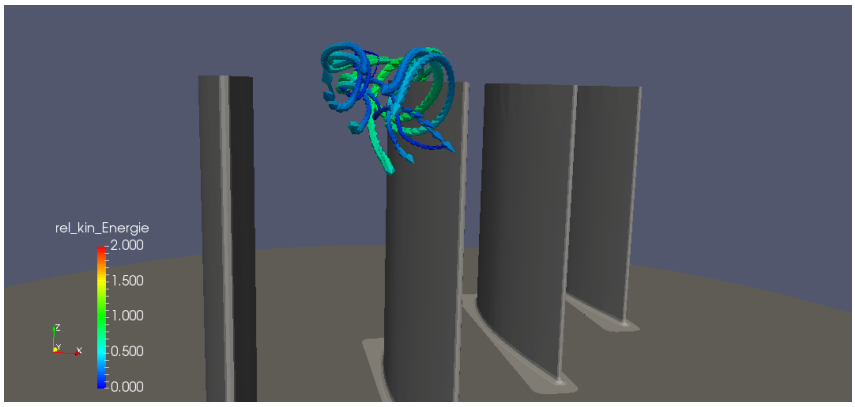

Figure 5.19: Double Vortex Structure: Relative Kinetic Energy. View from downstream (i=10º, Re=27.422, h=4%)

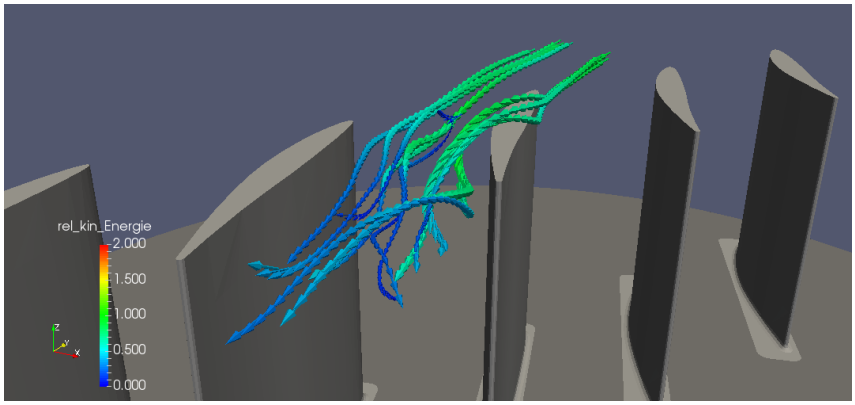

Figure 5.20: Double Vortex Structure: Relative Kinetic Energy. View from downstream (upper right side) (i=10º, Re=27.422, h=4%)

5.2.5 Reynolds Number dependency

During the analysis of the flow at an incidence angle of 10º, it could have checked that the influence of the Reynolds number in the flow phenomena is small. Varying the Reynolds number has not demonstrated noticeable changes in the flow behaviour. Some deviations in the value of the RKE have been noticed, produced during the calculation of the inlet flow velocity. It is obtained in the water channel in a simple way that might lead to some discrepancies. Because of that reason, and knowing that the RKE must be (aproximately) equal to 1 at the inlet of the blade cascade, the RKE values must be corrected.

After performing these corrections, measurements of different *Re* appear to have the same approximate values in the RKE and, most important, they show the same flow behaviour, no matter which Reynolds Number is tested. The changes of the pressure field around the airfoil do not modify the behaviour of the TLF, nor its vortex or any vortex system.

When observing Figures 5.1 and 5.3, the same phenomena happens in the passage. The flow accelerates at the passage in the suction side when reaching the highest curvature point, and then starts to decelerate. This behaviour is also seen in Figures 5.2 and 5.4 with the Absolute Acceleration, where the lighter colours right in the middle of the passage show a change in the acceleration (in this case negative, so deceleration).

5.3 Incidence Angle: $i = 19^o$. Unstable Behaviour

After describing and analysing the flow phenomena around the compressor cascade for the conditions studied at a stable and normal point of operation with an incidence angle of 10^o, the unstable flow conditions under an incidence angle of 19^o are being analysed. This unstable situation is reached when the operating point of the compressor exceeds the Stability Limit. This high incidence angle is translated into a lower flow coefficient of the stage than in the previous section. Such a low flow coefficient takes place in really low air mass flow conditions, such as Engine Start, but these extreme situations are more prone to happen during Engine Accelerations and Decelerations [16], rather than Engine Start.

5.3.1 General Flow Comparison

The first step in the comparison is checking whether the flow development inside the passage is the same as in stable conditions (i=10^o). In analogous way to 10^o of incidence, following, pictures from the passage are illustrated. They correspond to different views from top of the blade cascade and from downstream (at TE). The top views displayed are made performing a slide at around 50% of blade height (aproximately at 50mm from the base), to ignore at this very first moment the TLF effects.

Observing Figures 5.21 and 5.22, some particular characteristics have been found. Both images present a region near the LE of the blade where the flow is noticiable accelerated. Now, the incidence conditions have grown and 19^o of incidence is a high value of deflection of the flow when entering the passage. That means that the flow must turn considerably in order to adapt to the blade cascade direction. This produces an acceleration of the flow when avoiding this obstacle. That is why a colour orange/yellow area can be found in both images of the flow trajectories.

Additionally, when the flow enters the passage, it starts to decelerate inmediately. Quickly, the tonality of the trajectories turns green and light blue-green, which indicates a strong deceleration of the flow until RKE=0.50, in some cases. The deceleration of the flow continues all over the passage length, lightening the RKE trajectory colours an, hence, showing the slowing down the flow.

But the most important feature is seen at the blade suction side (right hand side of the blade passage). Here in this location can be observed a group of trajectories with low RKE (velocity), near zero. Besides, the trajectories of that flow part are more chaotic and they do not follow the general flow direction, which is kept trying to follow the direction designed by the blades, as it happens with 10^o of incidence. This zone that starts approximately at around 1/3 of the blade chord is a detachment flow. Under high incidence conditions, the flow cannot follow and adapt to the path that the blades determine, so the flow detaches and generates a recirculation zone there.

Even when Figures 5.21 and 5.22 are taken under different *Re* conditions, they show the same flow characteristics. In that sense, the Reynolds number has few influence on the flow behaviour in these conditions.

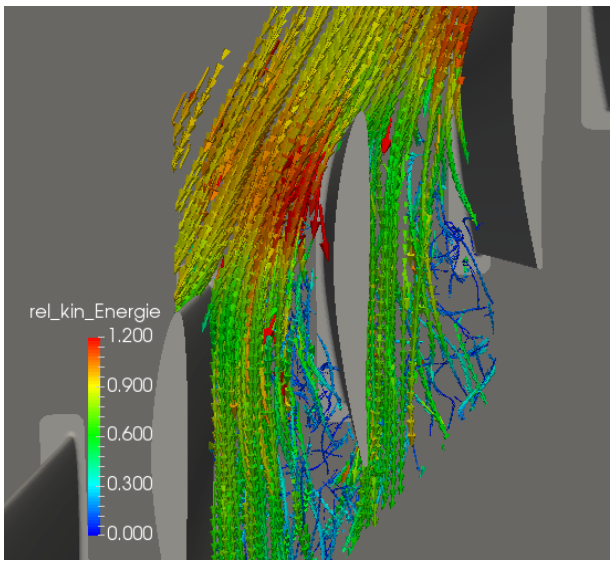

Figure 5.21: Relative Kinetic Energy of the flow around the centre blade. View from top. Cut at 50% blade height (i=19º, Re=19.065, h=4%)

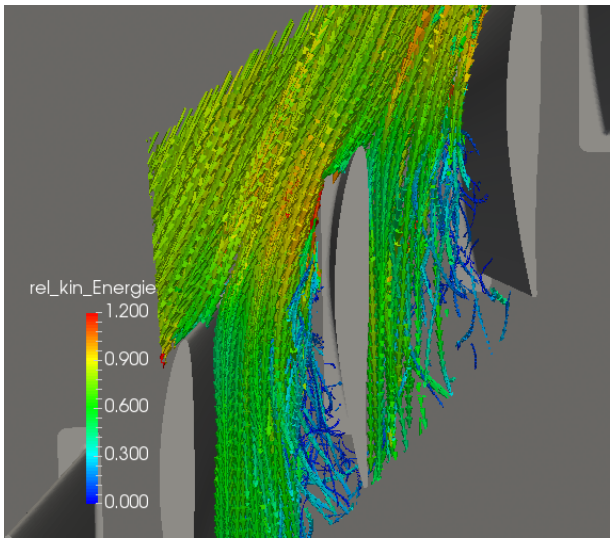

Figure 5.22: Relative Kinetic Energy of the flow around the centre blade. View from top. Cut at 50% blade height (i=19º, Re=30.023, h=4%)

When comparing 19º of incidence (Figures 5.21 and 5.22) with 10º of incidence (Figures 5.1 and 5.3), the main difference that can be observed is the detachment flow. Under 10º, there is no recirculation region or, if it exists, it is really small, located at the TE. With 19º this region has grown and occupies more than 1/2 of the chord length.

Another effect of increasing the incidence angle, related with the detached flow, is the growth of the detachment zone in the suction side of the blade at mid blade height. When comparing 10º and 19º of incidence conditions, the zone where the flow is detached grows with increasing incidence. This characteristic is observed by paying attention to the zone with low RKE (or flow velocity) values, that also show a chaotic behaviour, as previously mentioned, with a no predefined direction of the flow.

The growth of the recirculation zone is the first clue of a change of the structure in the flow core, because when at first the zone of detachment and flow recirculation was small, now it gains importance. It is true that the reason of the detachment cannot be only attributed to the TLFV (also the normal stall phenomena of an airfoil induces these effects), but it shows the reduction of the effective flow cross-section.

Furthermore, the acceleration that suffers the flow at the first half of the chord length is higher under 19º, since it has to perform a higher deflection to adapt to the channel contour. And then, the flow the flow decelerates much faster than 10º of incidence, where the flow slows down its velocity more progressively.

While with 10º incidence, the deceleration in the passage is progressive and takes place along all the passage in streamwise direction (Figure 5.4), in the 19º incidence situation, the flow accelerates and decelerates faster. It can be observed when comparing Figures 5.2 and 5.4 with Figures 5.23 and 5.24.

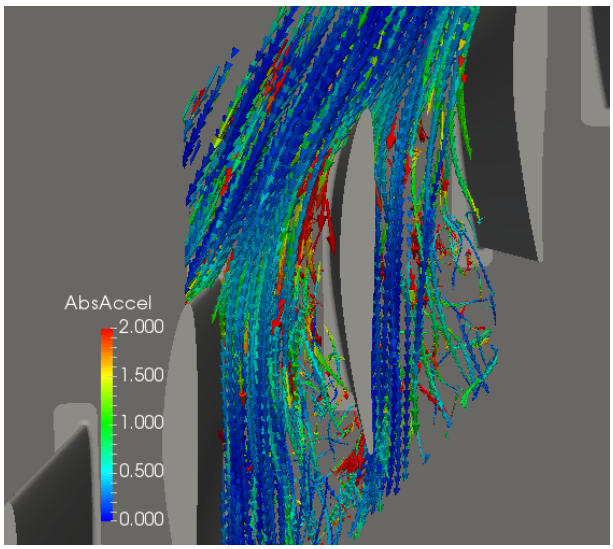

Figure 5.23: Absolute Acceleration in m/s^2 of the flow around the centre blade. View from top. Cut at 50% blade height (i=19º, Re=19.065, h=4%)

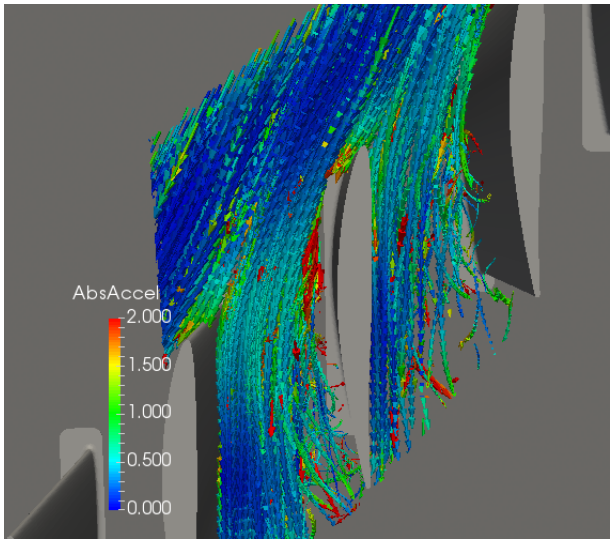

Figure 5.24: Absolute Acceleration in m/s^2 of the flow around the centre blade. View from top. Cut at 50% blade height (i=19º, Re=30.023, h=4%)

The values that shows Figure 5.24 are higher than before with 10º of incidence, and it displays a part with colour Red, which indicates an acceleration of 2 m/s^2. This part coincides with the higher RKE region and the start of the detachment region. Moreover, the values of the acceleration in the recirculation flow are kept higher. This is due to the rotation of the flow that is traduced in a high component of the centripetal acceleration.

The effects of increasing the incidence in a compressor cascade can be seen in the trajectories representation of RKE of the passage from downstreams (Figure 5.25).

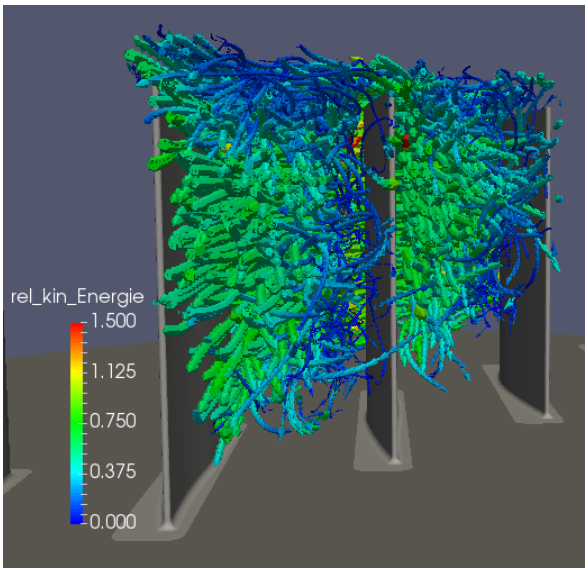

Figure 5.25: Relative Kinetic Energy of the flow around the centre blade. View from downstream (i=19º, Re=30.023, h=4%)

The increase of the recirculation zone in the blade suction side (right hand side of the passage) is clearly noticeable when comparing with Figure 5.6. In that case, the flow showed a rather uniform distribution of the RKE values. Almost all the passage was covered with green colour values of the RKE (around 0.75), with the exceptions of the TLFV on the top blade and a little portion on the TE (a small detachment). Now, all the superior part of the channel is covered in blue colour trajectories, which indicates a low or very low RKE and, thus, velocity. The detachment is better seen now, as well. And all the flow trajectories that does not belong to the recirculation or the vortices structure in the top of the channel show a lower value in the RKE. In Figure 5.6, the RKE was around 0.75, but in this case, the RKE has dropped to light-green/light-blue values, around 0.60.

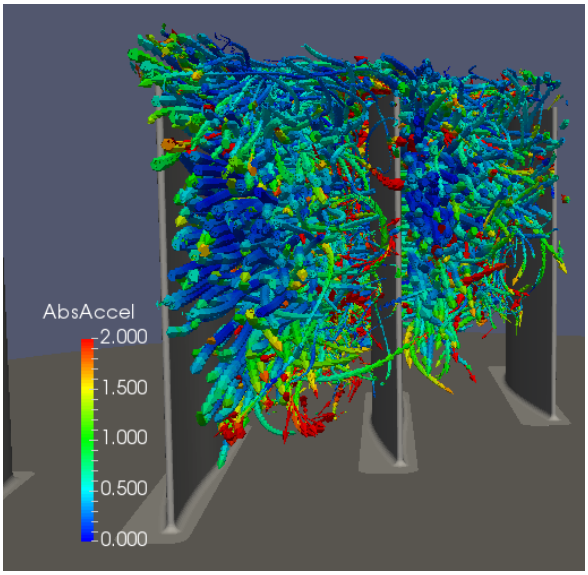

Figure 5.26: Absolute Acceleration in m/s^2 of the flow around the centre blade. View from downstream (i=19º, Re=30.023, h=4%)

If now the Absolute Acceleration is depicted (Figure 5.26), the difference with Figure 5.8 is considerable. Now all the top part is included with acceleration values that are around 0.5 m/s^2 (light-blue colour), plus the detachment zone and the bottom part that have values near green tonality (around 1 m/s^2). Just the blade pressure side (left hand side of the passage) shows blue/dark-blue value for the acceleration. In this situation, the higher values of acceleration are due to the centripetal component of the acceleration, motivated by the rotation and movement of the flow in the vortices and the recirculation zone.

5.3.2 Identification of different Flow Structures. Tip Leakage Flow and Tip Leakage Vortex

The next step to be carried out is the analysis of the different flow streams present in the passage for 19º of incidence. All the types were already presented in the corresponding section for 10º of incidence. The group types remain the same, but in these new conditions, the characteristics of everyone may differ a little bit.

Mainly, the TLF grows and tends to occupy all the passage width and the Double Vortex structure (DV) is not so easy to observe. The reason for this last thing is the unstability of the flow state, in terms of the Vortex Breakdown, which consists of the breakdown of the stable vortices structure present in the case of 10º incidence. So, it changes the flow situation all along time and sometimes the cameras cannot capture the whole phenomenon cycle.

Every measurement consists of the capture of 200 and 300 images at 50 or 60Hz. So, the exposure time of the flow phenomena to the cameras is around 5 seconds. Hence, depending on which part of the cycle the cameras record, one situation, the other one or both can be observed.

With Figure 5.27, a first identification of the trajectories for i=19º is shown. The colour legend for these images is the same as in the last section: Red colour for TLF, Green colour for Main Flow and Yellow colour for HSV and the flow influenced by HSV and TFLV. This time, another trajectory type is distinguished with the Blue colour. It represents the trajectories in the recirculation zone. Here can be seen that the coverage of the TLFV is bigger in these conditions than for 10º incidence and reaches the entire passage width, letting less free cross-section for the incoming main flow, as seen in Figure 5.25.

Besides, the flow is noticed to be more chaotic and present more variations than stable conditions. In Figure 5.27 it is not so evident to observe the vortices rotation, nor the Double Vortex structure, contrary to the situation in Figure 5.14 with an incidence of 10º. As mentioned above, the Vortex Breakdown, phenomenon present under unstable operating conditions, is unsteady, so the trajectories along time are not kept and the display of the vortices structure is made more difficult.

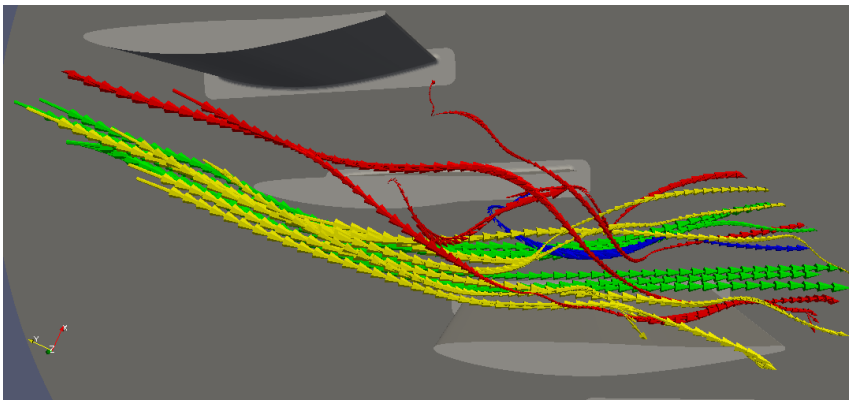

(a) Top view

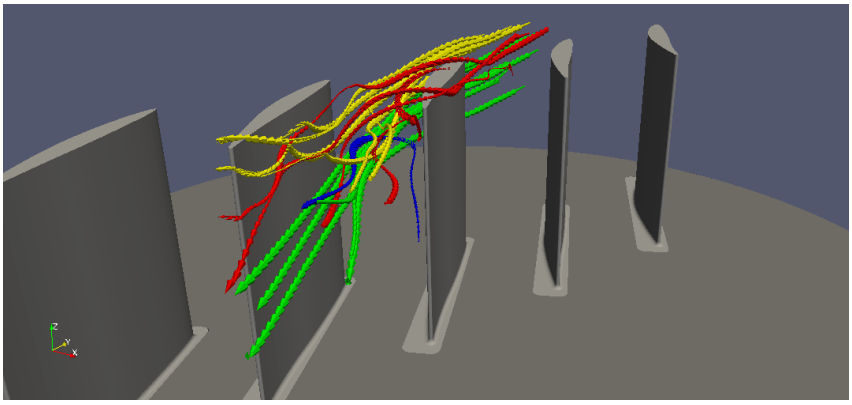

(b) Rear side view

Figure 5.27: Flow characteristic patterns in a compressor cascade (i=19º, Re=19.065, h=4%)

Under another different *Re* conditions and measurement in the compressor cascade, the Figure 5.28 has been taken. This picture is taken with a higher *Re* number than Figure 5.27. This image has the same colour legend than the other picture: Red for TLF, Yellow for HSV and partial flows influenced by it, Green for the main flow, and Blue for the trajectories in the recirculation zone. This time, the different senses of rotation of the TLFV and the HSV and influenced flow can be seen. Additionally, this capture displays diverse recirculation zone trajectories, which correspond to the detached flow of the blade.

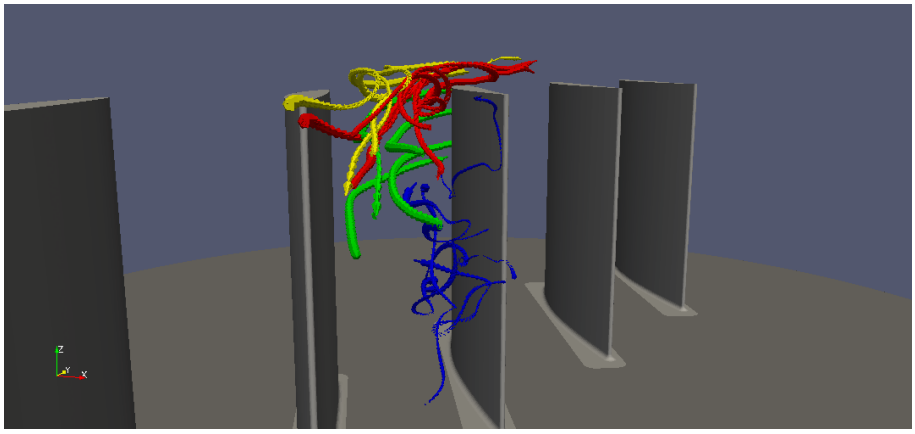

Figure 5.28: Flow characteristic patterns in a compressor cascade. Vortices (i=19º, Re=30.023, h=4%)

This recirculation zone is a key characteristic of the flow under unstable conditions, such as the 19º incidence tested in this project. Even when in i=10º the recirculation zone also exists, it is more noticeable with 19º and its existence is related to the increase in the incidence angle and the growing TLFV. Figure 5.29 shows the recirculation zone with a different perspective.

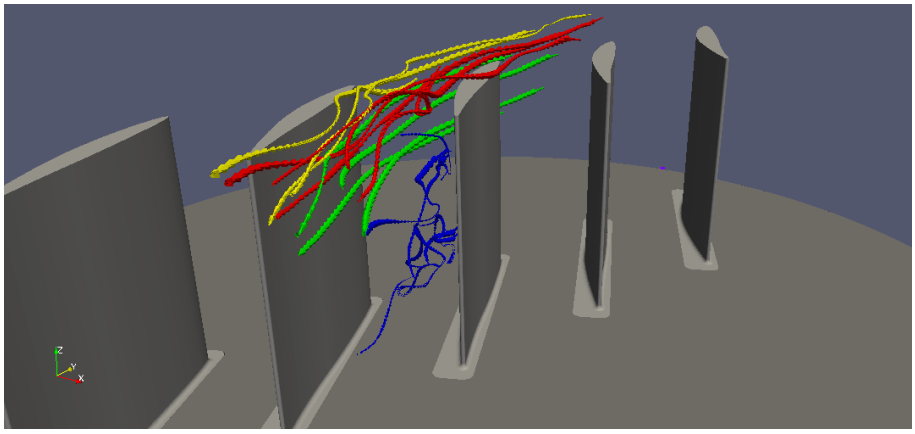

Figure 5.29: Flow characteristic patterns in a compressor cascade. Vortices. Lateral perspective (i=19º, Re=30.023, h=4%)

In the following Figures 5.30 and 5.31, the RKE and the absolute acceleration of the flow around the recirculation zone are displayed, respectively. These images are taken with the same concept as Figures 5.22 and 5.24, but with another different perspective. With this angle, the path of the trajectories around the detached flow can be observed.

From Figure 5.30 can be seen that the trajectories pass around the recirculation area, they get a little bit curved. It seems that the flow when enters in the passage tries to avoid the recirculation flow, and when it exits the channel, it attempsts to recover all the passage width at the TE.

When observing Figure 5.31 with the acceleration, the nearby trajectories got lighter colours in the acceleration scale. These trajectories are influenced by the high centripetal acceleration component of the recirculation and, moreover, the curving they suffer induce a higher component in their centripetal acceleration too.

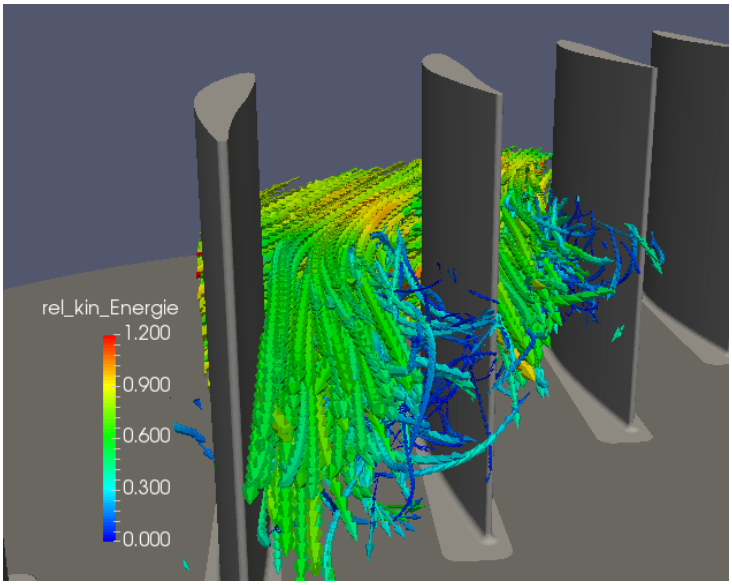

Figure 5.30: Relative Kinetic Energy of the flow around the center blade. View from downstream. Cut at 50% blade height (i=19º, Re=30.023, h=4%)

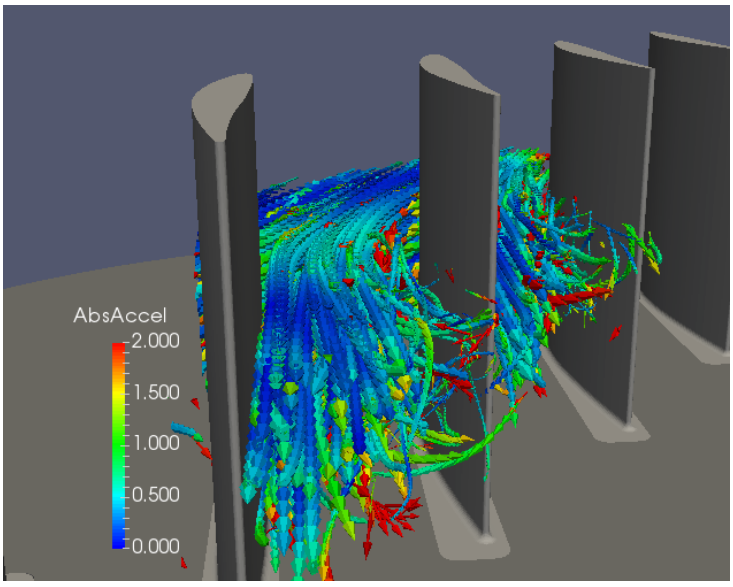

Figure 5.31: Absolute Acceleration in m/s^2 of the flow around the center blade. View from downstream. Cut at 50% blade height (i=19º, Re=30.023, h=4%)

When talking about the coverage of the TLFV, it is useful to observe the images of the RKE, like Figure 5.32, where the main trajectories involved in the phenomena are displayed for one measurement at high *Re*. But more important is the display of Figure 5.33, in terms of the Absolute Acceleration. Both together show the coverage of the TLFV and the flow behaviour, under these flow conditions.

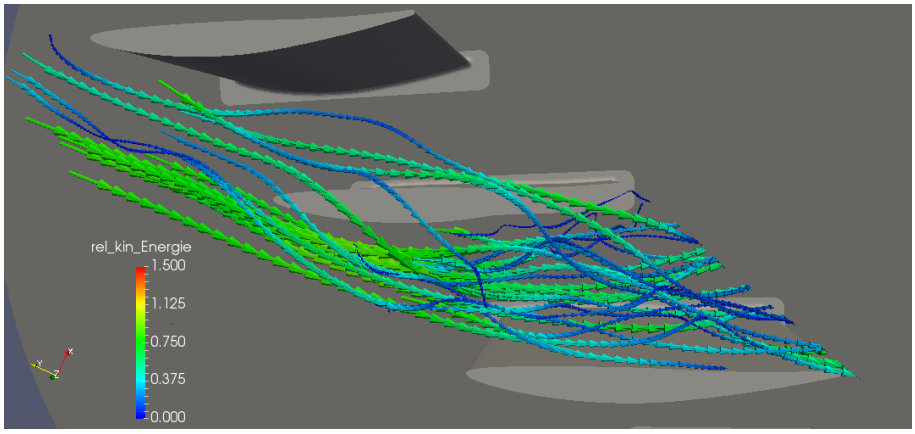

Figure 5.32: Relative Kinetic Energy of the flow around the centre blade. View from top (Compressor Blade view) (i=19º, Re=30.023, h=4%)

When comparing Figure 5.32 with Figure 5.15 (10º of incidence), the range of RKE is seen to be similar. But the biggest difference between them is seen when comparing the RKE distribution in the trajectories. For i=10º, the blue colour trajectories where mainly located near the TE of the blade at the suction side of the passage, but in this case, this type of trajectories covers all the passage pitchwise. Another feature observed is the value of the RKE inside the passage, which is lower than in 10º. In Figure 5.30, the deceleration of the flow is higher. Related to the recirculation zone and the TLFV, the high velocity gradients between different flow streams induce a high viscous dissipation of energy and a high drop in the RKE along one single trajectory.

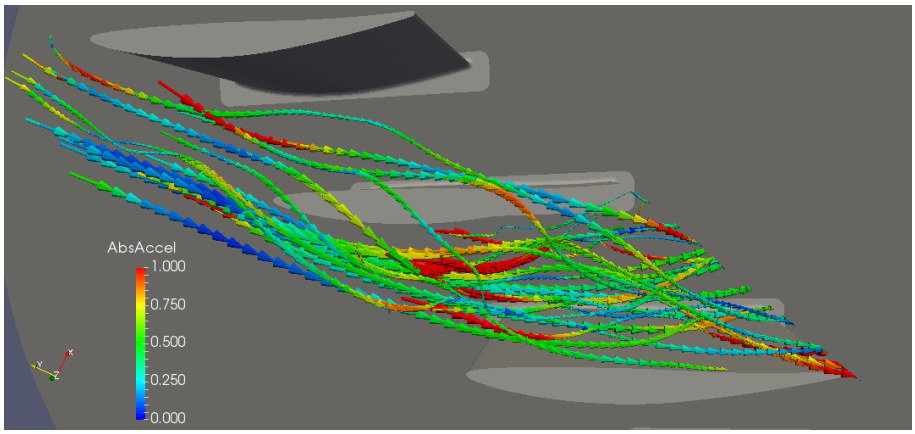

Figure 5.33: Absolute Acceleration in m/s^2 of the flow around the centre blade. View from top (Compressor Blade view) (i=19º, Re=30.023, h=4%)

When observing Figure 5.33 compared to Figure 5.16, the values of the acceleration are bigger all over the whole passage, streamwise and pitchwise, with respect to the case with 10º incidence. These higher values show the decelerations of the flow in the passage, due to the high dissipation of energy and the direction changes in the vortices flow because of the centripetal acceleration.

Another fact to keep in mind in this situation with 19º incidence is the non-periodicity of the images. In the 10º incidence cases the structures seen in the images of every measurement were roughly the same in space location. But with these new conditions, the different flow streams seem to change in every measurement, which means over time. Therefore, when one given type of trajectories is noticed in one measurement, it is usual not observing them in the followings. This fact proves the fluctuations of the flow in 19º incidence.

But the main clue for the instability of the flow is the group of trajectories coloured in blue in Figures 5.27, 5.28 and 5.29. All these trajectories belong to the recirculation zone of the passage in the suction side. Even when they are distributed all along the blade height, it does not mean that every trajectory belongs to one portion of the blade height. It is possible that one trajectory is initiated at the near-hub region at the TE, it ascends right to the tip region and, then, it follows the main flow direction again (for instance: Figure 5.34).

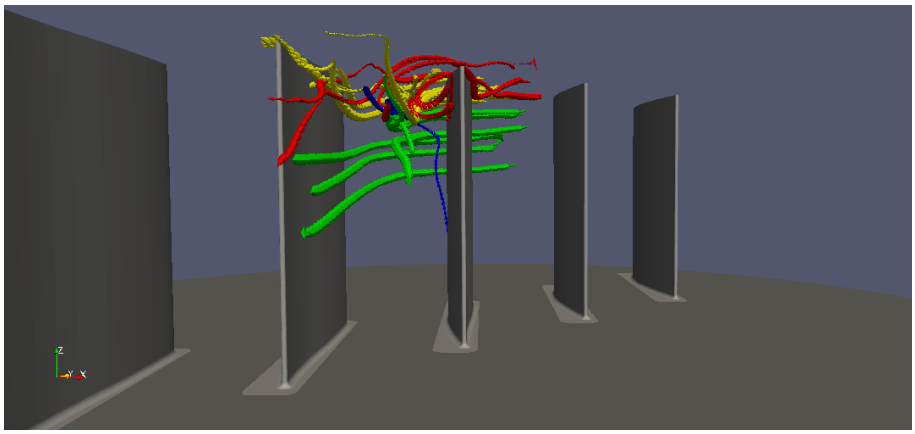

Figure 5.34: Flow characteristic patterns in a compressor cascade. View from downstream (i=19º, Re=19.065, h=4%)

This kind of trajectories appear essentially with high incidence angle, like 19º, when the Stability Limit of the compressor cascade is reached. All of them appear basically in the recirculation zone, where the flow is detached from the blade and it appears to no longer follow the main flow direction, at first sight. These recirculating trajectories appear also with 10º of incidence, when observing Figure 5.3 and/or 5.7. However, in these situations the recirculation zone is not big and its effects are located in a small region, apparently with low effect in the general flow.

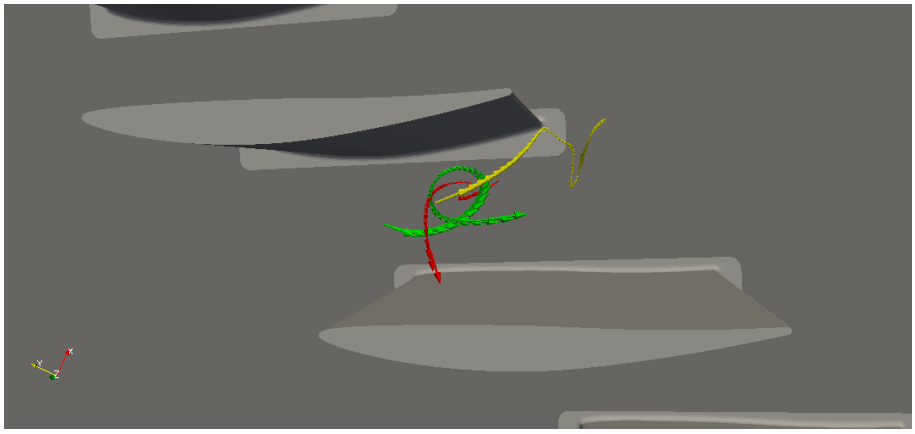

Figure 5.35: Flow unstable patterns in a compressor cascade. View from top (i=19º, Re=30.023, h=4%)

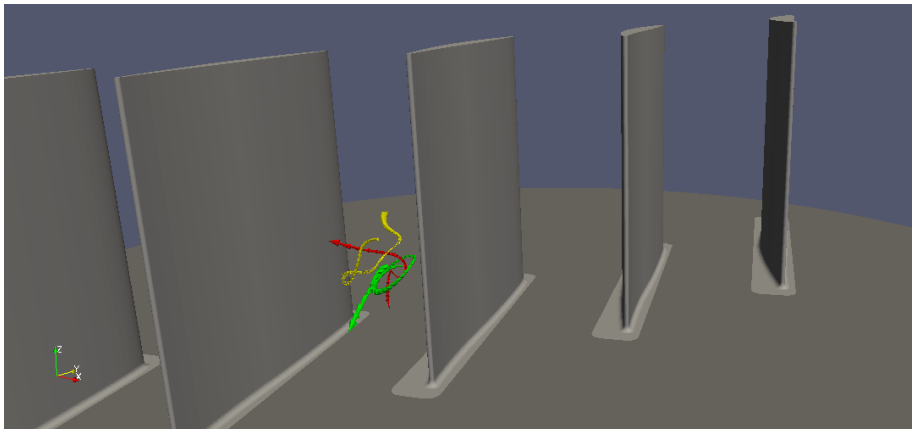

Figure 5.36: Flow unstable patterns in a compressor cascade. View from right lateral side (i=19º, Re=30.023, h=4%)

The first thing to say about this kind of trajectories is that they show no-coherence in their movement. For example, Trajectory 1 (green) comes from the front part of the passage and in the middle of it makes a "loop" and continues its path. Trajectory 2 (red) comes from the hub, makes an "S" movement and redirects towards the nearby blade. And Trajectory 3 (yellow) comes from forward and makes diverse direction changes of 90º and 180º. So, apparently, those three trajectories do not follow any coherence nor similar pattern in their movements, which seem to be random and chaotic. Hence, the analysis of these kind of trajectories with the Absolute Acceleration has been performed and it is shown in Figure 5.37. This pictures displays the recirculation region trajectories that have been depicted in Figures 5.28 and 5.29.

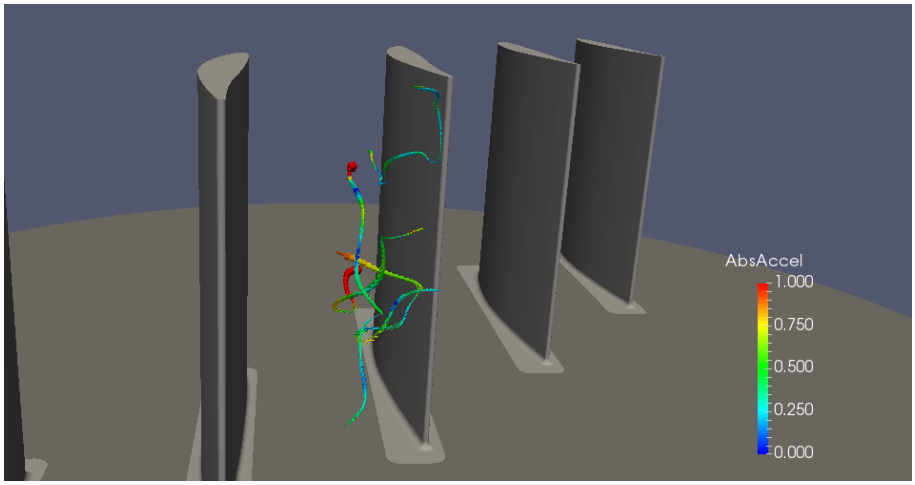

Figure 5.37: Flow unstable patterns in a compressor cascade. Absolute Acceleration in m/s^2 (i=19º, Re=30.023, h=4%)

This image is good for observing the acceleration characteristics of the flow in the recirculation zone. Apart from the high values of acceleration, it is easy to appreciate the big variations of it along one single trajectory. It is logic that the trajectories in this region have high acceleration, since the flow particles moving in it have quick and sudden changes of direction, so the centripetal acceleration of them is big. But, the acceleration changes its value considerably in one trajectory. This shows a high degree of fluctuations in this region and changes in the trajectory directions.

5.3.3 Double Vortex Structure

The Double Vortex Structure has been previously introduced and presented when analysing the different vortices structures in Figure 5.17-5.20. This structure of the flow is a system formed by two vortices: the HSV and the TLFV, which rotate in different senses, originating the Double Vortex Structure.

The DV has come to be a little bit difficult to observe under 19º incidence, when trying to compare it with the 10º incidence one. Different causes for this phenomenon have been considered. The first one might be the change in strength of both vortices. The HSV part is weaker than the TLFV and tends to move towards and under it or, in some occasions, to get mixed in the core flow. Thus, in 19º incidence the TLF is more important and can cover all the passage width, so it disturbs and interact more than before with the HSV, making difficult its observation. Another option, presumed to be more willing to be the reason of this disappearance of the DV, is the Vortex Breakdown. The increase of incidence angle leads to an unstable state of the vortices structures, which tend to change and collapse, generating an increase in the recirculating region, and hence, obstructing the passage.

Figures 5.38 and 5.39 on one side and Figures 5.40 and 5.41 on the other side represent the situation in which the DV is observed or not. The first two are taken from a different measurement than the last two ones, but under the same Reynolds number, incidence and velocity conditions. The only difference between them is the moment in which the measurements were taken.

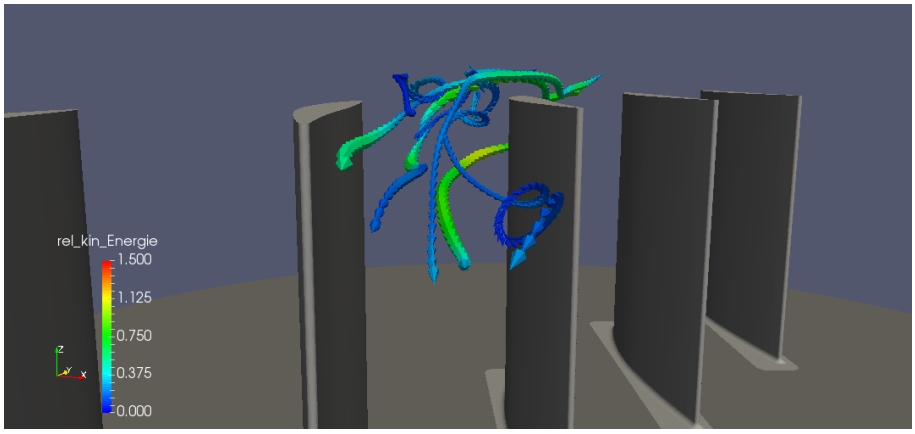

Figure 5.38: Double Vortex Structure: Relative Kinetic Energy. View from downstream (i=19º, Re=30.023, h=4%)

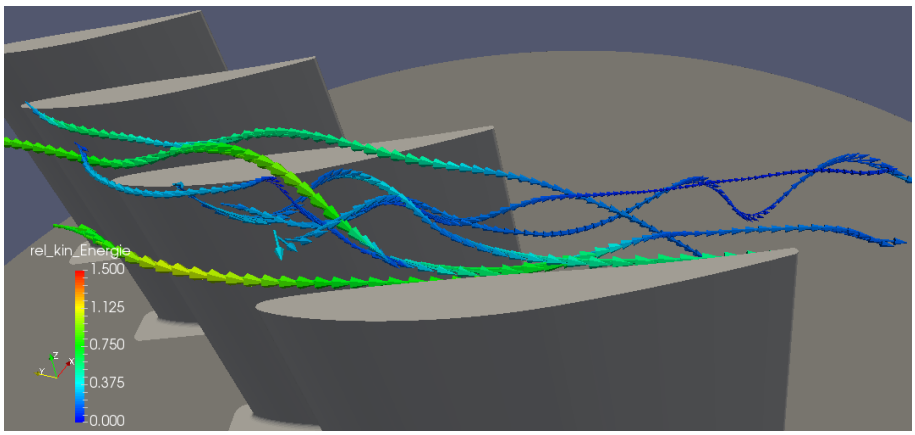

Figure 5.39: Double Vortex Structure: Relative Kinetic Energy. View from lateral (i=19º, Re=30.023, h=4%)

Figures 5.38 and 5.39 represent the Double Vortex Structure when the vortices have broken. Here, the DV is hardly seen, since only a TLFV structure is recognized with really low RKE values, which shows a huge deceleration in that zone. With these images up to two TLF structures can be appreciated, but only one turns into a vortex. Even the rotation of this one is displaced downwards and deviated with respect to the last examples observed in the section with 10º of incidence angle.

On the other hand, Figures 5.40 and 5.41 represent the DV for the same incidence and *Re* conditions as before.

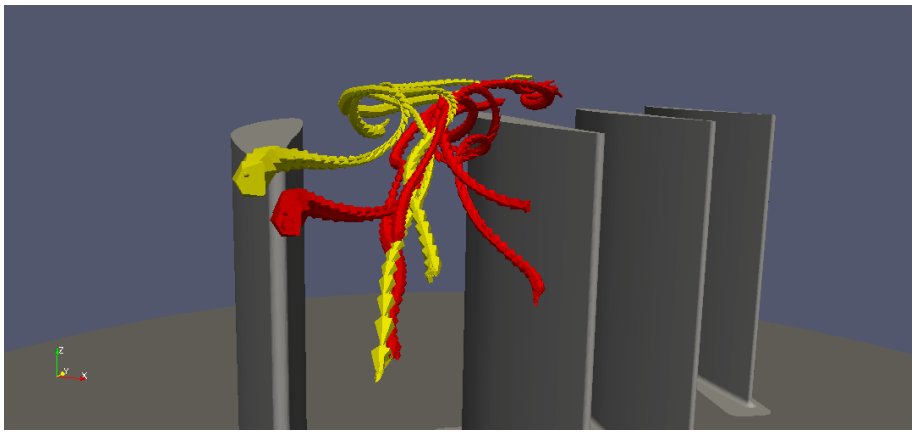

Figure 5.40: Double Vortex Structure. HSV and TLFV (i=19º, Re=30.023, h=4%)

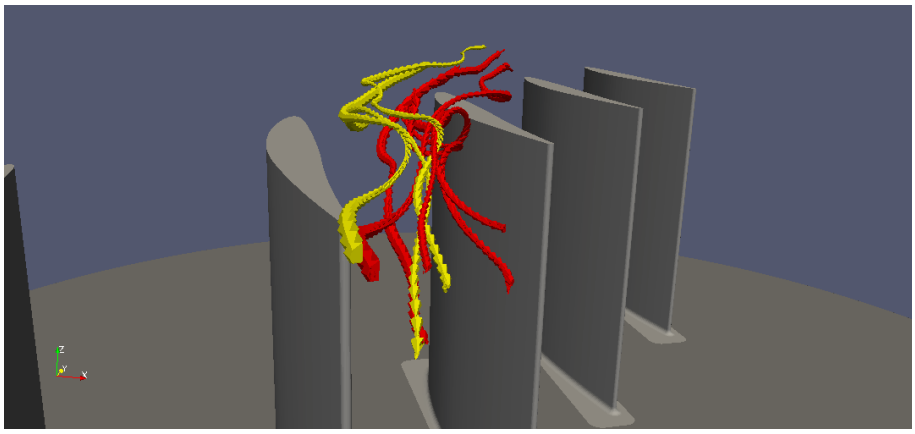

Figure 5.41: Double Vortex Structure. HSV and TLFV. View from rear-top (i=19º, Re=30.023, h=4%)

This time, in both images the DV can be clearly identified, specially in Figure 5.40, which is seen from downstreams. In colour Yellow the HSV part is represented and in Red, the TLFV part. As expected, the HSV trajectories rotate in counterclockwise direction with respect to flow direction. The TLFV comes from across the tip clearance between the tip blade and the casing. It rotates clockwise in the flow direction as seen in the images. Even when the TLFV trajectories are supposed to remain near the suction side of the passage, some trajectories seem to cross the passage pitchwise. This fact might be due to the Vortex Breakdown phenomena. So, these trajectories could have been taken moments before the Vortex Breakdown takes place and the vortices structure collapses.

Chapter 6

Conclusions

In the present work, the flow behaviour at a compressor cascade in the region of the blade tip has been investigated with the help of the Particle Tracking Velocimetry (PTV) measuring technique. All the measurements were carried out in the flat bed water channel at the facilities of the Institut für Luftfahrtantriebe (ILA) of the Universität Stuttgart. A compressor blade cascade has been introduced in the measuring region of the water channel, which allows performing different tests, simulating the cascade under diverse operating conditions. Different flow conditions in stable and unstable behaviour, under two different incidence angles (10^o and 19^o), were tested to analyse the flow phenomena in such different flow situations, as well as to compare the main characteristics of both operating performances. Two different incidence angles with three Reynolds number conditions each with the same tip gap clearance are presented in the project.

The PTV measurements allow the tracking of single tracer particles in a fluid in time and space by taking pictures of a fluid control volume. Synchronous coupled cameras are placed in different positions and orientations. By crossing picture rows of all cameras, particles can be tracked and spatially be located. The spatial location of all particles in a trajectory lets us obtain quantitative parameters such as velocity and acceleration, so not only it can be known how the particles move, but how much they move. By applying different kind of filters after the image processing, the flow trajectories can be analysed, depending on different main characteristics. For instance, Boundary Layer flow can be distinguished by its low velocity and energy component. Hence, by filtering low velocity flow near a wall region, the Boundary Layer can be analysed. Or, recirculation regions can be located by combining low velocity and high acceleration filters.

To analyse the flow in stable conditions, it has been chosen 10^o of incidence. The definition of stable behaviour is defined by the performance and the characteristics of the flow at these situations. With stable operation, it has been observed that the flow in the passage core is homogeneous and follows the direction predefined by the blade contours in a smooth way. The flow decelerates, as expected, smoothly, all along the passage.

Additionally, the existence of recirculation zones in the channel are mainly limited to a small flow detachment in the blade suction side surface and to the flow near the hub. But both recirculation zones seem to be of minor importance. Then, apart from these two zones, the flow seems to be coherent with the blade predefined direction.

When observing the flow from downstream, at the Trailing Edge position, it has been noted that the detachment zone occupies a small percentage of the whole passage cross-section. Besides, the vortex and the flow generated of the Tip Leakage can be also observed. In this case, both phenomena are limited in size and effect, reducing their contribution to the general flow. But in any case, it is seen how the TLF crosses the blade tip from the pressure side to the suction side. When it enters in contact with the main flow, it turns clockwise in the direction of the main flow, due to the presence of the main flow and the casing. Another interesting fact is the Boundary Layer flow, or at least the main flow disturbed by it, that when interacts with the blade in the end-wall casing zone, turn into a Horseshoe Vortex, whose pressure side leg rotates in opposite sense than the TLFV.

The TLFV and the HSV represent a well consolidated vortices system, in which both moves towards each other due to the presence of the casing [5]. Since the TLFV is stronger than the HSV, its path is curved and tends to move underneath the TLFV [5]. Both vortices tend to move towards the centre of the passage, causing its blockage, due to the recirculation they generate. This structure of two vortices has been named Double Vortex.

Reducing the flow coefficient of the compressor leads to the growth in the tip leakage flow, increasing the passage blockage, and in late stages, motivating the inception of rotating stall in the compressor. The reduction in the flow coefficient is achieved in the water channel by increasing the incidence angle.

The second angle of incidence that has been tested is 19^o. This incidence is over the Stability Limit of the compressor stage, thus, in principle, unstable conditions are expected.

The first thing noticed when observing the general flow behaviour at 19^o of incidence is the growth in the detachment and recirculation region. While 10^o of incidence showed a low detachment region in the blade surface, under 19^o conditions, the detachment grows. This recirculation region is analysed at mid-height span, far from the tip effects, but when observing it from downstream, the detachment is effective all along the blade span, specially in the tip, where the growth of the TLF has covered all the passage pitchwise. Even when some part of the flow passage follows the blade contour, most of it belongs to the recirculation zone. In that case, the main flow passing across the passage is limited to a reduced region in the pressure side of the channel. This confirms that the increase of incidence increases the TLFV.

One interesting fact of the flow at 19º of incidence, which corroborates the unstable assumption, is the unsteadiness of it. It is clearly seen in the no recurrence of the flow among different measurements with the same conditions. This is recognized with the Vortex Breakdown phenomenon. That type of event consists of the actual breakdown or disintegration of the vortex structure generated in the channel. That means that the TLFV seems to appear and disappear. The prove of this behaviour is that in some measurements the Double Vortex structure can be seen and, in another ones, not. In some occasions, the DV structure was clearly seen as in 10º of incidence, with the two vortices perfectly defined. But in other measurements, the trajectories show a huge recirculation in the zone the DV would be expected. The TLF trajectories are observed to avoid this zone and cross all the passage pitchwise without rotating and generating the TLFV. Furthermore, unexpected trajectories appear. These trajectories presented not a logical flow pattern. They seemed to not follow any direction. For example, some of them come backward (opposite flow direction), change from one passage to the other, rise from the hub to the tip region or vice versa, etc.

Some possible further improvements to the analysis of the flow phenomena in the compressor cascade at the ILA water channel have been found. The first of them have been encountered to improve the visualization of the trajectories. Along the analysis of the trajectories in this project, it has been noticed that the trajectories near the suction surface of the study blade (center blade of the cascade of 5) often disappear. That generates two issues. First, some trajectories that cross those zones seem to be cut, when both ends seem to be found. And second, it appears an empty space in the suction side of the blade. This fact has been checked along different images of different measurements to ensure whether it was a big recirculation zone or a measurement problem. Finally, it was concluded that the white lateral surface of the blades reflects too much light towards the camera, so when particles cross this region, from the point of view of the camera, the bright white background "hides" the particles and, then, the tracking program is unable to find and track them. This problem might be solved by covering the blade in black tape or substituting the center blade by a black-colour material blade. In this case, unwanted reflection would be eliminated.

An interesting further study would be the identification and characterization of the transition incidence angle between a stable and unstable operating point. It has been proved in previous projects and articles [4–6, 8, 9, 39] that this point is around 17.5º of incidence angle, for the given compressor blade cascade. So, the PTV technique can provide a further and deeper approach to the flow behaviour understanding in this incidence angle range. It could let analyse the dependency of the stability limit with respect other parameters like the *Re* and the tip clearance. Moreover, some interesting information could be obtained by analysing the flow patterns during the transition. Thus, a better understanding of the Stability Limit and its borders would allow improving the performance and operating limits of compressors.

Another possible development would be introducing the Time as a forth Degree of Freedom in the tracking routine. Apart from knowing all three spatial components, it would be very useful knowing the time moment in which a trajectory is still present, and when another different one is generated. This would be very interesting when analysing in deep the Vortex Breakdown, which is an unsteady phenomenon.

Chapter 7

Bibliography

[1] "Airbus desvela su visión 2050 para un "Cielo más Inteligente"", AIRBUS, 2012. [Online]. https://www.airbus.com/newsroom/press-releases/es/2012/09/airbus-unveils-its-2050-vision-for-smarter-skies.html [Accessed: 14 August 2018]

[2] "La aviación reducirá a la mitad las emisiones contaminantes en 2050", TENDENCIAS21. NAVEGACIÓN AÉREA, 2012. [Online]. https://www.tendencias21.net/La-aviacion-reducira-a-la-mitad-las-emisiones-contaminantes-en-2050_a4855.html [Accessed: 14 August 2018]

[3] SARAVANAMUTTOO, H.I.H., ROGERS, G.F.C., COHEN, H. and STRAZNICKY, P.V., "Gas Turbine Theory", Pearson Education, 6th Edition, 2009

[4] LEITNER, M.W., ZIPPEL, M., and STAUDACHER, S., "The Interaction of Tip Leakage Flow with Incoming Flow in a Compressor Cascade", *DLR Kongress*, Vol. 420023, 2016

[5] LEITNER, M.W., ZIPPEL, M., and STAUDACHER, S., "Interaction of Tip Leakage Flow with Incoming Flow in a Compressor Cascade exceeding the Stability Limit", *DLR Kongress*, Vol. 450090, 2017

[6] PAPAYANNIS, "Untersuchung der Spitzenspaltströmung in einer Verdichterkaskade am Flachbettwasserkanal bei hoher Inzidenz", Diploma's Thesis, ILA, Universität Stuttgart, 2015

[7] KUKE, T., "Untersuchung der Einsatzfähigkeit der Particle Tracking Velocimetry (PTV) am Flachbettwasserkanal", Master's Thesis, ILA, Universität Stuttgart, 2016

[8] AL-TAIE, R., "Untersuchung der Spitzenspaltströmung in einer Verdichterkaskade mit Hilfe der Particle Tracking Velocimetry (PTV)", Master's Thesis, ILA, Universität Stuttgart, 2017

[9] SCHWÄBLE, M., "Untersuchung der Strömung im Spitzenspaltbereich einer Verdichterkaskade mit Hilfe der Particle Tracking Velocimetry", Bachelor's Thesis, ILA, Universität Stuttgart, 2018

[10] "Fluid Mechanics for MAP/Dimensional Analysis", WIKIVERSITY, 2017. [Online]. https://en.wikiversity.org/wiki/Fluid_Mechanics_for_MAP/Dimensional_Analysis [Accessed: 14 May 2018]

[11] VOGT, H. and ZIPPEL, M., "Sekundärströmungen in Turbinengittern mit geraden und gekrümmten Schaufeln; Visualisierung im ebenen Wasserkanal", Forschung im Ingenieurwesen, Vol. 62, 1996, pp. 247-253

[12] "Densidad del agua líquida entre 0ºC y 100ºC", VAXASOFTWARE. [Online]. http://www.vaxasoftware.com/doc_edu/qui/denh2o.pdf [Accessed 03 April 2018]

[13] "Viscosity", SAYLOR. [Online]. https://www.saylor.org/site/wp-content/uploads/2011/04/Viscosity.pdf [Accessed 03 April 2018]

[14] "Compressor Stall", WIKIPEDIA. [Online]. https://en.wikipedia.org/wiki/Compressor_stall [Accessed 04 June 2018]

[15] STAUDACHER S. "*Turbomachinery II*", Lecture Material, Institut für Luftfahrtantriebe (ILA), Universität Stuttgart, 2017

[16] GIL, A. "*Actuaciones de Aerorreactores*", Lecture Material, Departamento de Máquinas y Motores Térmicos (CMT), ETSID, Universitat Politècnica de València (UPV)

[17] SAEID, N. and SANKAR, L.N. "Numerical Simulation of Rotating Stall and Surge Alleviation in Axial Compressors", School of Aerospace Engineering, Georgia Institute of Technology, 2016

[18] CHEN, N., "Aerothermodynamics of Turbomachinery. Analysis and Design", WILEY, 2010

[19] STAUDACHER S. "*Turbomachinery I*", Lecture Material, Institut für Luftfahrtantriebe (ILA), Universität Stuttgart, 2018

[20] KEARNEY, D., PUNCH, J. and GRIMES, R., "An Experimental and Theoretical Investigation of the Pumping Performance of Geometrically Similar Flow Fields Within Miniature-Scale Centrifugal Pumps",Proceedings ASME-JSME Thermal Engineering and Summer Heat Transfer Conference, HT2007-321519, Vancouver, BC, Canada, July 8-12, 2007

[21] GOLDSTEIN, R.J. and SPORES, R.A., "Turbulent Transport on the Endwall in the Region Between Adjacent Turbine Blades", AMSE J. Heat Transfer, Volume 110, pp. 862-869, 1988

[22] INOUE, M., and KUROUMARU, M., "Structure of Tip Clearance Flow in an Isolated Axial Compressor Rotor", ASME Journal of Turbomachinery, Vol. 111, 1989, pp. 250-256

[23] TAN, C.S., DAY, I., MORRIS, S. and WADIA, A., "Spike-Type Compressor Stall Inception, Detection and Control", Annual Review of Fluid Dynamics, Vol. 42, 2010, pp. 275-300

[24] VO, H.D., "Role of Tip Clearance Flow on Axial Compressor Stability", 2001

[25] HOYING, D.A., TAN, C.S., VO, H.D. and GREITZER, E.M., "Role of Blade Passage Flow Structures in Axial Compressor Rotating Stall Inception", ASME Proceedings, 1998, pp. 89-GT-588

[26] LEIBOVICH, S., "The Structure of Vortex Breakdown", Ann. Rev. Fluid Mech., 1978

[27] FURUKAWA, M., INOUE, M., SAIKI, K. and YAMADA, K., "The Role of Tip Leakage Vortex Breakdown in Compresso Rotor Aerodynamics", ASME Journal of Turbomachinery, Vol. 121, 1999, pp. 469-480

[28] "Particle Tracking Velocimetry", WIKIPEDIA, 2017. [Online]. https://en.wikipedia.org/wiki/Particle_tracking_velocimetry [Last Accessed: 06 August 2018]

[29] VIRANT, M. and DRACOS, T., "3D PTV and its application on Lagrantian motion", *Meas. Sci. Technology*, 1997

[30] LÜTHI, B., "Some Aspects of Strain, Vorticity and Material Element Dynamics as Measured with 3D Particle Tracking Velocimetry in a Turbulent Flow", Dissertation, Swiss Federal Institute of Technology Zürich, 2002

[31] MAAS, H.-G. "Digitale Photogrammetrie in der dreidimensionalen Strömungsmeßtechnik", 1992

[32] "Epipolar Geometry", WIKIPEDIA, 2018. [Online]. https://en.wikipedia.org/wiki/Epipolar_geometry [Accessed: 06 August 2018]

[33] "Snell's Law of Refraction", LUMEN, 2018. [Online]. https://courses.lumenlearning.com/austincc-physics2/chapter/25-3-the-law-of-refraction/ [Accessed: 08 August 2018]

[34] "Collinearity Equations", WIKIPEDIA, 2018. [Online]. https://en.wikipedia.org/wiki/Collinearity_equation [Accessed: 06 August 2018]

[35] SCHENK, T. "Introduction to Photogrammetry", Department of Civil and Environmental Engineering and Geodetic Science, The Ohio State University, 2005

[36] "ParaView", WIKIPEDIA, 2018. [Online]. https://en.wikipedia.org/wiki/ParaView [Accessed: 06 August 2018]

[37] "Benutzerhandbuch PTV. Ringgitterwasserkanal. Flachbettwasserkanal", ILA, Universität Stuttgart, 2017

[38] WEIMER, M., "Modifikation des Wasserkanals zur Untersuchung der Spitzenspaltströmung und deren Wechselwirkung mit anderen Strömungsregionen", Diploma's Thesis, ILA, Universität Stuttgart, 2014

[39] ERHARD, S., "Untersuchung der Spitzen-Spalt-Stromung und deren Wechselwirkung mit der Zuströmung in einer Verdichter-Kaskade", Master's Thesis, ILA, Universität Stuttgart, 2017

[40] CUMPSTY, N.A., "Compressor Aerodynamics", Krieger Publishing Company, Malabar, Florida, 2004

[41] CUMPSTY, N.A. and HEYES, A., "Jet Propulsion. A simple guide to the aerodynamics and thermodynamic design and performance of jet engines", Cambridge University Press, 3rd Edition, 2015

[42] DAY, I.J, "Axial Compressor Stall", PhD Dissertation, University of Cambridge, 1976

[43] GUEZENNEC, Y.G., BRODKEY, R.S., TRIGUI, N. and KENT, J.C. "Algorithms for fully automated three-dimensional particle tracking velocimetry", 1994

[44] LÜTHI, B., TSINOBER, A. and KINZELGACH, W., "Lagrangian measurements of vorticity dynamics in turbulent flow", *J. Fluid Mech.*, Vol. 528, pp. 87-118, 2005

[45] MATTINGLY, J. D., HEISER, W. H. and DALEY, D. H., "Aircraft Engine Design", AIAA Education Series, 1987

[46] OATES, G. C., "Aerothermodynamics of Gas Turbine and Rocket Propulsion", AIAA Education Series, Second Printing, 1988

[47] VO, H.D., TAN, C.S. and GREITZER, E.M., "Criteria for Spike Initiated Rotating Stall", Journal of Turbomachinery, *ASME*, Vol. 130, Issue 1, 2008